Cold Plasma deposition of organosilicon films with different monomers in a dielectric-barrier discharge

Sara Lovascio

Università degli Studi di Bari

Dottorato di Ricerca In Scienze Chimiche

XXI CICLO

Université Pierre et Marie Curie

Ecole doctorale:

Génie des procédés et Technologies Avancées

COLD PLASMA DEPOSITION OF ORGANOSILICON FILMS WITH DIFFERENT MONOMERS IN A DIELECTRIC-BARRIER DISCHARGE

Ph.D. Thesis

Sara Lovascio

UNIVERSITA' DEGLI STUDI DI BARI

Dipartimento di CHIMICA

DOTTORATO DI RICERCA IN SCIENZE CHIMICHE

CICLO XXI

Settore Scientifico Disciplinare CHIM03

COLD PLASMA DEPOSITION OF ORGANOSILICON FILMS WITH DIFFERENT MONOMERS IN A DIELECTRIC-BARRIER DISCHARGE

Coordinatore: Ch.mo Prof. Pietro Favia

Supervisore: Ch.mo Prof. Riccardo d'Agostino

Dottoranda: Sara Lovascio

THESE DE DOCTORAT DE
L'UNIVERSITE PIERRE ET MARIE CURIE

Spécialité: **Génie des procédés et technologies avancées**

Présentée par **Melle Sara Lovascio**

Pour obtenir le grade de **DOCTEUR de l'UNIVERSITÉ PIERRE ET MARIE CURIE**

Sujet de la thèse :
COLD PLASMA DEPOSITION OF ORGANOSILICON FILMS WITH DIFFERENT MONOMERS IN A DIELECTRIC-BARRIER DISCHARGE

soutenue le **30 Mars 2010**

devant le jury composé de:

M. Riccardo d'Agostino, *Professeur de l'Université de Bari*, **Directeur de thèse**
Mme. Farzaneh Arefi-Khonsari, *Professeur de l'UPMC,* **Directeur de thèse**

Mme. Emma Paola Maria Virginia Angelini, *Professeur de Politecnico di Torino*, **Rapporteur**
M. Khaled Hassouni, *Professeur de l'Université Paris 13*, **Rapporteur**

M.Gianluca Farinola, *Professeur de l'Université de Bari*, **Examinateur**
M.Michel Cassir, *Professeur de l'UPMC*, **Examinateur**

INDEX

ACKNOWLEDGEMENTS

This thesis was developed in the framework of a “co-tutele” between the University of Bari (Italy) and the University Pierre et Marie Curie (France). Different periods were spent at the Department of Chemistry of University of Bari, in the Istituto di Metodologie Inorganiche e Plasmi (IMIP)-CNR, and at the Ecole Nationale Superieure de Chimie Paris (ENSCP) in the Laboratoire de Génie des Procédés Plasma et Traitement de Surface (LGPPTS).

I would like to thank my two supervisors, prof. R. d’Agostino and prof. F. Arefi-Khonsari, and my co-supervisor prof. F. Fracassi, for their guidance in the development of this project. Dr. F. Fanelli is firstly acknowledged for her scientific support and assistance and, secondly, for the XPS and GC-MS analyses.

Finally I would like to express my sincerest gratitude to all ones, in both laboratories, contributed, in whatever way, to the realization of this work and supported me in the entire period of this Ph.D. thesis.

PREFACE

Nowadays textile materials cannot be restricted to clothes, linen, tablecloth and curtains, but they have to be regarded also as high-tech products that, in addition to the traditional clothing industry, find application in many technological fields, like construction, agriculture, automotive, aerospace, medicine. Due to the increasing growth of textile market, in the last decades there is a growing demand for improving the methods for the finishing of textile fabrics as well as of materials with new characteristics. Further the traditional wet techniques are not always environment friendly and at low energy consumption, so dry, environmentally safe, and energetically efficient processes are required as alternatives to the classical/old textile finishing methods. All these issues, along with the statement of fact that some properties are needed only on the textile surface, make non-thermal plasma technologies quite appealing for the textile industry. In particular non-thermal plasma produced at atmospheric pressure are challenging for the modification of the fabrics surface, as this technology is compatible with continuum, on-line processing.

Recently both surface activation and deposition of thin functional coating by means of atmospheric pressure plasma have been investigated in order to confer to textiles various properties, such as affinity for painting and dyeing, stain-resistance, antibacterial, no-shrinking and no-felting character. At this purpose different feeding gas mixtures have been used, from non-polymerizing ones (air, Ar, He, N_2, O_2), to hydrocarbon, fluorocarbon and organosilicon precursors. Thin organosilicon coatings, in particular, are quite challenging for various textiles finishing, as, due to their inorganic/organic character, they can exhibit different suitable properties, such as thermal stability, abrasion resistance, anti-reflective character, dielectric and hydrophilic/hydrophobic tuneable features.

This thesis, developed in “co-tutele” between the University of Bari (Italy) and the University Pierre et Marie Curie (France), reports a fundamental study on the deposition of thin organosilicon coating in a Dielectric Barrier Discharge (DBD) which is very interesting for application to the textiles finishing. Although this topic is receiving widespread attention in the scientific community, as stated by the recent literature, very few works investigate organosilicon precursors different from hexamethyldisiloxane (HMDSO) and get inside the occurring deposition mechanism in DBD. The first goal of

this work was the investigation of other precursors: in addition to the HMDSO, pentamethyldisiloxane (PMDSO) and tetramethyldisiloxane (TMDSO) were used as organosilicon monomers. Both gas phase and thin films produced in Ar/HMDSO/O_2, Ar/PMDSO/O_2 and Ar/TMDSO/O_2 DBD, with different oxidant content, were investigated with the aim of giving an overview of the three disiloxanes performances. At this purpose a GC-MS detection of by-products in the exhaust gases was carried out and correlated to the coating properties.

The first chapter of this thesis gives an overview of the available plasma processes for the textile treatment, with regard for the atmospheric pressure plasma processes and the employment of organosilicon coating in the textile finishing.

In the second chapter a description of Dielectric Barrier Discharges fundamentals is presented. The third chapter describes the state of the art of organosilicon thin films deposition in both low and atmospheric pressure; a particular attention is given to deposition mechanism investigations.

The experimental apparatus along with the adopted diagnostic techniques are presented in the fourth chapter. The fifth and sixth chapter are respectively devoted to the obtained coatings characterization and to the experimental results from the GC-MS investigations.

INTRODUCTION

A nos jour les matériaux textiles ne sont pas seulement utilisé dans le domaine de l'habillement et les linges de maison (draps, nappes, rideaux, etc.), mais il sont très utilisés comme produits d'une haute technicité employées dans divers domaines industriels, comme la construction, l'agriculture, la médecine, l'industrie aérospatiale et de l'automobile. En raison de la rapide expansion du marché des textiles, l'amélioration des méthodes de finission, ainsi que des matériaux avec des nouvelles propriétés ont été demandées dans les dernières décennies. Par ailleurs les techniques traditionnelles par voie humide sont souvent néfaste pour l'environnement et demandent une consommation d'énergie importante. Les procédés par voie sèche, sans danger pour l'environnement et économiques, constituent une solution alternative aux méthodes traditionnelles. De plus elles permettent de modifier l'extrême surface sans affecter les propriétés massiques des matériaux. Tout particulièrement les plasmas non-thermiques à la pression atmosphérique sont intéressants pour l'industrie textile, car cette technologie est compatible avec la chaîne de production continue.

Récemment l'activation de la surface, ainsi que le dépôt des couches minces fonctionnels par plasmas à la pression atmosphérique, ont été étudiées afin de conférer des nouvelles propriétés aux textiles, comme l'amélioration de l'adhésion vis à vis des peintures et de la teinture, les propriétés anti-tache, antibactérienne, anti-raccourcissement et anti-feutrage. Pour ce faire, une large gamme de précurseur non-polymérisable (air, Ar, He, N_2, O_2) et polymérisable (hydrocarbures, fluorocarbures, organosiloxanes), ont été utilisés. En particulier les couches minces obtenues à partir de composés d'organosiloxanes, grâce à leur large gamme de caractéristiques chimiques différentes selon leur caractère, organique ou inorganiques, peuvent conférer des propriétés très intéressantes et variées aux textiles, à savoir la résistance à la chaleur et à l'abrasion, l'isolation électriques, propriétés anti-reflet, ou hydrophobes/hydrophiles.

Cette thèse, développée en co-tutelle entre l'Université de Bari (Italie) et l'Université Pierre et Marie Curie (France), est consacrée à une étude fondamentale de la déposition des couches minces d'organosiloxanes, réalisées par des Décharges à la Barrière Diélectrique (DBD), un procédé très intéressant pour l'application aux textiles. Même si ce sujet est en train de recevoir beaucoup d'attention de la part de la communauté scientifique, la littérature la plus récente étant une preuve, en très peu

d’études des organosiloxanes différents de l’hexaméthyldisiloxane (HMDSO) ont été utilisés comme précurseurs. De plus, jusqu’à présent, les mécanismes du dépôt des couches minces d’organosiloxanes par DBD ont été peu abordés. Le premier but de cette étude a été, donc, d’examiner d’autres précurseurs: outre le HMDSO, tels que le pentaméthyldisiloxane (PMDSO) et le tetraméthyldisiloxane (TMDSO) ont été utilisés. La phase gazeuse, ainsi que les couches minces déposées en DBD alimentées par Ar/HMDSO/O_2, Ar/PMDSO/O_2 et Ar/TMDSO/O_2, avec différentes proportions de l’oxygène, ont été étudiés dans le but d’avoir une vue d’ensemble des performances des trois disiloxanes utilisés. Pour cette raison les sous-produits générés dans la phase plasma ont été recueillis à partir du gaz sortant du réacteur, et analysés par GC-MS; une corrélation entre les résultats GC-MS et les propriétés des couches minces obtenues a été établi.

Dans le premier chapitre de ce manuscrit nous présentons une introduction sur l’ensemble des procédés plasma disponibles pour le traitement des textiles, avec une attention particulière pour les procédés plasma à la pression atmosphérique et l’utilisation des couches minces d’organosiloxanes comme précurseur.

Le deuxième chapitre est consacré à la description des principes de base des Décharges à la Barrière Diélectrique (DBD). Ensuite nous présentons dans le chapitre 3 l’état de l’art sur les mécanismes du dépôt des couches minces d’organosiloxanes par procédés plasma à basse pression ainsi qu’ à la pression atmosphérique.

Le réacteur DBD et les techniques de diagnostiques utilisés sont présentés dans le quatrième chapitre. L’ensemble des résultats expérimentaux obtenus est présenté dans les chapitres 5 et 6: l’analyse phisico-chimiques des couches minces dans le chapitre 5, et les analyses des gaz sortant du réacteur par GC-MS dans le chapitre 6.

PREFAZIONE

Oggigiorno i materiali tessili non sono utilizzati solamente nel campo dell'abbigliamento e della biancheria per la casa (lenzuola, tovaglie, tende, etc.), ma sono considerati dei prodotti altamente tecnici adoperati in diversi settori industriali, come quelli edile, agricolo, dell'automobile, aeronautico e medico. A causa della forte espansione del mercato tessile, negli ultimi decenni c'è stata una crescente richiesta sia di metodi più efficaci per il finissaggio dei tessuti, sia di materiali con caratteristiche nuove. Inoltre le tecniche tradizionali per via umida non sono sempre eco-compatibili e a basso consumo di energia, perciò la ricerca è rivolta a metodi alternativi a quelli tradizionali, che cioè non utilizzino acqua e/o solventi e che non siano dannosi per l'ambiente. Per tutte queste ragioni, in aggiunta al fatto che spesso alcune proprietà sono necessarie solo sulla superficie di un tessuto, laddove i metodi tradizionali influiscono sull'intero materiale, i plasmi freddi risultano particolarmente interessanti per l'industria tessile. Ancor più interessanti sono i plasmi freddi prodotti a pressione atmosferica, data la loro compatibilità con i processi industriali in continuo.

Recentemente, al fine di conferire ai tessuti diverse proprietà, come l'affinità per la tintura e lo stampaggio, la resistenza alle macchie, il carattere antibatterico, antirestringimento o antinfeltrimento, sono state studiate sia l'attivazione della superficie, sia la deposizione di film sottili mediante plasmi a pressione atmosferica. A questo scopo sono stati usati diversi precursori, dai gas non-polimerizzanti (aria, Ar, He, N_2, O_2) agli idrocarburi, fluorocarburi, organosilani. I film sottili organosilanici, in particolare, sono molto indicati per vari finissaggii tessili, poiché, grazie al loro carattere inorganico/organico, possono mostrare diverse proprietà utili al tessile, come la stabilità termica, la resistenza alle abrasioni, il carattere anti-riflesso, isolante, idrofobo/idrofilo.

Questa tesi, sviluppata in co-tutela tra l'Università di Bari (Italia) e l'Université Pierre et Marie Curie (Francia), è uno studio fondamentale sulla deposizione di film sottili organosilanici in Scariche a Barriera di Dielettrico (DBD), molto interessante per l'applicazione ai tessuti. Sebbene questo argomento stia ricevendo molta attenzione dalla comunità scientifica, come provato dalla letteratura recente, pochissimi lavori si occupano di precursori diversi dall'esametildisilossano (HMDSO) e approfondiscono lo studio dei meccanismi di deposizione nelle DBDs. Il primo obiettivo di questo lavoro è

stata l’indagine di altri precursori organosilanici: oltre a l’HMDSO sono stati usati anche il pentametildisilossano (PMDSO) ed il tetrametildisilossano (TMDSO). Allo scopo di fornire una panoramica sulle prestazioni dei tre organosilossani, sono stati studiati sia la fase gas sia i film sottili prodotti in DBD alimentate da miscele gassose di $Ar/HMDSO/O_2$, $Ar/PMDSO/O_2$ ed $Ar/TMDSO/O_2$, con differenti concentrazioni di ossidante. A tal fine sono stati analizzati i gas esausti delle scariche mediante GC-MS e la loro composizione è stata correlata alle proprietà dei film depositati.

Nel primo capitolo di questa tesi sono brevemente descritti i processi plasmochimici usati per il trattamento di tessuti, in particolare i processi plasmochimici a pressione atmosferica e l’uso di organosilani per il finissaggio.

Nel secondo capitolo sono presentati i principi fondamentali delle Scariche a Barriera di Dielettrico. Nel terzo capitolo è mostrato lo stato dell’arte sulla deposizione di film sottili in plasmi a bassa pressione e pressione atmosferica; particolare attenzione è stata rivolta agli studi sui meccanismi di deposizione.

L’apparato sperimentale e le tecniche diagnostiche impiegate sono descritte nel capitolo 4. Nei capitoli 5 e 6 sono infine presentati i risultati sperimentali relativi, rispettivamente, alla caratterizzazione dei film sottili e alle analisi GC-MS degli esausti.

CHAPTER 1: INTRODUCTION

1.1 General aspects of textile manufacturing

The production of textiles, from fibres to their end products, has a history as long as the human civilization and in the centuries has kept up with it. Nowadays it constitutes a global industry not limited to the apparel marketing, but well linked to many industries, including construction, agriculture, automotive, aerospace, where the unique properties of natural and synthetic fibres, filaments and fabrics are exploited. Textiles for clothing are increasingly becoming high-tech products offering special functionalities, such as hydrophobicity, breathability, UV-stability, flame-protection, antibacterial properties. Anyway these technical textiles comprises not only garments for outdoor sports and safety clothing, but also geotextiles, textiles for architecture, for vehicles or aircrafts (i.e.: reinforcing components, seat belts, airbags), for packaging, filtration, medical and healthcare [1].

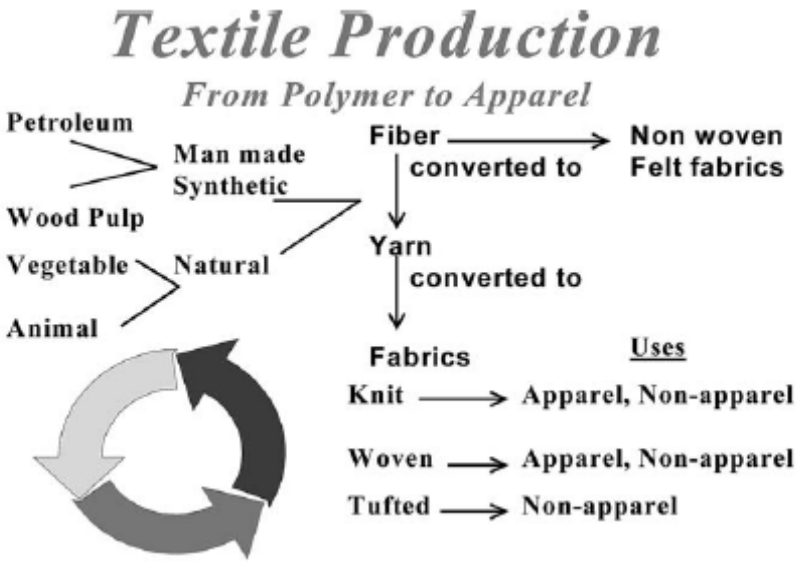

Figure 1.1.1: *Textile production chain [2].*

The great number of textile chain steps, as sketched in Figure 1.1.1, can be summarized in some main points: the fibres production from natural renewable (plant and animal kingdom) and from synthetic non-renewable sources (petroleum hydrocarbons), the fibres conversion into yarns that are finally employed in the fabrics weave (woven, knitted and tufted fabrics), or their conversion in non-woven fabrics [2].

The production line from the yarn manufacturing to value-added products moves through many wet processes, from the textile pre-treatments, such as desizing, scouring, cleaning, bleaching, to the fabric dyeing and chemical finishing (Figure 1.1.2). At this purpose large amounts of toxic wastewaters are produced [3]. On the other hand some properties (i.e.: the improvement of dyeing process, the stain resistance, antibacterial or antistatic properties etc.) are needed only on the textiles surface, whereas the traditional wet techniques may affect also the intrinsic bulk features, such as comfort, touch, porosity and air/water permeability. Moreover, after a wet chemistry finishing process the textile needs to be dried causing a rise in the productive energetic costs [4]. Therefore dry, environmentally safe, and energetically efficient processes are required as alternatives to classical/old textile finishing methods [5].

In response to this demand, plasma technologies represent eco-friendly, energy efficient and economic alternatives to classical textile finishing processes: they can contribute to make a selection of production based more on quality than on cost, thus reducing the urgency of the problems associated with the global challenge [6].

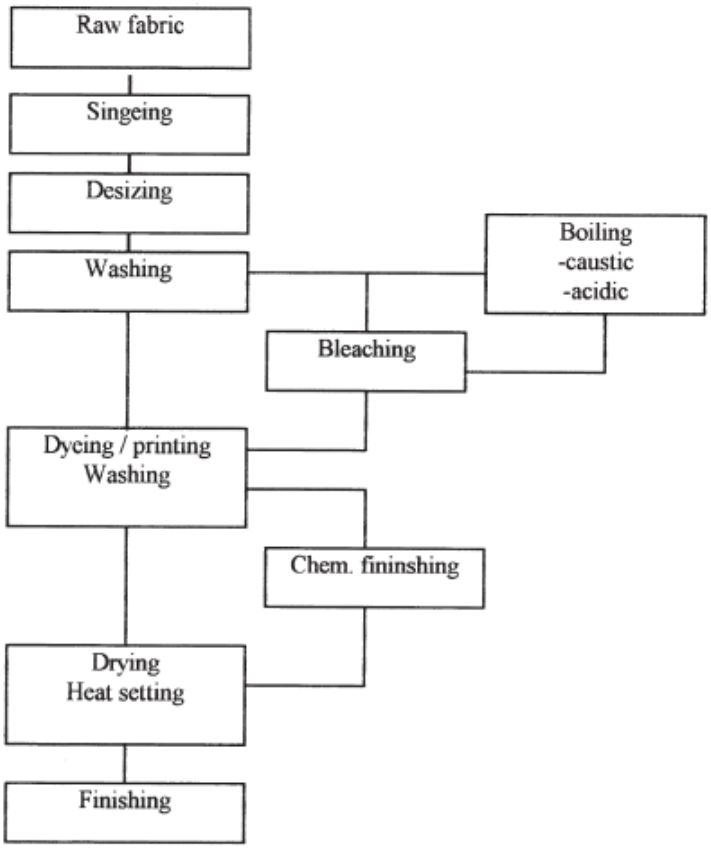

Figure 1.1.2: *Wet processing of woven fabric [3].*

1.2 Plasma technologies and textiles

A non-thermal plasma is a partially ionized gas containing high-energy electrons mixed with low-energy molecular species (ions, free radicals, meta-stable excited species, etc.) in a way that the overall system remains close to room temperature. Non-thermal plasma has been intensively studied and applied for the practical industrial requirements on high quality, high productivity, low cost and environmentally clean surface treatment processes, as it is able to tailor the surface properties without changing the physical and mechanical properties of the bulk materials. Surface

modifications may be accomplished through surface activation, ablation, etching, cross-linking, functionalization, film deposition or by some combination of these effects [6, 7].

Since the plasma gas remains at room temperature and textiles are not temperature resistant materials, cold plasma technologies are particularly suited to textile processing. An enormous variety of feeding gases can be used to perform a great number of surface chemistry: a large variety of chemically active functional groups can be incorporated onto the textile surface with the aim of cleaning or disinfecting, or improving wettability, printability, adhesion of coating, or inducing hydro- and/or oleophobic properties, or changing physical features. Further, a plasma treatment can be developed in a wide pressure range, and large reactor chambers and roller systems for large webs, are nowadays available with competitive costs [6].

The earliest plasma processes studies were carried out in low pressure gas systems, however, the integration of these processes, typically running at pressures between 0.1 and 1 mbar, into textile production line is often complex. As a matter of fact vacuum systems are not compatible with continuum, on-line processing and can be used only in batch mode or in semi-continuous *vacuum-vacuum-vacuum* roll-to-roll systems; additionally vacuum equipments are expensive, so there are high costs also for industrial scale-up. Finally, manufacturers are generally distrustful of vacuum system, mainly for ignorance problems. In the field of textile, in particular, processes are applied to wide areas (fabrics are meters wide and kilometres long) and, moreover, textiles have large specific surfaces: these facts make the desorption/adsorption of gases to become a real problem associated with vacuum systems [4].

Hence non-thermal plasma processes produced at atmospheric pressure are advantageous for the textile industry, as they can be introduced into the production line without major changes or system interruption and they are consistent with fabric large dimensions, high speed and continuous processing. In recent years a number of non-thermal processes, including Plasma Enhanced Chemical Vapour Deposition (PECVD), which were limited to low pressure apparatus, have been successfully transferred to the atmospheric pressure range, making atmospheric pressure plasma usable for substrate pre-treatment, cleaning, etching and plasma chemical coating from either gaseous or liquid precursors. Although the research in the field of low pressure plasma processes

for textiles have not been abandoned [8-12], the scientific world has developed a growing interest for the challenge of atmospheric pressure processes [6, 7].

1.3 Plasma treatments for textiles

As before mentioned plasma phase is made of various chemical species, i.e. electrons, ions, radicals, excited atoms/molecules, UV radiation: by tuning the feeding gas and the process parameters a great number of surface effects could be achieved. This fact well match the complexity of textile chain, as plasma processes could be adopted as any step of the production line, from pre-treatment to finishing.

The surface processes available to the textile industry can be classified as activation, etching/cleaning and coating, but a real distinction between the first two processes is hard to do as they are often contributory factors of the same treatment. Further the different targets in the field of textiles and fibres surface treatment have promoted the development and employment of various plasma apparatus, especially at atmospheric pressure (i.e corona treaters, DBDs system, Atmospheric Pressure Plasma Jet (APPJ)) [13-15].

Ambient air treatments carried out in corona discharges [15-21] on numerous kind of fibres have been widely investigated and compared to processes performed in controlled atmosphere DBDs [22-27] and APPJ [28-30]. The main effect of oxygen containing plasma is the introduction of polar groups, such as hydroxyl, carbonyl, carboxyl, ether, hydroperoxide, that enhance the hydrophilic properties of the treated textiles; anyway oxygen-free plasma create surface active sites that can easily react with ambient air or any other liquid or gaseous environment which the textile is exposed to. These processes often result in a surface energy enhancement aimed at the improving wettability and adhesion properties of the substrate [7, 13, 32].

Wettability is an important parameter for subsequent dyeing or printing of synthetic and natural textiles. Adhesion between fibres and a composite matrix play a fundamental role in composite materials [31-34] and it is involved also in the application of finishing coatings onto fabrics [35-40]. The chemical changes cannot be separated from the physical ones: several studies are focused on the occurring surface

micro-roughening that, if it does not turn into a surface damage, strongly improves wettability and adhesion properties of the treated fibres [41-44].

The textiles finishing can be obtained also by the deposition of thin conformal films: plasma promotes both the precursor fragmentation and the creation of surface reactive bonding sites, thus a solid phase material forms at the plasma-surface interface. The PECVD process delivers a dry coating, well-adhered to the substrate and conformal to each individual fibre accessed by the plasma [13]. In atmospheric pressure systems not only gases but also liquids, atomised into droplets and injected in the plasma phase, can be used as thin films precursors [45].

Several examples of PECVD onto fabric can be stated: acrylic acid was plasma polymerized onto polyester and polyamide fabrics to confer them a permanent hydrophilic character [46]; hydrocarbon (ethene, acethylene) and ammonia mixtures were used for the deposition of a-C:H:N coatings in order to introduce and preserve N-containing groups for a long period [47-48]; thin films from plasma fed with fluorocarbon gases were investigated to give water and stain repellence properties [45, 49-51]. Organosilicon compounds are also widely adopted as precursor for the coatings deposition onto fabrics: their suitability for the textile industry will be detailed in the next paragraph.

1.4 Role of silicones in textile finishing

Organosilicon compounds and their derivatives are often non-toxic and easy handling substances widely used in many technological fields. Due to their inorganic/organic character, thin organosilicon coatings can exhibit different properties, from thermal stability to abrasion resistance, anti-reflective character, dielectric and hydrophilic/hydrophobic tuneable properties, that make them suitable for various textiles finishing.

Organosilicon fed plasma result in a complex plasma-phase chemistry and in the tunability of films composition from the silicone-like character, when a great number of organic moieties (CH_x) is present in the film, to SiO_2-like inorganic coatings, normally if an oxidant is added to the feeding gas [52]. Silicone-like coatings can exhibit a Water Contact Angle (WCA) up to 110° on flat surfaces, but due to the microstructure of

textile fabrics, knitwear and non-woven, superhydrophobic effects can easily be obtained. Hydrophobic and stain-repellent textiles have a large market impact and are subject to strong demand from textile industry. Among the organosilicon precursor hexamethyldisiloxane (HMDSO) is widely used for the deposition of hydrophobic coatings onto fabric and fibres due to the retention of $-CH_3$ groups within a Si-O network [53-55].

Organosilicon thin films can confer also high washing permanence and abrasion resistance. HMDSO plasma-polymerized films were recently investigated as anti-pilling finishing for knitted wool fabrics [56]. In another work the barrier properties of HMDSO plasma coating were evaluated in order to control the moisture vapour transmission rate of wound dressings [57]. Other monomers were also investigated: anti-reflective coating layers were deposited onto PET fabrics by means of DBD fed with hexamethyldisilane and tris(trimethylsilyloxy)vinylsilane with the aim of increasing the PET colouring intensity [58].

Organosilicon compounds were also employed in the liquid state onto plasma activated surfaces. In order to obtain stable conductive textiles vinyltrimethoxysilane was grafted onto plasma activated polypropylene and viscose fabrics to ensure a surface covalent bonding of a pyrrole-functionalized silane: the silane back-bone provides a scouring and abrasion resistance to the polypyrrole outer-layer [59]. Hydrogen silicone fluid was grafted onto PET fabrics through corona discharge activation to improve the textile water repellency [60] or onto polyamide fabrics to create a gas-tight airbag [6].

The use of organosilicon substances for textiles treatment cannot be limited to plasma processes. Several studies report on the textiles modification by means of silicon alkoxides sol-gel coatings. The diluted alkoxides can be easily hydrolyzed leading to silanols groups that have a strong tendency to undergo condensation reactions; the basically formed inorganic network can be modified over a wide range by using other additives [1]. Examples could be the investigation of phosphorus doped SiO_2 thin films for giving flame retardancy properties to fabrics [61], the preparation of photoactive transparent thin SiO_2-TiO_2 films to confer self-cleaning properties to cotton fabrics [62], the sol-gel treatment with glycidylpropyloxytrimethoxysilane- and tetraethoxysilane-solutions to minimize the formaldehyde release in durable press finishing of cotton [63-64].

REFERENCES

[1] T. Textor, F. Schröter, E. Schollmeyer, *NanoS* 01.07, 14-17.

[2] S. B. Moore, L. W. Ausley, *Journal of Cleaner Production*, 12 (**2004**), 585-601.

[3] E. Kalliala, P. Talvenmaa, *Journal of Cleaner Production*, 8 (**2000**), 143-154.

[4] T. Stegmaier, A. Dinkelmann, V. von Arnim in, *Plasma Techology for textiles,* ed by R. Shishoo, The Textile Institute, WP, **2007**.

[5] E. Ozturk, U. Yetis, F. B. Dilek, G.N. Demirer, J*ournal of Cleaner Production*, 17 (**2009**), 239-247.

[6] R. Shishoo, *Plasma Techology for textiles,* ed by R. Shishoo, The Textile Institute, WP, **2007**.

[7] R. Morent, N. De Geyter, J. Verschuren, K. De Clerck, p. Kiekens, C. Leys, *Surface & Coating Technology* 202 (**2008**) 3427-3449.

[8] U. Vohrer, M. Müller, C. Oehr, *Surface and Coating Technology* 98 (**1998**) 1128-1131.

[9] G. Rosace, R. Canton, *Journal of Applied Polymer Science,* Vol. 107, 3702–3706 (**2008**).

[10] A. Vesel, M. Mozetic, S. Strnad, Z. Peršin, K. Stana-Kleinschek, N. Hauptman, *Vacuum* 84 (**2009**) 79–82.

[11] C. Kan, C. M. Yuen, *Plasma Processes and Polymers*, **2006**, 3, 627-635.

[12] K. Vaideki, S. Jayakumar, R. Rajendran, G. Thilagavathi, *Applied Surface Science* 254 (**2008**) 2472–2478.

[13] T. Herbert in "Plasma Technology for textiles", ed by R. Shishoo, The Textile Institute, WP, **2007**.

[14] Y. Akishev, M.Grushin, A. Napartovich, N.Trushkin, *Plasmas and Polymers*, Vol. 7, No. 3, **2002**, 261-289.

[15] E. Temmerman, Y. Akishev, N. Trushkin, C. Leys, J. Verschuren, *J. Phys. D: Appl. Phys.* 38 (**2005**) 505–509.

[16] V. A. Titov, E. V. Kuvaldina, S. A. Smirnov, A. N. Ivanov, V. V. Rybkin, *High Energy Chemistry*, Vol. 36, No. 2, **2002**, pp. 121–125.

[17] W. Xu, X. Liu, *European Polymer Journal* 39 (**2003**) 199–202.

[18] A. V. Ulesova, A. A. Grechko, S. F. Sadova, *Fibre Chemistry*, 40, 2, **2008**, 143-146.

[19] S. Nourbakhsha, M. E. Yazdanshenas, *Color. Technol*., 124, 43–47 (**2008**).

[20] X. Wang, G. Cao, W. Xu, *Journal of Applied Polymer Science*, 112, 1959–1966 (**2009**).

[21] P. Ma, X. Wang, W. Xu, G. Cao, *Journal of Applied Polymer Science*, 114, 2887–2892 (**2009**).

[22] G. Borcia, C.A. Anderson, N.M.D. Brown, *Surface & Coatings Technology* 201 (**2006**) 3074–3081.

[23] N. De Geyter, R. Morent, C. Leys, *Surface & Coatings Technology* 201 (**2006**) 2460-2466.

[24] Y. Shin, K. Son, D. I. Yoo, S. Hudson, M. McCord, S. Matthews, Y.-J. Whang, *Journal of Applied Polymer Science*, 100, 4306–4310 (**2006**).

[25] H. A. Karahan, E. Özdoğan, A. Demir, H. Ayhanb, N. Seventekin, *Color. Technol.*, 124, 106–110 (**2008**).

[26] C. Zhang, K. Fang, *Surface & Coatings Technology* 203 (**2009**) 2058–2063.

[27] N. Yaman, E. Özdoğan, N. Seventekin, H. Ayhan, *Applied Surface Science* 255 (**2009**) 6764–6770.

[28] Y. Ren, C. Wang , Y. Qiu, *Surface & Coatings Technology* 202 (**2008**) 2670–2676.

[29] C.X. Wang , H.L. Xu , Y. Liu, Y.P. Qiu, *Surface & Coatings Technology* 202 (**2008**) 2775–2782.

[30] H. Xu, S. Peng, C. Wang, L.Yao, J. Sun, F. Ji, Y. Qiu, *Journal of Applied Polymer Science*, 113, 3687–3692 (**2009**)

[31] C. Canal, F. Gaboriau, R. Molina, P. Erra, A. Ricard, *Plasma Processes and. Polymers*, **2007**, 4, 445–454.

[32] I. Holme, *International Journal of Adhesion & Adhesives* 19 (**1999**) 455-463.

[33] Y. Kusano, H. Mortensen, B. Stenum, P. Kingshott, T. L. Andersen, P. Brøndsted, J.B. Bilde-Sørensen, B.F. Sørensen, H. Bindslev, *Plasma Processes and. Polymers*, **2007**, 4, S455-S459.

[34] J. Janca, P. Stahel, J. Buchta, D. Subedi, F. Krcma, J. Pryckova, *Plasmas and Polymers*, Vol. 6, Nos. 1/2, June **2001**.

[35] M.J. Tsafack, J. Levalois-Grützmacher, *Surface & Coatings Technology* 200 (**2006**) 3503– 3510.

[36] M. Okubo, N. Saeki, T. Yamamoto, *Journal of Electrostatics* 66 (**2008**) 381–387.

[37] J.-D. Liao, C. Chen, Y.-T. Wu, C.-C. Weng, *Plasma Chemistry and Plasma Processing*, 25, 3, June **2005**.

[38] F. Hochart, R. De Jaeger, J. Levalois-Gru¨tzmacher, *Surface and Coatings Technology* 165 (**2003**) 201–210.

[39] D. Hegemann, *Advanced Engineering Materials*, **2005**, 7, 5, 401-404.

[40] W.-H. Yao, J.-C. Chen, C.-C. Chen, *Polym. Adv. Technol.* **2008**, 19, 1513–1521.

[41] R. Molina, J.P. Espinós, F. Yubero, P. Erra, A.R. González-Elipe, *Applied Surface Science* 252 (**2005**) 1417–1429.

[42] J. Yip, K. Chan, K. M. Sin, K. S. Lau, *Applied Surface Science* 253 (**2006**) 2493–2497.

[43] C. Kan, C. M. Yuen, *Journal of Applied Polymer Science*, 102, 5958–5964 (**2006**).

[44] K. K. Samanta, M. Jassal, A. K. Agrawal, *Surface & Coatings Technology* 203 (**2009**) 1336–1342.

[45] F. Leroux, C. Campagne, A. Perwuelz, L. Gengembre, *Applied Surface Science* 254 (**2008**) 3902–3908.

[46] A. Cireli, B. Kutlu, M. Mutlu, *Journal of Applied Polymer Science*, 104, 2318–2322 (**2007**).

[47] M. M. Hossain, A.S. Herrmann, D. Hegemann, *Plasma Process. Polym.* **2007**, 4, 135–144.

[48] M. M. Hossain, D. Hegemann, G. Fortunato, A. S. Herrmann, M. Heuberger, *Plasma Process. Polym.* **2007**, 4, 471–481.

[49] J. Zhang, P. France, A. Radomyselskiy, S. Datta, J. Zhao,W. van Ooij, *Journal of Applied Polymer Science*, 88, 1473–1481 (**2003**).

[50] M. G. McCord, Y. J. Hwang, Y. Qiu, L. K. Hughes, M. A. Bourham, *Journal of Applied Polymer Science*, 88, 2038–2047 (**2003**).

[51] D. Sun, G.K. Stylios, *Journal of Materials Processing Technology* 173 (**2006**) 172–177.

[52] A.M. Wróbel, M.R. Wertheimer in *Plasma deposition, treatment and etching of polymers*, R. d'Agostino ed., Academic Press, New York **1990**, p.163

[53] H. Höcker, *Pure Appl. Chem*., 74, 3, pp. 423–427, **2002**.

[54] D. Hegemann, D. Balazas, *NanoS* 01.07.

[55] Y. Y. Ji, H. K. Chang, Y. C. Hong, S. H. Lee, *Current Applied Physics*, **2009**, 9, 253-256.

[56] F. Rombaldoni, R. Mossotti, A. Montarsolo, M. B. Songia, R. Innocenti, G. Mazzuchetti, *Fibers and Polymers* **2008**, 9, 5, 566-573.

[57] X. J. Dai, J. S. Church, M.G. Huson, *Plasma Process. Polym*. **2009**, 6, 139–147.

[58] H.-R. Lee, D. Kim, K.-H. Lee, *Surface and Coatings Technology* 142-144 (**2001**) 468-473.

[59] M. Mičušík, T. Nedelčev, M. Omastová, I. Krupa, K. Olejníková, P. Fedorko, M. M. Chehimi, *Synthetic Metals* 157 (**2007**) 914–923.

[60] J. Lei, M. Shi, J. Zhang, *European Polymer Journal* 36 (**2000**) 1277-1281.

[61] A. Cireli, N. Onar, M. F. Ebeoglugil, I. Kayatekin, B. Kutlu, O. Culha, E. Celik, *Journal of Applied Polymer Science*, 105, 3747–3756 (**2007**).

[62] T. Yuranova, R. Mosteo, J. Bandara, D. Laubb, J. Kiwi, *Journal of Molecular Catalysis A: Chemical* 244 (**2006**) 160–167.

[63] C. Schramm, W.H. Binder, R. Tessadri, *Journal of Sol-Gel Science and Technology* 29, 155–165, **2004**.

[64] C. Schramm, B. Rinderer, W.H. Binder, R. Tessadri, H. Duelli, *Journal of Materials Science* 40 (**2005**) 1883 – 1891.

CHAPTER 2: ATMOSPHERIC PRESSURE PLASMA AND DIELECTRIC BARRIER DISCHARGES

2.1 Generalities about plasmas

Plasma is a partially ionized gas made of electrons, ions and neutrals in fundamental and excited states; although it is electrically conductive due to the presence of free charge carriers, from a macroscopic point of view plasma is electrically neutral. Excited species can undergo radiative relaxation processes emitting light in the visible-UV region, thus plasma is usually characterized by a glare: flames, lightnings, the aurora borealis, solar corona, interstellar space are some of the numerous examples of natural plasma. Anyway plasma can be artificially generated by giving energy to a gas by means of heat, radiation, electric or magnetic field: examples are the neon tube and the plasma display panels [1-3].

On the base of electron density and gas temperature, plasmas are generally classified in equilibrium and non-equilibrium plasmas. In equilibrium plasmas the high number of elastic collisions occurring between electrons and neutral species, that constitute the main part of the gas phase, promotes the enhancement of neutral kinetic energy. As a consequence the heavy particles in the plasma achieve the same electrons temperature ($\sim 10^4$ K), so this kind of plasma is also called thermal plasma. Due to their high temperature thermal plasmas are used for elemental spectroscopic analysis and for industrial processes like welding, cutting and waste destruction.

In non-equilibrium plasmas, instead, high energy electrons are involved in few elastic collisions, whereas they result quite effective in anelastic collisions, thus producing excited species, radicals and ions: electrons remain the more energetic species in the plasma (~ 10 eV), while heavy particles, if compared to the fast electrons, could be considered static, so their translational temperature remain close to the ambient one (~300 K). As heavy particles are the most abundant species in the plasma, they also determine the plasma temperature: for this reason non-equilibrium plasmas are also called cold plasmas. Non-equilibrium plasmas are widely used as surface modification technique, also for thermally unstable materials like polymers, paper, textiles, etc., and

have found application also in pollution control, volatile organic compounds removal, ozone generation and lamps [1, 3-4].

The working pressure play a fundamental role in determining the plasma temperature: at pressures lower than 10 Torr non-equilibrium plasmas are easily generated due to the large particles mean free path and, consequently, few electron-neutral elastic collisions; at higher pressures collisions become more frequents, therefore plasma temperature approaches the electrons one (Figure 2.1.1). Since the 70th cold plasmas generated in low pressure discharges (some hundred of mTorr), with regard to radio frequency (13.56 MHz) and microwave (2.54 GHz) plasmas, have been widely investigated. More recently new technical solutions allowed to obtain non-thermal plasmas at atmospheric pressure. In the last decade great attention has been paid to the atmospheric plasma technology as it can overcome some vacuum systems drawbacks that limit the plasma processes scale up, thus resulting very attractive for many industrial applications [5-8].

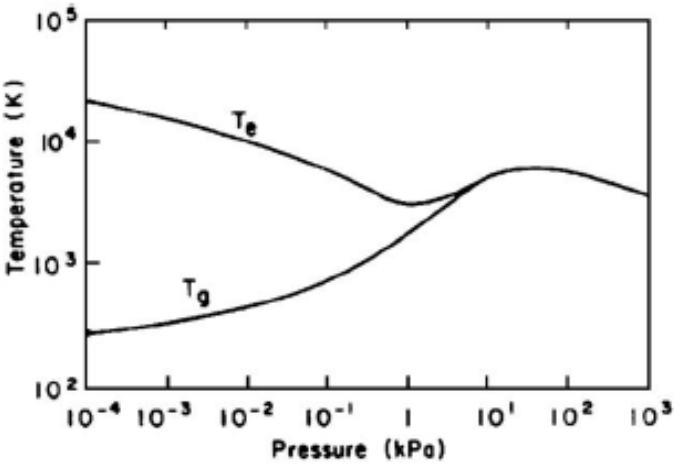

Figure 2.1.1: *Evolution of electrons and heavy particles temperature as a function of the pressure in a mercury plasma arc [7, 50].*

2.2 General aspects of atmospheric pressure plasmas

Non-thermal plasmas at atmospheric pressure can be generated by various type of electrical discharges. Their main feature is the production of high energy electrons promoting the formation of chemically active species, while the gas molecule remain cold. Different approaches can be used to maintain the neutral species at low temperature, that is limiting the input energy adsorbed in the discharge, providing an efficient cooling of the plasma stream or decreasing the residence time of the gas in the discharge gap [5-6, 8].

Many authors conveniently classify atmospheric pressure discharges on the base of applied excitation frequency and three main groups are defined: the direct current (DC) and low frequency alternating current discharges (1-100 kHz range), the radiofrequency discharges (100 kHz -100 MHz), the microwave (MW) discharges (>100 MHz) [5-7].

In the perspective of atmospheric pressure plasma sources developed for the surface treatment and the deposition of thin films (PECVD), probably due to the difficulty of designing a convenient equipment for wide areas coverage and sustaining MW discharges at low power avoiding high plasma temperatures [6], very few examples of MW sources working at atmospheric pressure can be found, mainly operating in a remote system configuration [9-10]. The Atmospheric Pressure Plasma Jet (APPJ), the cold plasma torch and the hollow cathode systems are the main type of RF plasma sources adopted for the AP-PECVD processes. Here plasma is generated in a narrow inter-electrode gap, normally with coaxial geometry, and it is blown outside that region by gas flow directly onto the substrate: the plasma treatment or deposition thus occurs in downstream mode [7, 11]. These systems have been investigated for the deposition of oxides onto small and large surfaces [6, 12-13].

The DC and low frequency discharges can work in continuous and pulsed mode. Pulsed DC power supplies are adopted for Corona Discharges, that are generated in highly asymmetric electrodes configuration, like sharply pointed needle or thin wire opposing flat planes or large diameter cylinder (Figure 2.2.1): when a high voltage is

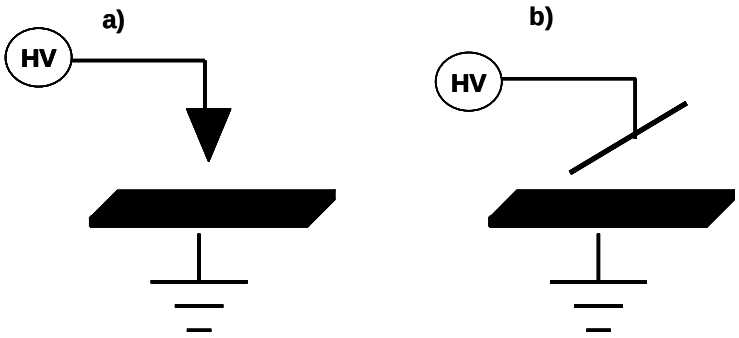

Figure 2.2.1: *Corona systems: a) point-to-plane geometry; b) wire-to-plane geometry.*

applied to the smaller electrode an intense electric field is generated around it, so plasma ignites in the form of streamers. Although this kind of discharges has been scaled–up for open-air surface modifications, the plasma volume is very small and streamers mainly generate in the same place, limiting its application to narrow areas and causing often non–homogeneous treatments [7, 11]. These drawbacks have been partially overcome by DBDs, characterized by the insertion of a dielectric layer in the discharge path; as a consequence, they operate at low frequencies alternating currents. DBD technology is quite appealing for industries as DBDs work at atmospheric pressure, at strongly non-equilibrium conditions, and at reasonably high power levels, with the use of simple design and relatively simple power supplies [7, 11, 14-16].

It is worth mentioning that some DBD systems are referred as Corona Treaters because plasma industry has developed equipments having the corona plasma type's asymmetric electrode configuration, typically a metal rod opposing a large diameter metal cylinder, together covered with the DBD's dielectric, generally ceramic (Figure 2.2.2): these systems run a hybrid corona/DBD plasma type adopted for large web treatment [11].

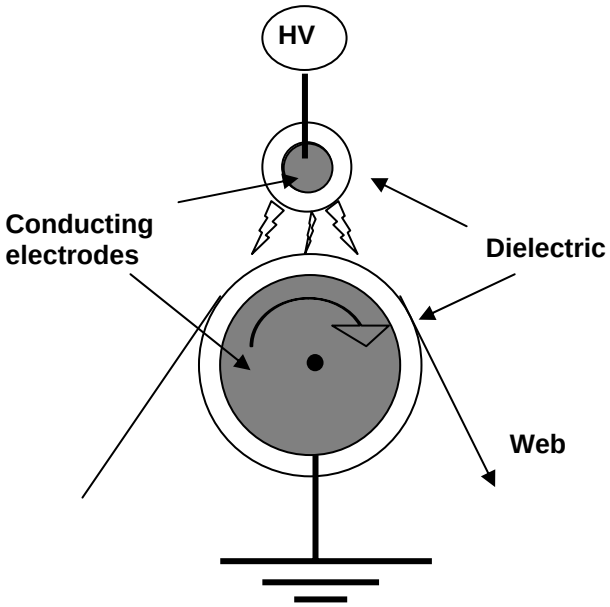

Figure 2.2.2: *Schematic of a corona treater (adapted from reference 11).*

2.3. Historical background of Dielectric Barrier Discharge

Although only in recent years scientific community has shown a growing interest for DBDs and their possible application in different technological fields, this kind of discharge has a long history [17]. Its birth is ascribed to Werner von Siemens who in 1857 developed a new discharge tube for the ozone production (Figure 2.3.1), whose novelty was that electrodes were positioned outside the discharge chamber and, thus, they were not in contact with the plasma: an oxygen or air flow was forced in an annular gap between two coaxial glass tubes, and an alternating voltage sufficiently high to promote the electrical gas breakdown was applied to two external coaxial electrodes [18]. As the electric current was forced to pass through the tube glass walls acting as dielectric barrier, nowadays this kind of discharge is commonly referred to as Dielectric Barrier Discharge, but in the first time it was called Silent Discharge due to the absence of sparks, usually accompanied by local shock waves and noise [19].

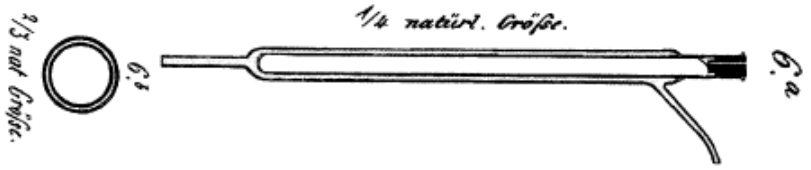

Figure 2.3.1: *Historic ozone discharge tube of W. Siemens [17-18].*

After the experimental investigation of Siemens for many decades interest for DBDs was mainly focused on their suitability for ozone production at industrial level [20-22]. At the beginning of 20th century various studies on the nature of the DBDs were carried out. Among them the work made by the electrical engineer K. Buss is worth of notice: in 1932 he found that when a planar parallel electrode system with dielectric layer on both electrodes is used at atmospheric pressure, the air breakdown occurs in a large number of tiny short lived current filaments; moreover he was able to take the first photographic traces, called Lichtenberg figures, of these microdischarges, and the current-voltage oscilloscope recordings [23]. Other authors [24-29] investigated the nature of these current filaments and in 1943 T. C. Manley proposed a method for the evaluation of dissipated power in the DBDs based on closed voltage/charge Lissajous figures and derived the power formula for ozonizers [30].

For many years, up to 80th, great efforts for the ozone production by DBDs were done, but around 1970 researchers started to adopt modern diagnostic and modelling tools for a better understanding of plasma physical and chemical processes in ozonizers: these efforts have resulted not only in an improvement of ozone production technology, but also in the extension of DBDs application fields. Nowadays, indeed, DBDs are widely used also in pollution control, in excitation of CO_2 lasers and excimer lamps, in flat plasma display panels, for surface treatments especially in the web conversion industry, and result quite appealing for the deposition of thin films in low-temperature atmospheric pressure plasmas [14-17, 31-35].

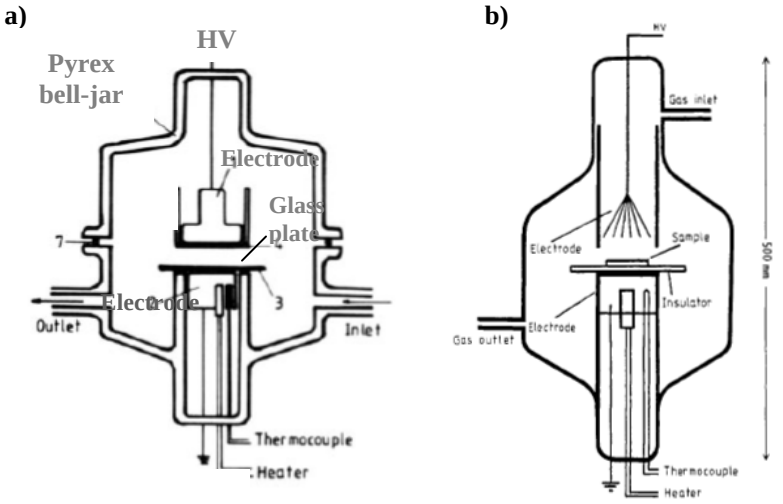

Figure 2.3.2: *Schematic of the reactors employed by Kogoma and co-workers [37-40]: a) plane-style upper electrode; b) brush-style upper-electrode.*

An important advance in the DBDs technology has been the achievement of homogeneous discharges also at atmospheric pressure. For a long time it was believed that uniform glow discharges could be produced only at low pressure, as the known discharges at atmospheric pressure were not homogeneous. The first evidence of a glow discharge at atmospheric pressure was recorded by von Engel in the 1933 [36], who used cooled metal electrodes in hydrogen gas. Anyway the research in the field of homogenous DBDs really started in the 1987 with the studies carried out by Kogoma and co-workers [37-40]. They developed an experimental set-up devoted to obtain a stable uniform discharge, that they named atmospheric-pressure glow (APG), avoiding in the same time the transition to an arc discharge. They stated that some requirements needed: a) the use of helium as main gas, also if later they obtained an APG with argon/acetone mixtures, too; b) the use of a high-frequency source, in the kilohertz or radio frequency range; c) an insulating plate on the lower electrode or on the bottom of the upper electrode depending on the reactor geometry adopted: the APG were, indeed, produced in a Pyrex bell jar containing a plate lower electrode, acting also as sample

holder, and, at the bottom, a brush-style electrode, made of sharp-pointed fine tungsten wires, for the treatment of dielectric materials, or another plate electrode for electrically conductive substances (Figure 2.3.2). By using fine wire mesh electrodes, a 50 Hz source and suitable dielectric plates, they obtained stable homogeneous glow discharges also in argon, nitrogen and air [40].

Other authors investigated the nature of homogeneous discharges produced at atmospheric pressure. F. Massines and co-workers gave a strong input in understanding homogeneous regimes by experimental and theoretical methods. They mainly studied helium and nitrogen discharges and they found that in He sub-normal discharges, very similar to normal glow discharges, are produced, while in N_2 a Townsend-like mechanism occurs [41-46].

Independently of these activities in 1995 J.R. Roth and co-workers developed a uniform glow discharge, named One Atmosphere Uniform Glow Discharge Plasma (OAUGDP), produced in atmospheric pressure air and other different gases [47-48].

Up to now several teams have focused their research activity on spectroscopic and electrical measurements as well as on the development of theoretical models aimed to a better understanding of the DBDs physic and chemistry, but great efforts are done also in the fields of numerous applications with the aim of the industrial scale up.

2.4 Fundamentals on DBDs

2.4.1 General description

By definition a Dielectric Barrier Discharge device is characterized by one or more dielectric layers located in the current path between two metal electrodes. Ceramics, glass, quartz, polymer layers or other material of low dielectric loss and high breakdown strength are used as dielectric barriers. Due to the presence of an insulating material capacitively coupled with the gas gap, DBDs require alternating voltages. Driving voltages from few hundred volts to several kilovolts with frequencies in the 50 Hz – 500 kHz range are normally used [8, 17]; some examples of DBDs generated at 13.56 MHz can also be found [49].

The dielectric role in the DBD set-up is to avoid the arc formation by limiting the average current density in the gas space. The amount of displacement current that can be passed through a dielectric depends on its dielectric constant, thickness and on the time derivative of the applied voltage, dV/dt. As a consequence of the presence of an insulator and the use of alternating voltage, DBDs are always pulsed discharges.

When electrical breakdown occurs in most gases a large amount of microdischarges, distributed in the discharge gap, appears: this discharge regime, that is also the most common DBD mode, is called filamentary regime. Under certain experimental conditions, depending on the gas mixtures, electrode configurations and operating parameters, homogeneous regimes, the so-called glow-discharges, can be obtained. Moreover apparently homogeneous, diffuse discharges and regularly spaced glow discharges patterns have been observed [8, 17, 50].

2.4.2 DBD apparatus

On the base of the application field different electrode configurations are available in literature, as shown in Figure 2.4.1 [8, 15-17]. The cylindrical geometry is widely used for CO_2 lasers, UV excimer lamps, for ozone and gas synthesis, and for depollution of gas streams. For the environmental control processes the packed-bed configuration is also extensively used: the interelectrode gap is filled with dielectric pellets, so a non-equilibrium plasma is generated in the voids between them [8]. Planar arrangements, with one or both electrodes covered by a dielectric, are mainly adopted for the surface treatment and the deposition of thin films. In cylindrical and planar geometries a volume discharge in the electrode gap is obtained, while in the coplanar and surface electrode geometry, mainly adopted in plasma display panels, discharge develops as a thin layer onto the dielectric surface, the so-named surface discharges [51].

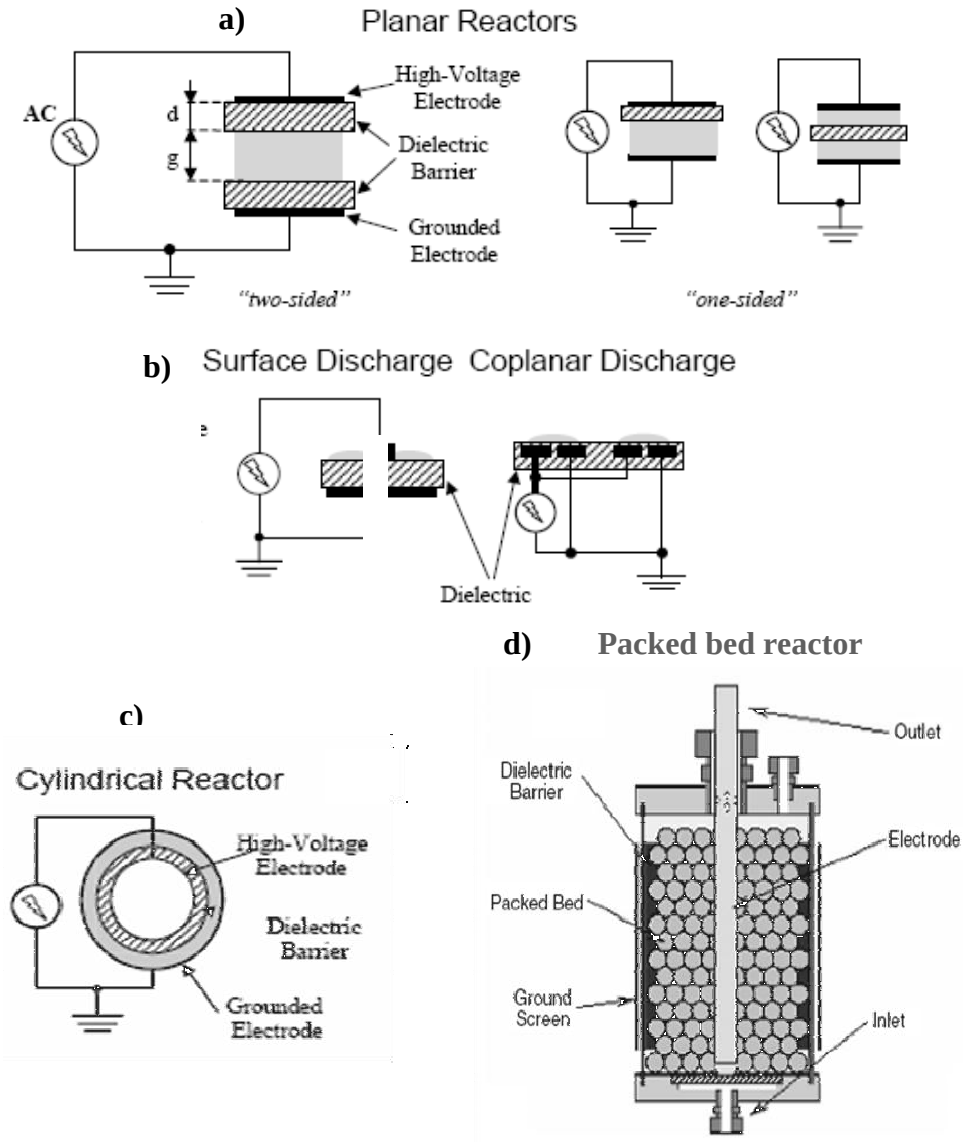

Figure 2.4.1: *Basic DBD electrode configurations [8, 16].*

The electrode gap, which typically varies from 0.1mm to several centimetres, is filled with gas at atmospheric pressure. The working gas can either flow through the gap as for surface treatment, pollution control and ozone production, or it can be recirculated as in CO_2 lasers, or it can be fully encapsulated as in excimer lamps and plasma display panels [17].

The electrode geometry and the related gas injection systems adopted for surface treatment and PECVD, and based on the planar arrangement, can be further detailed and are sketched in Figure 2.4.2 [52-53]. The basic geometry employed in deposition processes is a parallel plate configuration where identical electrodes are both covered by a dielectric layer; a lateral gas injection, where feeding gas is introduced in the discharge gap by means of an inlet slit and is pumped out in the opposite side, is normally adopted with this system (Figure 2.4.2a) [41-46, 54].

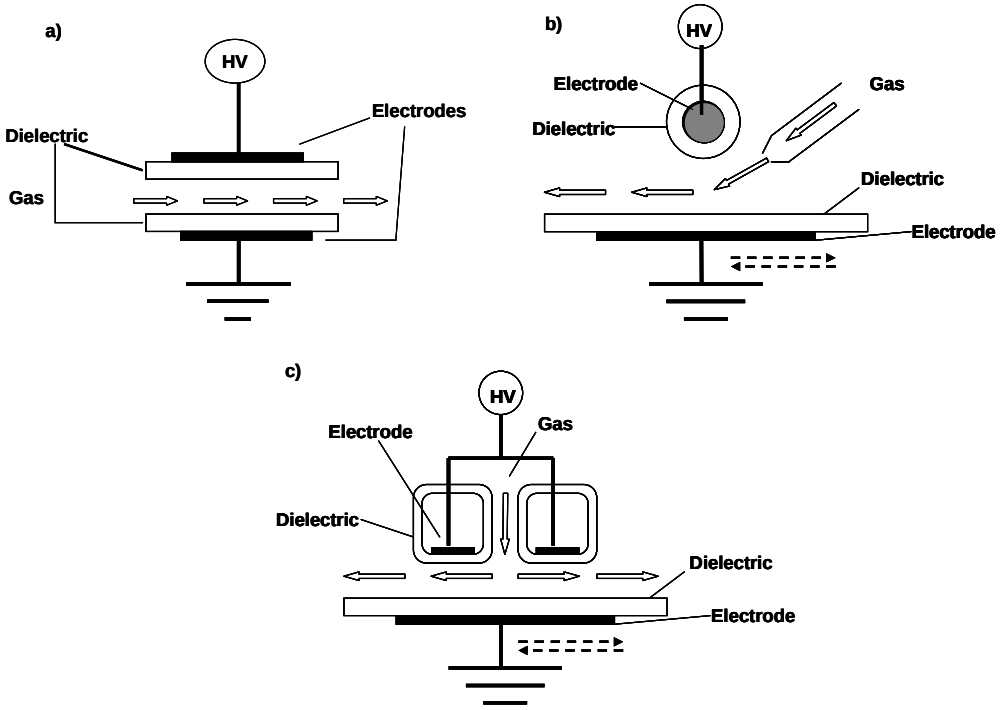

Figure 2.4.2: *Typical DBD electrode configuration adopted for PECVD.*

Other approaches adopt an asymmetric geometry and the movement of the larger electrode, generally the grounded one, in order to overcome some drawbacks of the lateral gas injection, such as the possible variation of coating thickness and chemical composition as a function of the gas residence time in the discharge area. In such systems the high voltage (HV) electrode can be a cylindrical metallic rod covered by a coaxial dielectric tube, so the gas is injected through a gas diffuser faced with the discharge region (Figure 2.4.2b) [55-56], or it can be made of two identical HV

electrodes symmetrically placed respect to the gas injection slit in a way that the gas is introduced from above (Figure 2.4.2c) [57-58]; the grounded electrode is usually a large plate, covered by a dielectric, that acts as sample holder and moves back and forward at controlled speed in order to ensure homogeneous thin films deposition over large areas. In the case of filamentary DBDs, in particular, the substrate movement is a technical solution to reduce the surface exposure to microdischarges that could cause a lack of homogeneity and surface damage. This same approach is used in roll-to-roll systems, like the before mentioned corona treaters (Figure 2.2.2), employed for the treatment of polymeric webs as continuous in-line processes [11, 16-17].

2.5 Dielectric Barrier Discharge regimes

Dielectric Barrier Discharges are usually classified in two main categories: the filamentary discharges (FDBDs) and the glow discharges (GDBDs). Different discharge regimes arise from different electrical breakdown mechanisms, that is the formation of a conductive gas channel caused by an applied electric field more intense than a critical value. In spite of differences among the breakdown mechanisms, all usually start with an electron avalanche, that is the multiplication of some primary electrons in a cascade ionization [8].

At the typical pressure-gas gap product (P x d) in an atmospheric pressure DBD the electron mean free path is very small in comparison with the gas gap, so an electron can generate a large size avalanche resulting in the streamer breakdown mechanism. A streamer is a thin ionized channel growing fast between electrodes; the condition of streamer formation, also called Meek's condition, is fulfilled when the space charge of a primary electron avalanche is large enough to create an electric field with a strength comparable to the applied electric field [59]. When a streamer breakdown occurs microdischarges are generated, thus the discharge works in the filamentary regime [8, 15-17, 50]

In particular experimental conditions, depending on the feeding gas and the working frequency and voltage, a Townsend breakdown can occur. This ignition mechanism typically takes place at low P x d values (less than 20 Torr x cm) and generates self-sustained discharge due to a feedback of electrons coming from the cathode secondary

electron emission: primary electrons, generated near the cathode and drifting to the anode, produce positive ions that, moving back towards the cathode, knock out secondary electrons; as soon as the electric field becomes high enough, the breakdown occurs and a self-sustaining discharge is initiated. This mechanism well explain the ignition of low-pressure glow discharges [59]; when a Townsend breakdown occurs at atmospheric pressure the discharge works in the glow regime [41-46].

2.5.1 Filamentary DBD

The filamentary regime is the most common DBD operational mode and it was the first to be observed in atmospheric pressure discharges. In filamentary DBDs the electrical breakdown starts almost simultaneously at many points of the surface and proceeds with the development of a large number of short-lived microdischarges, each one generated from a streamer breakdown. An initial electron, starting from some point in the discharge gap, produces secondary electrons by direct ionization and develops an electron avalanche and, if the Meek's condition is fulfilled, a streamer. The streamer bridges the gap in few nanoseconds and forms a conducting channel, typically of about 100 μm radius, of weakly ionized plasma; intense electron current flows through this channel, promoting ionization, until the local electric field collapses. As a matter of fact electrons deposit onto the anode dielectric barrier causing a charge accumulation and dissipate from the gap in about 40 ns, while heavy ions remain in the gap for some microseconds: the charges accumulated on the dielectric surface and the ionic space charge cause the collapse of the local electric field, thus the streamer extinction. A microdischarge is the group of local processes occurring in the discharge gap from the electron avalanche until the end of electron current [8, 15-17, 50]. Typical characteristics of DBDs microdischarges in air are summarized in Table 2.1.

Table 2.1: *Characteristic micro-discharge properties in a 1mm gap atmospheric-pressure air [8, 16, 50].*

Duration time	1-10 ns
Filament radius	about 0.1 mm
Peak current	0.1 A
Current Density	100-1000 A cm^{-2}
Total Charge	10^{-10}-10^{-9} C
Electron density	10^{14}-10^{15} cm^{-3}
Electron energy	1-10 eV

The charge accumulation onto the anode dielectric barrier prevents the formation of new streamers nearby until the voltage polarity reverses, but at the same time promotes new avalanches and streamers in the same spot when the voltage polarity reversal occurs. When the electron current stops, the excited species and ionic charges remain in the microdischarge channel volume and slowly move to the electrodes resulting in a low and long falling ion current; this ion current along with the charges deposited onto the surface, define a region in the discharge gap, called microdischarge remnant, that facilitate the formation of new microdischarges in the same spot as the voltage polarity reverses. The fact that the microdischarge remnant does not dissipate before a new microdischarge starts is called the memory effect and its main consequence is that in DBDs single filaments can be observed: a filament is, indeed, a group of microdischarges forming on the same spot at each polarity reversal [8].

The microdischarges properties does not depend on the external circuit, but only on the gas composition, pressure and electrode configuration; a power increase just leads to a larger number of microdischarges per unit time and per unit of electrode area. As in the remnant region external electric field is perturbed, at rising external voltage other microdischarges preferentially strike at other locations outside the area of influence of the previous microdischarge. This experimental evidence suggests that in DBDs dielectric has two roles: it limits the amount of energy injected in a single microdischarge and distributes the microdischarges over the entire electrode area [50].

Due to the short duration of the microdischarges and their small volume in comparison with the entire gas gap, plasma remains strongly non-thermal. The charge accumulation on the dielectric surface promotes the current termination just several nanoseconds after the breakdown, thus a very low overheating of the streamer channel occurs. Moreover the gas in between the microdischarges is not ionized and serves as background reservoir to absorb the energy dissipated in the microdischarges and to collect and transport the created long-lived species [15-17, 50].

Although microdischarges are randomly distributed in the space and in time, microdischarge patterns, due to the mutual influence of microdischarges in a DBD, have been also observed. The mechanism of influence arise from the net positive charge of the plasma channel and microdischarge remnant due to the faster motion of electrons respect to heavy ions: positive charges reduce the electric field in the anode area, thus preventing the formation of neighbouring microdischarges. A typical repulsion distance between microdischarges cause the observation of a short-range order in their distribution. When the average distance between microdischarges is larger than the characteristic interaction radius, or at AC frequencies too low or too high (megahertz), no significant microdischarges interaction is observed [8, 60].

2.5.2 Glow DBD

As previously stated in the recent years other discharge regimes, with no evidence of microdischarges, have been also observed and widely investigated. A this purpose the electrical characterization of the discharge, with regard to the current-voltage (i-V) recordings, are a powerful tool. When a filamentary discharge occurs multiple current pulses per half cycle are observed; Figure 2.5.1a shows the current and voltage waveform of a filamentary DBD. Diffuse and homogeneous discharges, instead, exhibit a current waveform with a single pulse per half cycle, but a distinction should be done between a homogeneous appearance and a really glow regime: in glow discharges the single pulse has also always the same intensity and periodicity as the applied voltage, as shown in Figure 2.5.1b; anyway a single pulse is not sufficient to prove the homogeneity of a discharge, as, if there is a very large number of streamers generated in way that they spatially overlap and the instrument cannot resolve very narrow current pulses, a wide single pulse can be showed [39-44, 50].

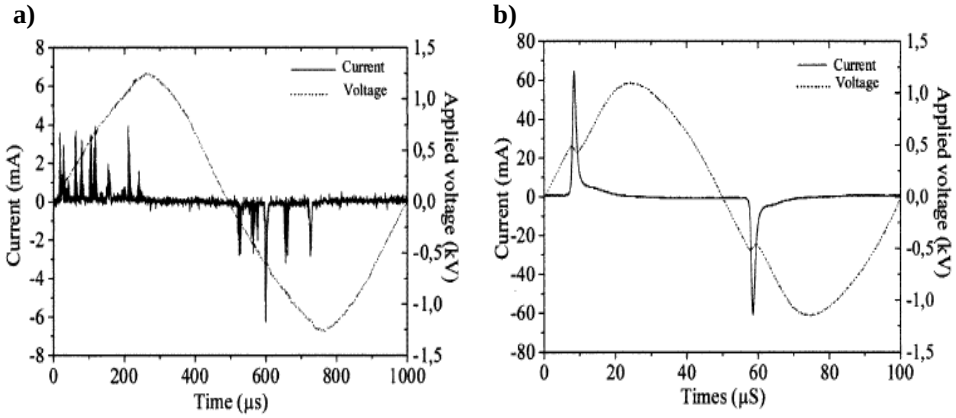

Figure 2.5.1: *Typical oscillograms of the sinusoidal voltage and pulsed current in a) a FDBD in He at1 kHz excitation frequency, b) a GDBD in He at 10 kHz excitation frequency [42].*

In addition to electrical measurements, short-exposure-time photographs is a second diagnostic method: photographs taken with exposure times in the order of streamers

lifetime (1-10ns) show a uniform region extending uniformly over the whole electrode surface in the case of glow discharges, while several localized discharges are visible for a filamentary discharge [41-45, 50]. Studies on pure gas GDBD carried out by Whertheimer and co-workers revealed that the homogeneous character of a discharge is proved by the total light emission signal from the gap and for a glow discharge a periodicity is recorded. Further in helium they observed a multi peak-regime, that they called pseudo-glow regime, as the discharge current is always periodical, but is formed by more than one current peak per half-cycle, each peak corresponding to a new discharge [61-62].

As reported in the paragraph 2.3 Kogoma and co-workers reported on the generation of an atmospheric pressure glow discharge (APGD) in helium and gave the necessary condition to obtain it, along with the evidence of the periodicity of the discharge current signal. Massines and co-workers confirmed these results and carried out several studies on the occurrence of glow discharges at atmospheric pressure in different atmospheres, with particular regard for helium and nitrogen. They proved that in helium and in noble gases subnormal glow discharges can be obtained, while in nitrogen Townsend discharges occur. Both these discharges at low pressure are generated by a Townsend breakdown, so Massines and co-workers stated that at atmospheric pressure only a Townsend breakdown can generate a glow discharges [42, 45].

Some conditions should verify to obtain a Townsend breakdown at atmospheric pressure: a high number of seed electrons, an ionization mechanism under low fields, a high value of the dielectric secondary emission coefficient. The condition to avoid streamers formation is the ability to produce electrons in small electric field in order to avoid a fast growth of electron avalanche. As an intense space-charge is not generated, ions have time to reach the cathode to promote the secondary electrons emission, so an increase of ion density is also necessary. Besides the electron-neutral collisions, metastables species play an important role in promoting ionization by Penning effect. It was found that in noble gases small amounts of impurities enhance the Penning effect thus promoting a glow discharge. On the other hand higher quantity of impurities can lead to the transition from a glow to a filamentary discharge [41].

An increase of the ionization and of the number of electrons emitted from the cathode is not sufficient to ensure a glow regime as also the number of electrons

remaining in the gas before the occurrence of a new discharge is quite important. As these electrons arrive at the insulator surface under low electric fields, they are slightly trapped: this is the so called memory effect. These electrons can be easier released in the next half period enhancing the value of secondary cathode emission and thus enhancing the probability of obtaining a glow discharge [41].

As before mentioned a Townsend breakdown generates a glow or a Townsend discharge: in glow discharges the memory from one discharge to the following one is based on electrons and ions trapped in a positive column formed during the discharge, and current densities of the order of mA/cm^2 are obtained; in a Townsend discharge gas metastables create electrons through cathode secondary emission and current densities are very low [45-46]. In comparison with value reported for micro-discharges (Table 2.1), in a diffuse discharge the number of electrons and their energy are in the 10^9-10^{11} cm^{-3} and 0.2-0.5 eV ranges, respectively [50].

REFERENCES

[1] B. Chapman, Glow discharge processes, J. Wiley & Sons ed., New York, **1980**.

[2] Plasma Deposition, treatment and etching of Polymers, R. d'Agostino ed., Academic Press, Boston **1990**.

[3] H. Conrads, M. Schmidt, Plasma Sources Sci. Technol. 9 (**2000**), 441-454.

[4] N. St. J. Braithwaite, Plasma Sources Sci. Technol. 9 (**2000**), 517-527.

[5] A. P. Napartovich, Plasmas and Polymers, Vol. 6, Nos. ½, **2001,** 1-14.

[6] S. E. Alexandrov, M. L. Hitchman, Chem. Vap. Deposition **2005**, 11, 457-468.

[7] C. Tendero, C. Tixier, P. Tristant, J. Desmaison, P. Leprince, Spectrochimica Acta Part B 61 (**2006**), 2-30.

[8] A. Fridman, A. Chirokov, A. Gustol, J. Phis. D: Appl. Phis. 38 (**2005**) R1-R24.

[9] M. Brown, P. Hayes, P. Prangnell, Composites, Part A, **2002**, A33, 1403.

[10] V. Hopfe, R. Spitzl, I. Dani, G. Maeder, L. Roch, D. Rogler, B. Leupolt, B. Schoeneich, Chem. Vap. Deposition **2005**, 11, 497-509.

[11] T. Herbert in "Plasma Technology for textiles", ed by R. Shishoo, The Textile Institute, WP, **2007**.

[12] H. Ha, B. K. Moon, T. Horiuchi, T. Hinushima, H. Ishiwara, H. Koinuma, Mat. Sci. Eng. **1996**, B41, 143.

[13] S. E. Babayan, J. Y. Jeongy, V. J. Tuy, J. Parks, G. S. Selwynz, R. F. Hicks, Plasma Sources Sci. Technol. **1998**, 7, 286.

[14] J. Salge, Surface and Coatings Technology 80 (**1996**) 1-7.

[15] U. Kogelschatz, , B. Eliasson, W. Egli, Pure Appl. Chem., Vol. 71, N° 10, 1819-1828, **1999**.

[16] H. –E. Wagner, R. Brandenburg, K. V. Kozlov, A. Sonnenfeld, P. Michel, J. F. Behnke, Vacuum 71 (**2003**) 417-436.

[17] U. Kogelschatz, Plasma Chemistry and Plasma Processing, Vol. 23, N° 1 (**2003**), 1-46.

[18] W. Siemens, Poggendorff's Ann. Phys. Chem. 102, 66 (**1857**).

[19] T. Andrews, P. G. Tait, Phil. Trans. Roy. Soc. (London) 150, 113 (**1860**).

[20] E. Warburg, G. Leithäuser, Ann. Physik (4) 13, 464 (**1904**).

[21] H. Becker, Wiss. Veröff. Siemens-Konzern 3, 243 (**1923**).

[22] M.–P. Otto, Bull. Soc. Franç. Electr. 9, 129 (**1929**).

[23] K. Buss, Arch. Elektrotech. 26, 261 (**1932**).

[24] A. Klemenc, H. Hinterberger, and H. Höfer, Z. Elektrochem. 43, 708 (**1937**).

[25] M. Suzuki, Proc. Jpn. Acad. 26, 20 (**1950**).

[26] M. Suzuki, Y. Naito, *Proc. Jpn. Acad*. 28, 469 (**1952**).

[27] K. Honda, Y. Naito, *J. Phys. Soc. Jpn.* 10, 1007 (**1955**).

[28] H. Gobrecht, O. Meinhardt, F. Hein, *Ber. Bunsenges. f. phys. Chem.* 68, 55 (**1964**).

[29] M. A. Bagirov, M. A. Kurbanov, A. V. Shkilev, and N. E. Nuraliev, *Sov. Phys.-Tech. Phys.* 16, 1011 (**1971**).

[30] T. C. Manley, *Trans. Electrochem. Soc.* 84, 83 (**1943**).

[31] U. Kogelschatz, in *Proc. 16th Int. Conf. on Phenomena in Ionized Gases (XVI ICPIG)*, Düsseldorf (**1983**), Invited Papers, pp. 240–250.

[32] B. Eliasson and U. Kogelschatz, *IEEE Trans. Plasma Sci*. 19, 309 (**1991**).

[33] B. Eliasson and U. Kogelschatz, *IEEE Trans. Plasma Sci*. 19, 1063 (**1991**).

[34] B. Eliasson, W. Egli, and U. Kogelschatz, *Pure Appl. Chem.* 66, 1275 (**1994**).

[35] U. Kogelschatz, B. Eliasson, and W. Egli, *J. Phys. IV (France)* 7, C4–47 (**1997**).

[36] A. von Engel, R. Seeliger, M. Steenbeck, *Z. Phys.* **1933**, 85, 144.

[37] S. Kanazawa, M. Kogoma, T. Moriwaki, S. Okazaki, *J. Phis. D: Appl. Phis.* 21 (**1988**) 838-840.

[38] T. Yokoyama, M. Kogoma, S. Kanazawa, T. Moriwaki, S. Okazaki, *J. Phis. D: Appl. Phis.* 23 (**1990**) 374-377.

[39] T. Yokoyama, M. Kogoma, T. Moriwaki, S. Okazaki, *J. Phis. D: Appl. Phis.* 23 (**1990**) 1125-1128.

[40] S. Okazaki, M. Kogoma, M. Ueharat, Y. Kimura, *J. Phis. D: Appl. Phis.* 26 (**1993**) 889-892.

[41] F. Massines, A. Rabehi, P. Decomps, R. Ben Gadri, P. Ségur, C. Mayoux, *Journal of Applied Physic*, Vol. 83, N° 6, 2950-2957 (**1998**).

[42] F. Massines, G. Gouda, *J. Phys. D: Appl. Phys.* 31 (**1998**) 3411–3420.

[43] F. Massines, R. Massaoudi, C. Mayoux, *Plasmas and Polymers*, Vol. 3, No. 1, **1998**, 43-59.

[44] N. Gherardi, G. Gouda, E. Gat, A. Ricard, F. Massines, *Plasma Sources Sci. Technol.* 9 (**2000**) 340-346.

[45] F. Massines, P. Ségur, N. Gherardi, C. Khamphan, A. Ricard, *Surface and Coating Technology* 174-175 (**2003**) 8-14.

[46] F. Massines, N. Gherardi, N. Naudé, P. Ségur, *Plasma Phys. Control. Fusion* 47 (**2005**) B577-B588.

[47] J.R. Roth, P.P.-Y. Tsai, C. Liu, M. Laroussi, P.D. Spence, U.S. Patent N° 5,414,324, **1995**.

[48] J. R. Roth, J. Rahel, X. Dai, D. M. Sherman, *J. Phys. D: Appl. Phys.* 38 (**2005**) 555–567.

[49] T. Terajima, H. Koinuma, *Appl. Surf. Sci*. **2004**, 223, 259.

[50] U. Kogelschatz, Y. S. Akishev, K. H. Becker, E.E. Kunhardt, M. Kogoma, S. Kuo, M. Laroussi, A. P. Napartovich, S. Okazaki, K.H. Schoenbach in " Non- equilibrium air plasma at atmospheric pressure", K.H.Becker, U. Kogelschatz, K.H. Shoenbach ed., **2005**.

[51] V.I. Gibalov, G.J. Pietsch, *J. Phys. D: Appl. Phys.* 33, (**2000**) 2618.

[52] S. Meiners, J.G.H. Salge, E. Prinz, F. Förster, *Surface and Coatings Technology* 98 (**1998**) 1121–1127.

[53] F. Fanelli, R. d'Agostino, F. Fracassi in *Advanced Plasma Technology*, R. d'Agostino, P. Favia, Y.Kawai, I. Ikegami, N. Sato, F. Arefi-Khonsari ed., WILEY-VCH, **2008**.

[54] F. Fanelli, F. Fracassi, R. d'Agostino, *Plasma Process. Polym*. **2005**, 2, 688–694.

[55] K. Pochner, S. Beil, H. Horn, M. Blömer, Surface and Coatings Technology 97 (**1997**) 372–377.

[56] X. Zhu, F. Arefi-Khonsari, C. Petit-Etienne, M. Tatoulian, *Plasma Process. Polym.* **2005**, 2, 407.

[57] M. Heise, W. Neff, O. Franken, P. Muranyi, J. Wunderlich, *Plasmas and Polymers*, Vol. 9, No. 1, **2004**.

[58] J. Borris, M. Thomas, C.-P. Klages, F. Faupel, V. Zaporojtchenko, *Plasma Process. Polym.* **2007**, 4, S482–S486.

[59] Y. Raizer , *Gas Discharge Physics* (Berlin: Springer) **1991**.

[60] A. Chirokov, A Gutsol, A. Fridman, K.D. Sieber, J. M. Grace, K.S. Robinson, *Plasma Sources Sci. Technol.* 13 (**2004**) 623–635.

[61] I. Radu, R. Bartnikas, M.R. Wertheimer, *J. Phys. D: Appl. Phys.* 38 (**2005**) 539–546.

[62] A. Sublet, C. Ding, J-L Dorier, Ch Hollenstein, P. Fayet, F. Coursimault, *Plasma Sources Sci. Technol*. 15 (**2006**) 627–634.

CHAPTER 3: STATE OF THE ART

3.1 General introduction on organosilicon thin films

In the chapter 1 organosilicon thin films have been introduced with relation to the textile finishing, anyway this subject has been so far widely investigated due to the suitability of these coatings for many application field. Since the 70's the scientific community has devoted great attention to the PECVD of organosilicon thin films mainly due to the development of micro-electronic technologies: silicon is the cheapest semiconductor material and its oxide, SiO_2, is chemically stable and has excellent insulating properties, thus the VLSI (very-large-scale integrated circuit) technology bases on the silicon chemistry and, on the other hand, plasma processes constitutes a great part of all VLSI fabrication steps [1].

Nowadays plasma polymerized organosilicon thin films continue to be employed in the micro-electronic technology as electrical insulators and passivation layers against harmful external agents (moistures, alkali metal ions); further, in the last decade, the demand for new dielectric materials with low dielectric constant (low-k materials) have enhanced the investigation of plasma deposition from a large number of organosilicon precursors [2-8].

Several properties of organosilicon coatings, such as optical clarity, low absorption and low scattering losses, the possible tailoring of refractive index, hardness and abrasion resistance, make them suitable for optical application: plasma polymerized organosilicon coatings have been used for integrated optics and as scratch-resistant and antireflective coatings onto polycarbonate and polymethylmetacrylate, commercial plastics widely used for eyeglass lenses, automotive and aerospace windows [9-13]. Organosilicon thin films have shown also good corrosion protection for aluminium and other metals, along with barrier effect to the oxygen and water vapours: investigation on the organosilicon thin films production for the food and pharmaceutical packaging [14-16] and corrosion resistance [17-19] areas have been widely developed in the last two decades. Moreover organosilicon coatings have resulted useful in the preparation of permselective membranes for both gases and liquids separation [20-21] and attractive also for biomedical application [22].

Different classes of Si-based PECVD materials can be outlined: amorphous hydrogenated silicon films (a-Si:H), amorphous silicon carbide films (a-SiC:H), and organosilicon coatings with general formula $SiO_xN_yC_zH_w$. The hazardous silane (SiH_4), adopted in the beginning as silicon precursor and mixed with other gases (i.e. hydrocarbon for the a-SiC:H coatings or nitrous oxide (N_2O) and ammonia (NH_3) for silica-like thin films), is nowadays fully replaced by silicon-containing organic precursors. Organosilicones are relatively non-toxic substances, of low flammability, relatively cheap and available from commercial sources; also if the main part of them is liquid at the ambient temperature, a high number of compounds has a vapour pressure sufficiently high to make them suitable for both low and atmospheric pressure plasma processes. Further the available safety handling and relatively volatile organosilicon precursors are often complex molecules containing at least one silicon atoms and more than ten atoms between hydrogen, carbon, oxygen and/or nitrogen. Different chemistries, from the silicone-like type to SiO_2-like inorganic one, exhibit different properties, thus turning out in the so far enounced wide range of technological applications and the correlated available literature [1].

3.2 Low-Pressure PECVD

A great amount of studies on the deposition of thin films in low pressure organosilicon fed plasmas has been carried out in the last three decades. Plasma fed by linear and cyclic organosilicon compounds, with saturated and unsaturated groups, have been generated in reactors with different geometries, operating in the radiofrequencies (RF) or microwave (MW) range; all these monomers have been often used in mixtures with rare gas (Ar, He, N_2), and eventually oxidants (O_2, N_2O). Very often tetraethoxysilane (TEOS) and the hexamethyldisiloxane (HMDSO) have been used, but also tetramethyldisiloxane (TMDSO) and hexamethyldisilazane (HMDSN), respectively containing Si-H and Si-N bonds, have been investigated [1, 23].

Independently of the particular experimental conditions and the investigated monomer, a general trend can be found. Plasma parameters, such as the discharge power, the substrate temperature, the substrate bias voltage, the feeding gas composition, the gases flow rate and the partial and total pressure in the reactor,

strongly influence the structure and the composition of plasma-polymerized organosilicon thin films [1]. The overall organosilicon thin films deposition mechanism in PECVD, sketched in (Figure 3.2.1), was outlined by d'Agostino and co-workers by means of the Activated Growth Model [24], successfully used for the explanation of fluoropolymers plasma polymerization. The model consists of several steps: the monomer fragmentation in organic and inorganic film precursors which can be involved in adsorption/desorption equilibrium onto the surface; the precursors polymerization at the active sites created by ions impinging the surface; the substrate temperature and the ions energy effects onto the adsorption/desorption equilibrium are also taken into account.

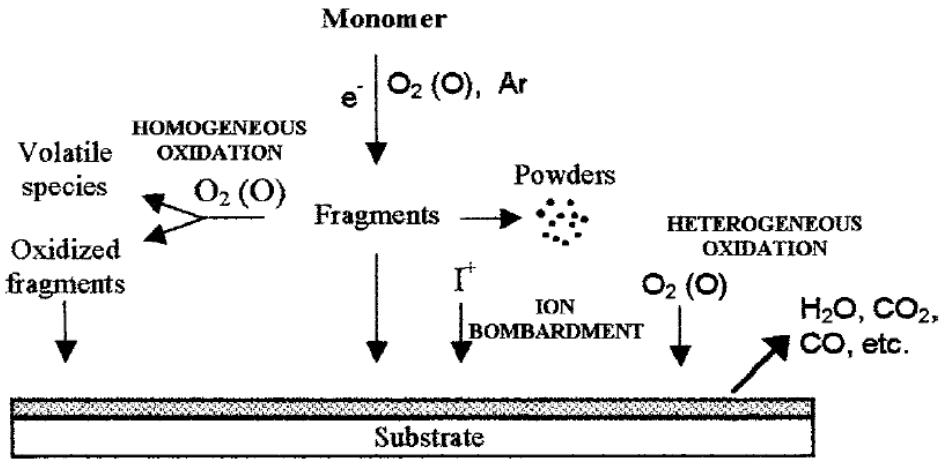

Figure 3.2.1: *General deposition mechanism in low pressure organosilicon fed plasma [47].*

The same authors, investigating the organosilicon deposition process by means of Actinometric Optical Emission Spectroscopy (AOES), found that substrate bias and temperature do not alter the plasma phase composition, but strongly influence the growing film, as they control the surface adsorption/desorption processes and the polymerization/etching competition. At high substrate temperature the growing film is affected by a continuous pyrolysis of the organic component and by the surface mobility of the precursor species, while a high bias voltage enhances the ionic bombardment:

increasing substrate temperature and ionic bombardment lead to more inorganic and crosslinked film due to the removal of carbon and hydrogen containing groups [24]. Similar effects are produced by high powers, which promote precursor activation and fragmentation.

Deposition rate is influenced by all these parameters: the film growth rate is reduced by the temperature increase, due to the dropping sticking coefficient of film precursors; low energy ions can enhance the film growth rate by creating active sites, while high energy ions depress precursor adsorption and can also promote an ion assisted etching; deposition rate can be enhanced by the increasing powers due to the greater monomer initiation. The precursor flow rate and the working pressure also contribute to determine the level of monomer fragmentation and the final deposition rate as they affect the species mean free path and their residence time in the reaction chamber [1].

The main effect of the monomer fragmentation is that the resulting coating often contains not only the functional groups of the starting monomer (i.e. -Si-alkyl (alkylsilane), -O(N)-Si-alkyl (alkylsiloxanes, alkylsilazanes), -Si-O-alkyl (alkoxysilane), -Si-H), but also new chemical bonds, thus the deposited coating stoichiometry always differs from that of the starting monomer. These effects are also more pronounced when an oxidant, commonly O_2, is added to the feeding gas: at increasing oxidant content the organic component of the starting monomer is drastically removed, thus the O/Si ratio approaches the silicon oxide (SiO_2) value and sometimes overcome it due to formation of Si-OH functionalities.

The O_2 addition to the organosilicon feed results in the modification of the plasma chemistry and the film precursors distribution. Oxygen molecules and atoms can react with both monomer and its fragments, thus increasing the monomer fragmentation on the one hand, and promoting oxidation processes on the other hand: the competition between the monomer activation and the organic fraction removal cause the deposition rate trends to decrease or to reach a maximum at increasing oxygen contents [12, 25-27]. Another point under debate is the main occurrence of oxidation reactions in the plasma phase or at the growing film surface: neither path can be excluded as their predominance depends on the particular experimental conditions, but heterogeneous film oxidation reactions seem to be more effective at high feed O_2 content [24].

3.3 Investigation of deposition mechanism in HMDSO low pressure plasma

Two main aspects of the plasma deposition from organosilicon precursors have been taken into account: the thin films composition and the plasma polymerization mechanism. In order to derive a general deposition mechanism and, secondly, to define the external parameters effect on the process, surface analysis has been well related to the plasma phase investigations.

HMDSO, one of the organosilicon precursor investigated in this work and widely used for the deposition of silicone- and silica-like thin films in low pressure plasmas, due to its non-toxic character, non-explosive behaviour and relatively high vapour pressure at room temperature, is without doubt also the more investigated monomer from the deposition mechanism point of view. Many diagnostic techniques, such as Fourier Transform Infrared Spectroscopy (FTIR-AS), Optical Emission Spectroscopy (OES), Mass Spectrometry (MS), have been employed in investigating HMDSO reactivity in low pressure plasmas.

Actinometric Optical Emission Spectroscopy (AOES) and Fourier Transform Infrared Absorbtion Spectroscopy (FTIR-AS) analysis of HMDSO/O_2 mixtures fed RF discharges were widely carried out in the d'Agostino research group [28-31]. It was found that in pure HMDSO plasma low monomer fragmentation occurs due to the absence of oxygen atoms and the consequently lower electron density in the plasma phase: as a consequence the film deposition is supposed to proceed through a condensation mechanism of HMDSO-like heavy fragments on the substrate [27-28]. On the contrary, high power and high O_2-to-HMDSO ratio in the feed promote high monomer fragmentation and the production of non volatile SiO radicals, considered the main silica-like film precursor, by means of homogeneous gas phase reactions [28]. For the purpose of obtaining inorganic SiO_2-like coatings with good gas barrier performance for the food packaging application, the same authors derived *in situ* process monitoring tools based on the evidence that the carbon and silanol content in the film are directly correlated respectively to the actinometric density of gas phase C atoms and CH radicals and to the plasma phase SiOH content, evaluated by FTIR-AS [28-31]. Similar results were obtained also by other authors [27, 32-33], who all agree that oxygen atoms play a role in the kinetic of monomer dissociation.

P. Raynaud and co-workers [34] adopted the FTIR-AS technique to investigate the by-products forming in HMDSO discharges generated in a microwave multipolar reactor. They found that under low power conditions the process is dominated by species produced during the primary HMDSO dissociation stage, as the gas phase contains mainly pentamethyldisiloxane (PMDSO), trimethylsilane (TriMS) and hydrocarbons; they also supposed the $(CH_3)_xSiO$ unit to be the main deposit precursor. On the other hand at higher powers longer siloxane chains were detected in the gas phase and the contribution of radicals resulting from the HMDSO by-products dissociation to the growing film was also taken into account.

Further insights into the HMDSO dissociation path in low pressure plasma were given by plasma phase MS investigations, often along with spectroscopic analysis techniques. Many authors state that, as the most intense peak in HMDSO mass spectra obtained with electron impact is the m/z 147 amu ion, the main HMDSO fragmentation route occurs via a methyl unit loss. M. R. Alexander and co-workers [35-36], comparing the mass spectra of neutral and positively charged species produced in the RF HMDSO plasma phase, proposed the formation of a $(CH_3)_3$-Si-O-Si^+-$(CH_3)_2$ ion and the production of oligomeric cations in the plasma phase via a linear chain growth due to cation-molecule interactions. D. Magni and co-workers [37] identified the CH_3 and the $OSi(CH_3)_3$ as the most abundant radicals formed in the HMDSO dissociation and suggested their involvement in homogeneous combustion reactions in O_2 rich atmospheres. Similar results were obtained by D.S. Wavhal and co-workers [38] who confirmed the occurrence of oxidation reactions both in the plasma phase and at the film surface, while K. Li and co-workers [39], describing the external parameters role in the HMDSO fragmentation extent, observed a complete HMDSO fragmentation, up to molecular hydrogen and light weight hydrocarbons, at high power inputs and oxygen concentrations.

M. Creatore and co-workers [40-41] studied the HMDSO dissociation path in remote Ar-fed expanding thermal plasma and found that cations formed in the primary dissociation reactions undergo dissociatively recombination reactions with low temperature electrons, thus promoting the Si-O dissociation with further methyl abstraction; they also supposed the $Si(CH_3)_2$ radical and the $OSi{=}CH_2$ molecule to be the most probable deposition precursors. D. Theirich and co-workers [42], on the other

hand, proposed three molecules having a mass of 148 amu and containing the silanon (Si=O) or the silanol (Si-OH) or the aldehyde (C=O) units, as reactive intermediate for SiO_x growth in HMDSO/O_2 plasmas.

3.3.1 GC-MS investigation of HMDSO fed low pressure plasma

Another diagnostic tool, useful to increase the knowledge on the deposition mechanism, is the analysis of exhaust gases by means of gas chromatography with mass spectrometry detection (GC-MS). Although an indirect analytical technique, not compatible with on-line and continuous sampling, GC-MS is a powerful tool which allows the evaluation of the precursor reactivity, the identification and eventually the quantification of the most abundant stable by-products generated by plasma activation. Besides the pioneering work of Wróbel and co-workers [1, 43-45], who widely used this technique for studying thin film deposition in low pressure remote plasma fed with siloxanes and silanes, few authors have reported on this technique. Among them Sarmadi et al. [46] and Fracassi et al. [47] investigated the exhaust gases of low pressure RF plasma fed with HMDSO/O_2. Light hydrocarbons [46] were detected along with different organosilicon compounds, most of them containing one or more dimethylsiloxane (-Me_2SiO-) groups [46-47], thus confirming the importance of this unit as building block in film growth. Moreover Fracassi and co-workers thanks to the GC-MS diagnostics suggested that O_2 has an important role in the plasma chemistry, as it promotes oxidation reactions, but it has a negligible effect on the monomer activation that is mainly due to electron collisions.

3.4 Organosilicon thin films deposition in DBDs

As shown in the previous paragraphs low pressure PE-CVD from organosilicon precursors is a well established technology, but the so far enounced advantages of non-equilibrium plasma at atmospheric pressure, along with the technological interest for organosilicon coatings, has resulted in many academic and industrial research groups studying the organosilicon thin film deposition in dielectric barrier discharges (DBDs)

[48]. At atmospheric pressure too HMDSO is the most investigated organosilicon precursor, but also TEOS, HMDSN, TMDSO and cyclic compounds have been used.

As described in the chapter 2 the critical point of the DBD technology is that uniform discharges (glow or Townsend regime) are difficult to obtain as they exist only in a narrow range of working parameters i.e. gas mixture composition, precursor concentration, frequency, applied voltage, etc.; in most cases filamentary, and hence intrinsically inhomogeneous, discharges are generated, with likely production of non uniform and damaged coatings. In order to obtain uniform and pinhole-free coatings in DBDs fed with organosilicon precursors, the following approaches are reported: i) the deposition in a homogeneous regime [48-59]; ii) the optimization of filamentary discharges [60-68].

One of the first works on organosilicon deposition process at atmospheric pressure was carried out by Sawada et al. [49], who investigated HMDSO/O_2 and TEOS/O_2 mixtures in He APGD generated in a parallel plate DBD system. They obtained transparent uniform coatings well comparable in quality and deposition rate to that produced in Low Pressure PECVD and they found that, in spite of the different starting molecules excitation mechanism, the decomposition and recombination processes of the two monomers were very similar to that reported in low pressure plasma. Further they observed that film obtained in O_2 free feeding gas mixtures showed high monomer structure retention, while at exceeding O_2 concentrations powders formation and increased deposition rates were recorded.

Other authors studied the deposition of thin homogeneous $SiO_xC_yH_z$ films in He [50] and in N_2 [51-57] APGD discharges. Among them Massines and co-workers [52-55], comparing the silica-like coatings produced in N_2-HMDSO-N_2O and N_2-SiH_4-N_2O APTD, found that in HMDSO-fed discharges denser SiO_2-like films were obtained and no powders were detected, probably due to a more efficient interaction of plasma activated radicals with the surface than with the other species in the gas phase. Further they found that the oxidant concentration strongly influences the film chemical composition without effects on the deposition rate, thus suggesting that HMDSO activation is due to the abundant N_2 metastables and not to oxidant.

Worth of noting is the study carried out by this research group on the deposition rate evolution along the gas flow direction in a parallel plate system, using both

experimental evidence and theoretical modelling [56-57]. The silica-like films thickness profile showed a maximum close to the gas entrance: here radicals produced near the surface mainly contribute to the growing film, while moving along the flow direction the coating is due to radicals coming from the gas bulk. The influence of external parameters (i.e. input power, monomer concentration, main gas flow) were evaluated and the chemical evolution of the deposited coating along the flow direction was recorded.

Similar results were obtained by Van de Sanden et al. [58-59]. A diffusive APGD with many gas mixtures was obtained by means of an electronic stabilization network. They found that a uniform discharge is not sufficient to guarantee an uniform film deposition; especially in presence of O_2, powders are produced, and working in a pulse mode it is possible to reduce powder production.

Schmidt-Szalowski et al. [60] investigated the thin film deposition from HMDSO and HMDSN, eventually mixed with O_2 or N_2O as oxidant, in Ar or N_2 filamentary DBD generated in a symmetric parallel plate system. They found that the substrate temperature does not significantly influence the film chemical composition and that also at exceeding concentration of oxidant agents the organic fraction cannot be totally removed. Moreover the presence of oxidants and longer deposition time promote powders formation, therefore not fully homogeneous coatings were obtained. More recently Morent and co-workers [61-62] working with a similar DBD system, reported on the deposition from HMDSO/Ar/Air mixture. Oxidant content influences not only the film chemistry, but also the discharge regime: when the air concentration increases the discharge moves from a glow-like to a filamentary type, resulting in very rough coatings.

Often the filamentary regime was investigated in DBD systems with movable grounded electrode. Thyen et al. [63] explored the thin films deposition from TEOS and tetramethylsylane in filamentary discharges fed by Ar and N_2 in a DBD system composed of four assembled rods as HV electrode and a movable plane as grounded electrode: they obtained softer and less cross-linked coatings respect of that produced in low pressure plasma, and suggested the importance of gas phase reactions in the filamentary regime due to the formation of particles during the film growth. Other

authors investigated HMDSO/N_2/O_2 filamentary DBDs generated in similar systems in order to deposit SiO_2-like thin films for metal corrosion protection [64-68].

Silicone- and silica-like thin films were deposited also injecting aerosol of various organosilicon liquid precursors in a DBD [69-73]. Twomey and al. [72-73], in particular, investigated also HMDSO and TMDSO: they found that the precursors does not influence the deposition rate and the difference among them become less important as siloxy-chemistry approaches the SiO_2 one. Moreover the level of plasma exposure reduce the deposition rate and moves the coating chemistry towards a more inorganic character.

Deposition of organosilicon films in remote DBD were investigated by Alexandrov and co-workers [74] who studied the deposition of silicon oxide films from HMDSO in an Ar and Ar/O_2 fed remote atmospheric pressure system. Nowling and al. [75] tested a chamberless plasma deposition from various organosilicon precursors, including HMDSO and TMDSO. Recently Y.S. Kim and co-workers [76] investigated the deposition of SiO_2-like thin films in a remote pin-to-plate type DBD from HMDSN/He/Ar/O_2 mixtures: smoother films were obtained in comparison with those produced in a HMDSN/Ar/O_2 direct pin-to-plate type DBD, where faster HMDS reactions in the gas phase occur, thus reducing the film quality [77].

3.5 Investigation of deposition mechanism in HMDSO DBD

Also if, compared to low pressure plasma investigations, few works can be mentioned, interesting results, concerning the correlation of the plasma chemistry with the chemical composition and structure of the coatings in HMDSO fed atmospheric pressure cold plasmas, have been published.

Alexandrov and co-workers [74] investigating their Ar/O_2 fed remote atmospheric pressure system coupled with HMDSO injection by means of optical emission spectroscopy and FT-IR of the streaming gas, suggested the role of excited argon atoms in metastable states and of ozone in the monomer activation and they found that the better deposition conditions were obtained with an O_2 amount sufficient to give active oxygen species, but not too much to reduce the likelihood of HMDSO activation by excited Ar metastables.

Vinogradov et al. [78-79] performed the FT-IRAS and OES analysis of DBDs fed with Ar/HMDSO/O_2 and He/HMDSO/O_2. In particular the investigation of the plasma phase with FT-IRAS suggested that monomer fragmentation mainly results in the production of four radicals: $(CH_3)_3SiO$, $Si(CH_3)_3$, $(CH_3)_3SiOSi(CH_3)_2$ and CH_3; these reactive fragments can be responsible for the formation of pentamethyldisiloxane, trimethylsilane and methane. The concentration of these species decreases with oxygen addition, with the production of CO, CO_2, H_2CO, O_3 and HCOOH.-

Also GC-MS was utilized to investigate organosilicon-containing atmospheric pressure plasmas. Sonnenfeld et al. [80] studied HMDSO- and TEOS-fed filamentary discharges sustained in Ar, N_2 and He. It was reported that, in HMDSO-plasma, methyl loss with formation of pentamethyldisiloxane is the main reaction path in monomer activation along with Si-O bond breaking and formation of $(CH_3)_3SiO$ and $(CH_3)_3Si$ units. Since only small amounts of unidentified oligomers were detected, the authors assumed that the polymerization processes mainly take place at the surface of the growing polymer.

REFERENCES

[1] A.M. Wróbel, M.R. Wertheimer in *Plasma deposition, treatment and etching of polymers*, R. d'Agostino ed., Academic Press, New York **1990**, p.163.

[2] A. Grill, V. Patel, *J. Appl. Phys.* **1999**,*85*, 3314-3318.

[3] A. Grill, *J. Appl. Phys.* **2003**, *93*, 1785.

[4] D.D. Burkey, K.K. Gleason, *J. Appl. Phys.* **2003**, *93*, 5143-5150.

[5] D.D. Burkey, K.K. Gleason, *Journal of The Electrochemical Society,* **2004**, 151 (5)**,** F105-F112.

[6] M. Creatore, W. M. M. Kessels, Y. Barrell, J. Benedikt, M. C. M. van de Sanden, *Mat. Sci. Semicond. Process.* **2004**, *7*, 283.

[7] A. Milella, J. L. Delattre, F. Palumbo, F. Fracassi, R. d'Agostino, *J. Electrochem. Soc.* **2006**, *153*, F106.

[8] A. Milella, F. Palumbo, J. L. Delattre, F. Fracassi, R. d'Agostino, *Plasma Process. Polym.* **2007**, *4*, 425.

[9] D. Korzec, K. Traub, F. Werner, J. Engemann, *Thin Solid Films*, 281-282, **1996**, 143-145.

[10] L. Zajíčková, V Buršíková, J. Janča, *Vacuum* **1998**, *50*, 19.

[11] W. Michaeli, I. Fonteiner, S. Goebel, *Macromol. Mater. Eng.* **2000**, *284/285*, 30–34.

[12] L. Zajíčková, V. Buršiková, V. Peřina, A. Macková, D. Subedi, J. Janča, S. Smirnov, *Surf. Coat. Technol.* **2001**, *142-144*, 449.

[13] B.W. Muir, H. Thissen, G.P. Simon, P.J. Murphy, H.J. Griesser, *Thin Solid Films* 500, **2006,** 34 – 40.

[14] M. Creatore, F. Palumbo, R. d'Agostino, P. Fayet, *Surf. Coat. Technol.* **2001**, *142-144*, 163.

[15] M. Creatore, F. Palumbo, R. d'Agostino, *Plasmas Polym.* **2002**, *7*, 291.

[16] A. Sonnenfeld, A. Bieden, P.R. von Rohr, *Plasma Process. Polym*. **2006**, 3, 606–617.

[17] J. Schwarz, M. Schmidt, A. Ohl, *Surface and Coatings Technology* 98 (**1998**) 859–864.

[18] F. Fracassi, R. d'Agostino, F. Palumbo, E. Angelini, S. Grassini, F. Rosalbino, *Surf. Coat. Technol.* **2003**, *174*, 107.

[19] Y.S. Li, S. Shimada, *Surf. Coat. Technol.* **2006**, 201, 1160-1165.

[20] K. Li, J. Meichsner, *Surf. Coat. Technol.* **1999**, 116-119, 841-847.

[21] S. Zanini, P. Massini, M. Mietta, E. Grimoldi, C. Riccardi, *Journal of Colloid and Interface Science* 322 (**2008**) 566–571.

[22] T. Hayakawa, M. Yoshinari, K. Nemoto, *Biomaterials* **2004**, *25*, 119.

[23] Y. Segui in "Plasma processing of polymers" NATO ASI Series E, edited by R. d'Agostino, P. Favia, F. Fracassi, **1996**.

[24] P. Favia, R. d'Agostino, F. Fracassi, *Pure Appl. Chem.*, 66, 6, 1373-1390, **1994**.

[25] D. Hegemann, U. Vohrer, C. Oehr, R. Riedel, *Surface and Coatings Technology* 116–119 (**1999**) 1033–1036.

[26] S. Saloum, M. Naddaf, B. Alkhaled, *Vacuum* **2008**, 82, 742.

[27] K. Aumaille, C. Vallée, A. Granier, A. Goullet, F. Gaboriau, G. Turban, *Thin Solid Films* 359 (**2000**) 188-196.

[28] R. Lamendola, R. d'Agostino in "Plasma processing of polymers" NATO ASI Series E, edited by R. d'Agostino, P. Favia, F. Fracassi, **1996**.

[29] R. Lamendola, R. d'Agostino, *Pure Appl. Chem.*, 70, 6, 1203-1208, **1998**.

[30] M. Creatore, F. Palumbo, R. d'Agostino, *Plasmas and Polymers*, 7, 3, **2002**.

[31] M. Creatore, F. Palumbo, R. d'Agostino, *Pure Appl. Chem.*, 74, 3, 407-411, **2002**.

[32] N. Benissad, C. Boisse-Laporte, C. Vallée, A. Granier, A. Goullet, *Surface and Coatings Technology* 116–119 (**1999**) 868–873.

[33] M. Goujon, T. Belmonte, G. Henrion, *Surf. Coat. Technol.* **2004**, *188-189*, 756.

[34] P. Raynaud, B. Despax, Y. Segui, H. Caquineau, *Plasma Process. Polym.* **2005**, *2*, 45.

[35] M. R. Alexander, F. R. Jones, R. D. Short, *Plasmas Polym.* **1997**, 2, 277.

[36] M. R. Alexander, F. R. Jones, R. D. Short, *J. Phys. Chem. B* **1997**, 101, 3164.

[37] D. Magni, Ch. Deschenaux, Ch. Hollenstein, A. Creatore, P. Fayet, *J. Phys. D: Appl. Phys.* **2001**, 34, 87.

[38] D. S. Wavhal, J. Zhang, M. L. Steen, E. R. Fisher, *Plasma Process. Polym.* **2006**, 3, 276.

[39] K. Li, O. Gabriel, J. Meichsner, *J. Phys. D: Appl. Phys.* 37 (**2004**) 588-594.

[40] M. Creatore, W. M. M. Kessels, Y. Barrell, J. Benedikt, M. C. M. van de Sanden, *Materials Science in Semiconductor Processing*, 7, (**2004**) 283-288.

[41] M. Creatore, Y. Barrell, J. Benedikt, M. C. M. van de Sanden, *Plasma Sources Sci. Technol.* 15 (**2006**) 421-431.

[42] D. Theirich, Ch. Soll, F. Leu, J. Engemann, *Vacuum*, 71 (**2003**) 349-359.

[43] A. M. Wróbel, G. Czeremuskin, H. Szymanowski, J. Kowalski, *Plasma Chemistry and Plasma Processing*, 10, 2, **1990**.

[44] A. M. Wróbel, A. Walkiewicz-Pietrzykowska, S. Wickramanayaka, Y. Hatanaka, *J. Electrochem. Soc.*, 145, 8, **1998**.

[45] A. M. Wróbel, A. Walkiewicz-Pietrzykowska, Y. Hatanaka, S. Wickramanayaka, Y. Nakanishi, *Chem. Mater.* **2001**, 13, 1884-1895.

[46] A. M. Sarmadi, T. H. Ying, F. Denes, *Eur. Polym. J.*, 31, 9, 847-857, **1995**.

[47] F. Fracassi, R. d'Agostino, F. Fanelli, A. Fornelli, F. Palumbo, *Plasmas Polym.* **2003**, 8, 259.

[48] S. E. Alexandrov, M. L. Hitchman, *Chem. Vap. Dep.* **2005**, 11, 457-468.

[49] Y. Sawada, S. Ogawa, M. Kogoma, *J. Phys. D: Appl. Phys.* 28 (**1995**) 1661-1669.

[50] R. Foest, F. Adler, F. Sigeneger, M. Schmidt, *Surface and Coatings Technology* , 163-164 (**2003**), 323-330.

[51] D. Trunec, Z. Navrátil, P. Sťahel, L. Zajíčková, V Buršíková, J. Čech, *J. Phys. D: Appl. Phys.,* 37 (**2004**) 2112-2120.

[52] N. Gherardi, S. Martin, F. Massines, *J. Phys. D: Appl. Phys.*, 33 (**2000**) L104-L108.

[53] F. Massines, N. Gherardi, F. Sommer, *Plasmas and Polymers*, Vol 5, Nos 3/4, **2000.**

[54] S. Martin, F. Massines, N. Gherardi, C. Jimenez, *Surface and Coatings Technology*, 177-178 (**2004**), 693-698.

[55] F. Massines, N. Gherardi, A. Fornelli, S. Martin, *Surface & Coatings Technology*, 200 (**2005**) 1855-1861.

[56] I. Enanche, H Caquineau, N. Gherardi, T. Paulmier, L.Maechler, F. Massines, *Plasma Process. Polym.*, **2007**, 4, 806-814.

[57] H Caquineau, I. Enanche, N. Gherard, N. Naudé, F. Massines, *J. Phys. D: Appl. Phys.*, 42 (**2009**) 12520.

[58] S. Starostine, E. Aldea, H. de Vries, M. Creatore, M. C. M. van de Sanden, *Plasma Process. Polym.* **2007**, 4, S440-S444.

[59] P.A. Premkumar, S.A. Starostine, H. de Vries, R.M.J. Paffen, M. Creatore, T.J. Eijkemans, P.M. Koenraad, M. van de Sanden, *Plasma Process. Polym.* **2009**, 6, 693-702.

[60] K. Schmidt-Szalowski, Z. Rżanek-Boroch, J. Sentek, Z. Rymuza, Z. Kusznierewicz, M. Misiak, *Plasmas and Polymers*, Vol. 5, Nos. 3/4, **2000**.

[61] R. Morent, N. De Geyter, S. Van Vlierberghe, P. Dubruel, C. Leys, E. Schacht, *Surf. Coat. Technol.* **2009**, *203*, 1366.

[62] R. Morent, N. De Geyter, S. Van Vlierberghe, P. Dubruel, C. Leys, L. Gengembre, E. Schacht, E. Payen, *Progress in organic coatings*, 64 (**2009**) 304-310.

[63] R. Thyen, A.Weber, C.-P. Klages, *Surface and Coatings Technology* 97 (**1997**) 426-434.

[64] X. Zhu, F. Arefi-Khonsari, C. Petit-Etienne, M. Tatoulian, *Plasma Process. Polym.* **2005**, *2*, 407.

[65] C. Petit-Etienne, M. Tatoulian, I. Mabille, E. Sutter, F. Arefi-Khonsari, *Plasma Process. Polym.* **2007**, *4*, S562.

[66] M. Šimor, A. Fiala, D. Kováčik, P. Hlídek, A. Wypkema, R. Kuipers, *Surface and Coatings Technology* 201 (**2007**) 7802-7812.

[67] J. Bardon, J. Bour, H. Aubriet, D. Ruch, B. Verheyde, R. Dams, S. Paulussen, R. Rego, D. Vangeneugden, *Plasma Process. Polym.* **2007**, 4, S445-S449.

[68] J. Bour, J. Bardon, H. Aubriet, D. Del Frari, B. Verheyde, R. Dams, D. Vangeneugden, D. Ruch, *Plasma Process. Polym.* **2008**, *5*, 788.

[69] L. O'Neill, L.-A. O'Hare, S. R. Leadley, A. J. Goodwin, *Chem. Vap. Dep.* **2005**, 11, 477-479.

[70] S. Paulussen, R. Rego, O. Goossens, D. Vangeneugden, K. Rose, *J. Phys. D: Appl. Phys.* 38 (**2005**) 568-575.

[71] D. Vangeneugden, S. Paulussen, O. Goossens, R. Rego, K. Rose, *Chem. Vap. Dep.* **2005**, 11, 491-496.

[72] B. Twomey, D. Dowling, G. Byrne, L. O'Neill, L.-A O'Hare, *Plasma Process. Polym.* **2007**, 4, S450-S454.

[73] B. Twomey, M. Rahman, G. Byrne, A. Hynes, L.-A O'Hare, L. O'Neill, D. Dowling, *Plasma Process. Polym.* **2008**, 5, 737-744.

[74] S. E. Alexandrov, N. McSporran, M. L. Hitchman, *Chem. Vap. Dep.* **2005**, *11*, 481-490.

[75] G. R. Nowling, M. Yajima, S. E. Babayan, M. Moravej, X. Yang, W. Hoffman, R.F. Hicks, *Plasma Sources Sci. Technol*. 14 (**2005**) 477-484.

[76] Y. S. Kim, J. H. Lee, J. T. Lim, J. B. Park, J. Y. Yeom, *Thin Solid Films*, (**2009**) 4065-4069.

[77] J. H. Lee, T.T.T. Pham, Y. S. Kim, J. T. Lim, S.J. Kyung, J. Y. Yeom, *Journal of The Electrochemical Society,* **2008**, 155 (3)**,** D163-D169.

[78] I. Vinogradov, D. Zimmer, A. Lunk, *Plasma Process. Polym.* **2007**, 4, S435-S439.

[79] I. Vinogradov, D. Zimmer, A. Lunk, *Plasma Process. Polym.* **2009**, 6, DOI: 10.1002/ppap.200931102.

[80] A. Sonnenfeld, T. M. Tun, L. Zajíčková, K. V. Kozlov, H. E. Wagner, J. F. Behnke, R. Hippler, *Plasmas Polym.* **2001**, 6, 237.

CHAPTER 4: EXPERIMENTAL

1.1 DBD reactor

Plasma processes were carried out in the home-made DBD reactor schematically shown in Figure 4.1.1. The discharge cell, enclosed in a Plexiglas chamber (volume of about 14 L), consists of two 50 x 50 mm^2 parallel plane electrodes both covered by a 2.54 mm thick 70 x 70 mm^2 Al_2O_3 plate (CoorsTek, 96 % purity). Alumina was chosen as dielectric layer because it has a good relative permittivity (9.5) and good mechanical properties.

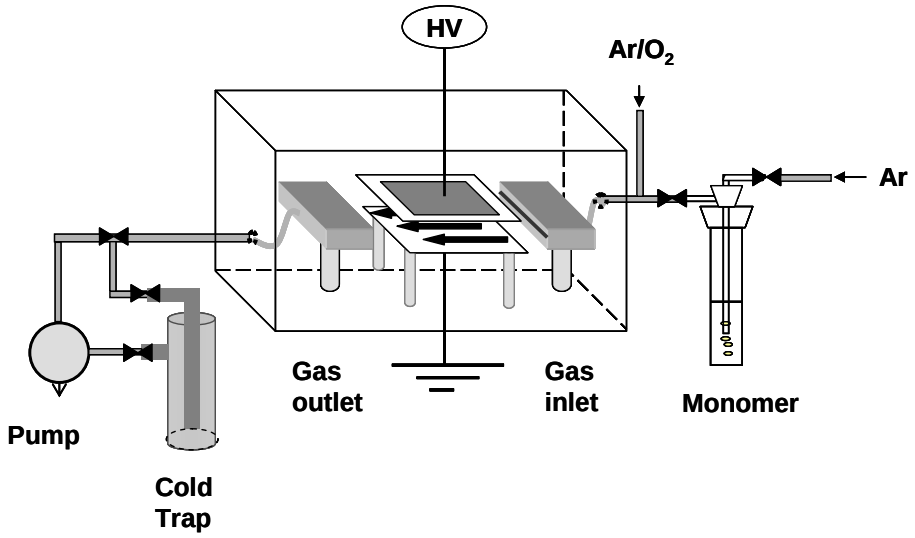

Figure 4.1.1: *Schematic of the experimental apparatus.*

The home-made electrodes were prepared applying a metallic layer onto one face of the alumina plate: this procedure allows the best metal-dielectric adhesion avoiding any kind of glue. Each alumina plate is painted with a silver-palladium containing screen-printing paint, then it is heated up to 825°C for 15 min. An electric cable, which allows the electrode connection to the power supply, is soldered to the metallization by a silver

loaded epoxy resin. To ensure a good electrical insulation the metallic layer is finally covered by an epoxy resin [1].

The electrodes are connected to an AC HV (high voltage) power supply (SG2 STT Calvatron), composed of a corona generator and a HV transformer, working in the 15-50 kHz frequency range. The inter-electrode distance can be easily regulated in the 1-5 mm range by means of proper spacers.

Feed gas is longitudinally injected in the discharge gap through a gas inlet slit and pumped out, by means of a membrane pump, through a slit placed at the opposite side of the gap. Gas flow canalization along the electrode length is assured by two glass spacers, symmetrically placed with respect to the metallization at a distance of 52 mm, which laterally confine the interelectrode gap.

The gas mean linear velocity (v) in the interelectrode gap can be evaluated by means of the equation 4.1.1:

$$v = \frac{\Phi}{d \cdot L} \qquad (4.1.1)$$

where Φ is the gas flow rate, d the interelectrode distance, and L the width of the region through which the gas flows, i.e. the distance between the two spacers. At the experimental conditions adopted in this thesis, i.e. at a total gas flow rate of 4000 sccm, interelectrode gap of 2 mm and spacers distance of 52 mm, the gas velocity is approximately 64 cm/s.

The pressure in the chamber, measured by a MKS baratron working in the 0-1000 Torr range, is maintained around 760 Torr by proper pumping speed regulation with a needle valve.

Discharges were fed with mixtures of Ar, O_2 and vapours of an organosilicon liquid precursor. Ar and O_2 gas flow rates were controlled by MKS electronic mass flow controllers; liquid precursor vapours were introduced by an Ar stream bubbling through a liquid monomer reservoir kept at constant temperature.

In order to collect stable by-products formed by plasma activation, a stainless steel liquid nitrogen trap was located between the reactor and the pump.

4.2 Electrical diagnostic of the discharge

The electrical characterization of a DBD mainly consists in the measurement of the applied voltage (V_a) and of the current flowing through the electrical circuit (I_m) or the total charge driven through the cell (Q_m). In this thesis both these approaches were adopted: the I-V_a curves were recorded in order to characterize the discharge regime and to control the working conditions; the Q_m-V_a plots, the so-called Lissajous figures, were instead used for measuring the discharge power P [2-5].

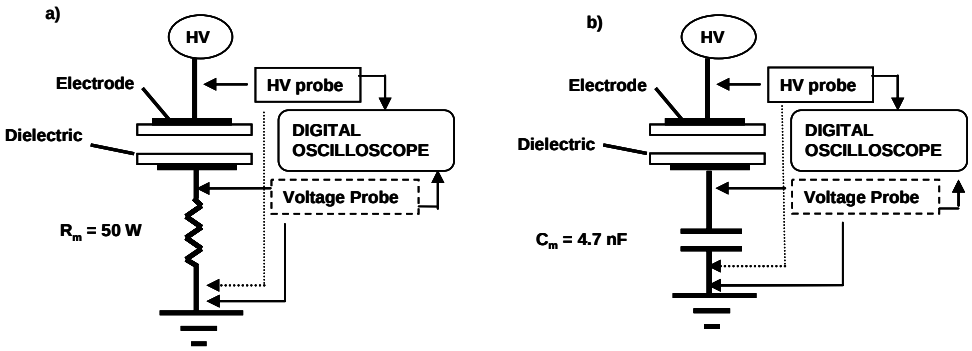

Figure 4.2.1: *Schematic of the experimental apparatus for the electrical characterization of the discharge.*

As schematically shown in Figure 4.2.1, the applied voltage was measured by a HV probe (Tektronix P6015A); a Tektronix P2200 probe was used for the current and charge measurements: the current was evaluated by measuring the voltage drop across a 50 Ω resistor (R_m) connected in series with the grounded electrode (Figure 4.2.1a), the charge, instead, by measuring the voltage drop across a 4.7 nF capacitor (C_m) that replaces the 50 Ω resistor (Figure 4.2.1b). The data were recorded by means of a digital oscilloscope (Tektronix TDS2014B).

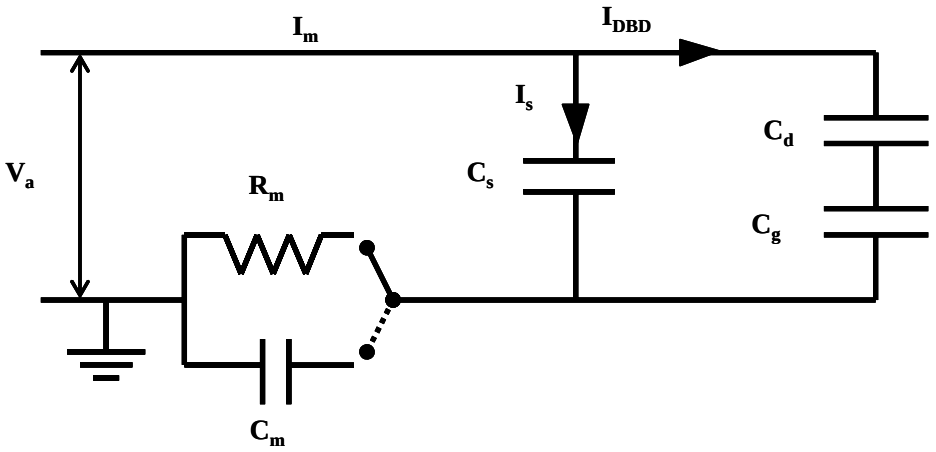

Figure 4.2.2: *Electrical equivalent circuit corresponding to the DBD system employed in this study, adapted from references [1, 4-5].*

Some electrical parameters of the DBD system can be evaluated; Figure 4.2.2 shows the equivalent circuit describing the DBD system [1, 4-5]. The cell capacitance C_{tot} is the total series capacitance of the gas (C_g) and dielectric layer (C_d) capacitances; C_g and C_d are known for a certain electrode configuration and interelectrode distance, and can be calculated by the following equations:

$$C_g = \varepsilon_0 \frac{A}{d} \qquad (4.2.1)$$

$$C_d = \varepsilon_0 \cdot \varepsilon_r \frac{A}{d_d} \qquad (4.2.2)$$

$$C_{tot} = \frac{C_d \cdot C_g}{C_d + C_g} \qquad (4.2.3)$$

where ε_0 is the vacuum permittivity ($8.85 \cdot 10^{-12}$ F/m), ε_r the alumina relative permittivity (9.5), A the electrode area (25 cm^2), d the interelectrode distance (2 mm), d_d the total thickness of dielectric plates (2 x 2.54 mm, as C_d is the total series capacitance of both dielectric layers). For the given parameters C_g and C_d are 11.1 pF and 41.4 pF, respectively. The total equivalent capacitance, C_{tot}, calculated by the equation 4.2.3, is thus 8.7 pF.

The measured current (I_m) is the result of the current connected to the dielectric barrier discharge (I_{DBD}) and a stray current (I_s) due to a stray capacitance (C_s) generally present in the electrical circuit:

$$I_m(t) = I_{DBD}(t) + I_s(t) = (C_{tot} + C_s)\frac{dV_a(t)}{dt} \qquad (4.2.4)$$

The stray capacitance can be easily calculated when the discharge is in off state as:

$$I_m = V_a \cdot 2\pi f \cdot (C_{tot} + C_s) \qquad (4.2.5)$$

where I_m and V_a are, respectively, the maximum measured current and the maximum applied voltage, and f is the working frequency. It was experimentally evaluated that in the adopted experimental conditions C_s is 7.5 pF.

The power dissipated in the discharge is defined as:

$$P = \frac{1}{T}\int_0^T I_m(t)V_a(t)dt \qquad (4.2.6)$$

If I(t) is replaced by the charge values, as I(t) = dQ(t)/dt, the equation 4.2.6 can be rewritten as:

$$P = \frac{1}{T}\oint V_a(Q_m)dQ_m = f \cdot E \qquad (4.2.7)$$

where f is the working frequency and E the electric energy consumed per voltage cycle: the integral in the equation 4.2.7 is mathematically the area of the Q-V diagram. When the voltage across the gas, V_{gas}, is lower than the ignition voltage, i.e. the discharge is off, the sinusoidal applied voltage V_a and the measured charge Q_m (i.e. the voltage V_m measured on the C_m capacitor) are in phase, and the Q-V plot is a straight line whose slope is the previously calculated C_{tot} + C_s. When the discharge is ignited, the phase of Q is shifted by the resistive losses of the discharge and the straight line opens into a parallelogram, whose area is the electric energy consumed per voltage cycle E.

This method was firstly derived by Manley (see section 2.3), who did not consider stray capacitance effects; however it is important to highlight that Falkestein et al. [3] demonstrated that the stray capacitance (see figure 4.2.2), does not change the area

enclosed by the Q-V plot, thus it does not influence the E and P calculus, but significantly affects the parallelogram shape, so its slopes and intercept with the axis.

A typical Q-V plot obtained in the present experimental conditions is shown in Figure 4.2.3. Power values averaged on three measures were reported.

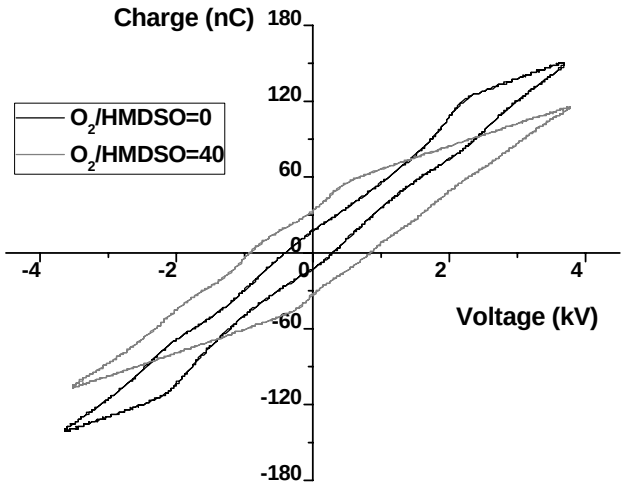

Figure 4.2.3: *Experimental charge-voltage plot obtained at O_2-to-HMDSO ratio of 0 and 40.*

4.3 Experimental conditions

All experiments were carried out with an Ar (Air Liquide Argon C) constant flow rate of 4000 sccm. Three organosilicon precursor were examined: hexamethildisiloxane (HMDSO, Fluka, 98.5 % purity), pentamethyldisiloxane (PMDSO, ABCR, 97 % purity) and 1,1,3,3-tetramethyldisiloxane (TMDSO, ABCR, 97 % purity). As before mentioned the vapours of each reactive monomer were added to the main gas by an Ar stream bubbling through a liquid monomer reservoir kept at 30°C for HMDSO and PMDSO, at 0°C for TMDSO. The effective amount of precursor injected into the reactor was evaluated by reservoir weight variation per unit of time. Assuming an ideal gas behaviour, the mass flow rate expressed in g/min was converted to flow rate Φ expressed in sccm by means of equation 4.3.1:

$$\Phi = \frac{\text{mass(g)}}{\text{t}_{\text{sampling}}\text{(min)}} \cdot \frac{22400(\text{cc}\cdot\text{mol}^{-1})}{\text{MW}(\text{g}\cdot\text{mol}^{-1})} \qquad (4.3.1)$$

where $t_{sampling}$ is the time interval adopted for the weight measure, MW is the precursor molecular weight. Each monomer vapour flow rate was kept constant at 1.0 sccm.

O_2 (Air Liquide Oxygen C) was added to Ar/HMDSO, Ar/PMDSO and Ar/TMDSO mixtures and its flow was changed in order to vary the O_2-to-monomer feed ratio in the range 0 – 40. Only for HMDSO, also the O_2-to-HMDSO feed ratio of 80 was investigated.

For each monomer, the interelectrode distance was fixed at 2 mm and discharges were driven at fixed excitation frequency and voltage of 30 kHz and 2.5 kV_{rms}, respectively.

Substrates were placed on the bottom grounded electrode. Thin films were deposited onto thin glass slides to perform deposition rate and water contact angle (WCA) measurements, XPS analysis and SEM investigations; for FT-IR analysis 0.7 mm thick c-Si(100) was used.

Before each experiment, the Plexiglas chamber was purged with 4000 sccm of Ar for 20 min to remove air contaminations. The deposition processes were carried out for

5 min in Ar/HMDSO/O_2 and Ar/PMDSO/O_2 mixtures fed discharges, for 10 min in Ar/TMDSO/O_2 mixtures fed discharges.

4.4 Surface diagnostic

4.4.1 Fourier transform infrared spectroscopy (FT-IR)

For the chemical characterization of the coatings, Fourier transform infrared spectroscopy (FT-IR) analyses were carried out with a commercial Brucker Equinox 554 FTIR Interferometer. The instrument is equipped with a Globar light source: the parallel IR beam is directed through the sample and then focused on a DGTS detector. As the light beam passes all the sample thickness, this technique provide a bulk chemical analysis investigation. To avoid water vapour and carbon dioxide (CO_2) interferences the optical path was purged with a continuous N_2 flow for 10 min between each measurement.

Infrared absorbance spectra were recorded in the 400-4000 cm^{-1} range, with a resolution of 4 cm^{-1}. The analyzed surface had a circular area of 27 mm^2 centred at a certain position along the gas flow into the discharge zone, i.e. at certain gas residence times. Before each sample scan the signal of the bare silicon substrate was taken as reference. After baseline correction, spectra were normalized to the most intense absorption band.

Table 4.4.1 reports the assignments of FT-IR peaks, as provided by published data, for organosilicon films. The reported wavenumber ranges refer to the published uncertainty of signal position.

Table 4.4.1 *Infrared absorbtion band assignements for organosilicon coatings.*

Wavenumber (cm^{-1})	Assignment	References
3700-3100	-OH stretching	[8, 10-11, 14-17, 20-21]
3650	-OH stretching of free Si-OH	[11, 15, 17]
2959-2970	$-CH_3$ asymmetric stretching	[8, 13-21]
2935-2915	$-CH_2$ asymmetric stretching	[8, 14-16, 18-19]
2906-2900	$-CH_3$ symmetric stretching	[8, 13-16, 18-20]
2880-2875	$-CH_2$ symmetric stretching	[8, 14, 16]
2000	-Si-H stretching in H-Si(Si_3)	[22-25]
2090-2165	-Si-H stretching in H-Si(Si_2O)	[8, 12-14, 16, 18-19 22-25]
2200-2178	-Si-H stretching in H-Si(SiO_2)	[8, 10, 22-25]
2260-2232	-Si-H stretching in H-Si(O_3)	[8, 10, 22-25]
1405-1412	$-CH_3$ asymmetric bending in -Si-$(CH_3)_x$	[8, 14, 16, 20]
1255-1250	$-CH_3$ symmetric bending in -Si-$(CH_3)_3$	[10, 15-16]
1260	$-CH_3$ symmetric bending in -Si-$(CH_3)_2$	[10, 15-16]
1270	$-CH_3$ symmetric bending in -Si-CH_3	[10, 15-16]
1020-1048	Si-O-Si stretching long chains or smaller rings	[6, 8-10, 14-17]
1077-1090	Si-O-Si stretching long chains with –OH or $–CH_3$ terminating units or opened smaller rings	[6, 8-10, 14-17]
1134-1138	Si-O-Si stretching short chains or larger rings	[6, 8, 10, 14-17]
1190-1183	Si-O-Si stretching short chains with –OH or $–CH_3$ terminating units or opened larger rings	[6, 8, 10, 14-17]
936-926	Si-OH stretching	[6, 11, 13, 18-20]
890-975	H-Si-(O_3) hybrid vibrations	[7-8, 22-25]
865-850	H-Si(SiO_2) hybrid vibrations	[8, 22-25]
780-790	H-Si(Si_2O) hybrid vibrations	[22-25]
850-830; 779-760	$-CH_3$ rocking and Si-C stretching in Si-$(CH_3)_3$	[6, 8, 12-16, 26]
904-885; 805-800	$-CH_3$ rocking and Si-C stretching in Si-$(CH_3)_2$	[6, 8, 12-16, 26]
810-800	Si-O-Si bending	[6-8, 12-13, 15-16]

4.4.2 X-ray photoelectron spectroscopy

For evaluating the atomic composition of the deposited films, XPS analyses were carried out with a Thermo VG Scientific spectrometer equipped with a monochromatic Al-Kα X-ray source (1486.6 eV), operated at a spot size of 400 μm. Elements were identified by survey spectra recorded from 0 to 1200 eV at a pass energy of 200 eV; high resolution spectra of the C1s, O1s and Si2p regions were acquired at a pass energy of 150 eV. All spectra were recorded at a take off angle of 37°. A flood gun was used to balance the surface charging. In order to remove carbon contamination from the sample surface sputtering cleaning was performed with Ar^+ ions for 10 s (1 kV, 500 nA, 3 mm raster size) before the analysis.

4.4.3 Deposition rate measurements

The deposition rate was evaluated by measuring the films thickness by means of an Alpha-Step 500 KLA Tencor Surface Profilometer. Partially masked substrates covering all the discharge length in the flow direction were used. Measurements were performed at different position along the gas flow, i.e. at different gas residence times. For each experimental condition the deposition rate mean value in the region between 20 and 30 mm from the gas entrance inside the discharge area, in this work referred to as central region of the discharge zone, was considered [27].

4.4.4 Water contact angle (WCA)

The wettability of deposited coatings was evaluated by means of static (sWCA) and dynamic water contact angle measurement (advancing and receding WCA). A Ramé-Hart manual goniometer (model A-100) was used. A 2 μl double distilled water drop was placed on the deposited coatings and the contact angles on both sides of the drop were recorded. For each coating the value averaged on five measures carried out in the central area (20-30 mm region from the gas entrance inside the discharge area) was reported.

Advancing (aWCA) and receding (rWCA) water contact angles were recorded in the same area applying the sessile drop method [28]. Also in this case a mean value on five measures was reported.

4.4.5 Scanning Electron Microscopy (SEM)

Morphological investigations of the deposited films were carried out onto 50 nm gold coated thin glass slides. A Zeiss Evo 40 scanning electron microscope was used. Surfaces were observed at working distance of 6.5 mm and a 30° tilt angle.

4.5 Gas phase diagnostic

4.5.1 Gas chromatography-mass spectrometry of exhaust gas (GC-MS)

In order to investigate the deposition mechanism of the organosilicon monomers used in this work, the analysis of stable by-products formed by plasma activation and contained in the gas effluent was performed by gas chromatography coupled with mass spectrometry (GC-MS).

As mentioned before a stainless steel trap, cooled in liquid nitrogen, was inserted between the reactor and the pump (Figure 4.1.1). The exhaust gas was forced through the trap before it was pumped off, so the stable long-lived by-products formed due to the plasma process were here condensed. After the sampling was carried out for 30 min, the trap was isolated from the system and, as soon as it was removed from the liquid nitrogen bath, 20 ml of acetone (Fluka, 99.8 % purity) were introduced to dissolve the condensate. Then the trap was slowly heated up to the ambient temperature and the solution was filtered and analyzed by means of a GC 8000^{Top} gas chromatographer (Thermoquest Corporation) coupled with a differential pumped quadrupole mass spectrometer (Voyager, Thermoquest Corporation). A Grace AT^{TM}-1MS fused silica capillary column (polydimethylsiloxane 0.25 μm thick stationary phase, length of 30 m, internal diameter of 0.25 mm) was utilized with He as carrier gas (2 sccm) under the following conditions: injector temperature of 200°C, column temperature programmed from 30°C to 200°C (1 min at 30°C, linear heating rate of $10°C \cdot min^{-1}$,

1 min at 200°C). Separated products were analyzed at the GC-MS interface and mass spectrometer source temperature of 250 and 200°C, respectively. Mass spectra were recorded in full-scan mode in the m/z range 15–500 amu at the standard ionizing electron energy of 70 eV.

Stable by-products were identified by means of available libraries [29], some species were tentatively identified through the interpretation of their mass spectra according to the typical fragmentations pattern of organosilicon compounds. The identification of some products was confirmed by the comparison of retention time and mass spectrum with standard compounds. Nonane (Aldrich, 99 % purity) was used as internal standard (IS) for quantitative analysis of identified species; calibration curves were calculated in the linear range using the area of the corresponding peaks in the chromatogram acquired in total ion current. The measured amounts were then converted in flow rate by mean of Equation 4.3.1 (here $t_{sampling}$ is the time interval adopted for the exhaust sampling). Considering the overall procedure used (sampling, CG-MS analysis conditions, etc.) the limit of quantification (LOQ) of by-products in the exhaust was 0.0001 sccm.

The extent of reacted monomer (HMDSO or PMDSO or TMDSO) percent, namely the monomer depletion ($Monomer_{depletion}$), was evaluated according to equation (4.5.1):

$$Monomer_{depletion}(\%) = \frac{Monomer_{off}(sccm) - Monomer_{on}(sccm)}{Monomer_{off}(sccm)} \cdot 100 \qquad (4.5.1)$$

where $Monomer_{on}$ and $Monomer_{off}$ are the precursor flow rate detected in the exhaust in plasma off and plasma on conditions, respectively.

REFERENCES

[1] F. Fanelli, Ph.D. Thesis **2005.**

[2] T. C. Manley, *Trans. Electrochem. Soc*. 84, 83 (**1943**).

[3] Z. Falkenstein, J.J. Coogan, *J. Phys. D: Appl. Phys*. 30 (**1997**) 817-825.

[4] H. –E. Wagner, R. Brandenburg, K. V. Kozlov, A. Sonnenfeld, P. Michel, J. F. Behnke, *Vacuum* 71 (**2003**) 417-436.

[5] U. Kogelschatz, *Plasma Chemistry and Plasma Processing*, 23, 1 (**2003**), 1-46.

[6] C.Y. Wang, Z.H. Shen, Z.J. Zheng, *Applied Spectroscopy*, 54, 2, **2000**, 209-213.

[7] A. Grill, *J. of Applied Physics*, 93, 3, 1785-1790 (**2003**).

[8] A. Grill, D. A. Neumayer, *J. Appl Phys*, 94, 10, 6697-6707, **2003**.

[9] K. Li, O. Gabriel, J. Meichsner, *J. Phys. D: Appl. Phys*. 37 (**2004**) 588-594.

[10] D.D. Burkey, K.K. Gleason, *Journal of The Electrochemical Society,* **2004**, 151 (5)**,** F105-F112.

[11] F. Massines, N. Gherardi, A. Fornelli, S. Martin, *Surface & Coatings Technology* 200 (**2005**) 1855-1861.

[12] P. Raynaud, B. Despax, Y. Segui, H. Caquineau, *Plasma Process. Polym.* **2005**, 2, 45-52.

[13] D. S. Wavhal, J. Zhang, M. L. Steen, E. R. Fisher, *Plasma Process. Polym.* **2006**, 3, 276-287.

[14] P. Supiot, C. Vivien, A. Granier, A. Bousquet, A. Mackova, D. Escaich, R. Clergereaux, P. Raynaud, Z. Stryhal, J. Pavlik, *Plasma Process. Polym.*, **2006**, 3, 100-109.

[15] A. Milella, J.L. Delattre, F. Palumbo, F. Fracassi, R. d'Agostino, *J. of Electrochemical Society*, 153 (6) F106-F114 (**2006**).

[16] A. Milella, F. Palumbo, J.L. Delattre, F. Fracassi, R. d'Agostino, *Plasma Process. Polym.* **2007**, 4, 425-432.

[17] A. Milella, M. Creatore, M.A. Blauw, M.C.M. van de Sanden, *Plasma Process. Polym.* **2007**, 4, 621-628.

[18] I. Vinogradov, D. Zimmer, A. Lunk, *Plasma Process. Polym*. **2007**, 4, S435-S439.

[19] I. Vinogradov, D. Zimmer, A. Lunk, *Plasma Process. Polym.* **2009**, *6*, DOI: 10.1002/ppap.200931102.

[20] J. Bour, J. Bardon, H. Aubriet, D. Del Frari, B. Verheyde, R. Dams, D. Vangeneugden, D. Ruch, *Plasma Process. Polym.* **2008**, *5*, 788.

[21] R. Morent, N. De Geyter, S. Van Vlierberghe, P. Dubruel, C. Leys, E. Schacht, *Surf. Coat. Technol.* **2009**, 203, 1366.

[22] G. Lucovsky, J. Yang, S.S. Chao, J.E. Tyler, W. Czubatyi, *Physical Review B*, 28, 6, 3225-3233, **1983**.

[23] D.V. Tsu, G. Lucovsky, B.N.Davidson, *Physical Review B*, 40, 3, 1795-1805, **1989**.

[24] L. He, T. Inokuma, Y. Kurata, S. Hasegawa, *Journal of Non-Crystalline Solids* 185 (**1995**) 249-261.

[25] N.D. Gupta, P. Chaudhuri, *Journal of Non-Crystalline Solids* 289 (**2001**) 168-174.

[26] *Handbook of Plastic analyses*, D. H. Lobo and J.V. Bonilla ed., **2003.**

[27] F. Fanelli, F. Fracassi. R. d'Agostino, *Plasma Process. Polym.* **2005**, 2, 688.

[28] Garbassi, Morra, Occhiello, *Polymer Surfaces from Physics to Technology*, J. Wiley & Sons, **1994**.

[29] NIST and Wiley libraries in *MassLab Release 1.4 (GC/MS Data System Software Finngan).*

CHAPTER 5: RESULTS AND DISCUSSION: THIN FILMS DEPOSITION

5.1 Electrical characterization of the discharge

Under the experimental conditions explored in this work, independently of the investigated precursor, filamentary DBDs are obtained: in the current-voltage plots, recorded at various O_2/monomer feed ratios, several peaks characteristic of filamentary discharges [1] appear. For each monomers discharges fed with the same O_2/monomer ratio gas mixtures exhibit the same current signals, thus the current-voltage curves obtained at different O_2/HMDSO feed ratios are shown in Figure 5.1.1 as example.

The filamentary character seems to increase with the oxygen content in the feed gas since the number of current peaks increases within each half-cycle. In particular at the O_2-to-monomer feed ratio of zero the discharge current is formed by a quasi-periodical multipeak signal and the filamentary discharge is characterized by a quasi-homogeneous appearance ascribed to stochastically distributed microdischarges. Under this condition only few filaments (defined in reference [2] as a family of microdischarges that generate in the same spot each time the polarity is reversed) are observed in the gas gap. Increasing the O_2 content more and more intense filaments are observed and at O_2-to-monomer ratios higher than 6 the typical current signal of a filamentary DBD characterized by intense and well-distinguished microdischarges is recorded.

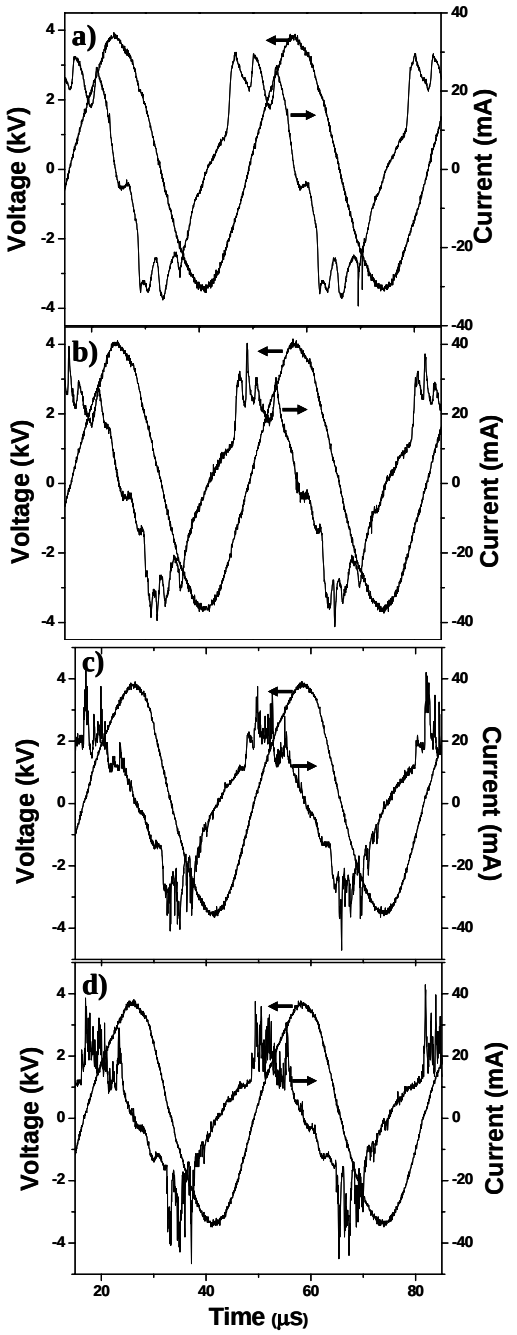

Figure 5.1.1: *Current and voltage waveforms of the DBD fed with Ar/HMDSO/O_2 gas mixtures, at different O_2/HMDSO feed ratios: a) 0, b) 1, c) 6, d) 25.*

For all the precursors the power delivered to the discharge, evaluated with the Lissajous method, steeply increases with O_2 addition to the feed (Figure 5.1.2) and then reaches a plateau, moving from ~ 5 W without O_2 in the feed, to 8 - 9 W at O_2-to-monomer feed ratio higher than 3. As Figure 5.1.2 shows, at the same O_2 content in the feed, the power delivered to HMDSO fed discharges is generally lower than for the other two precursors.

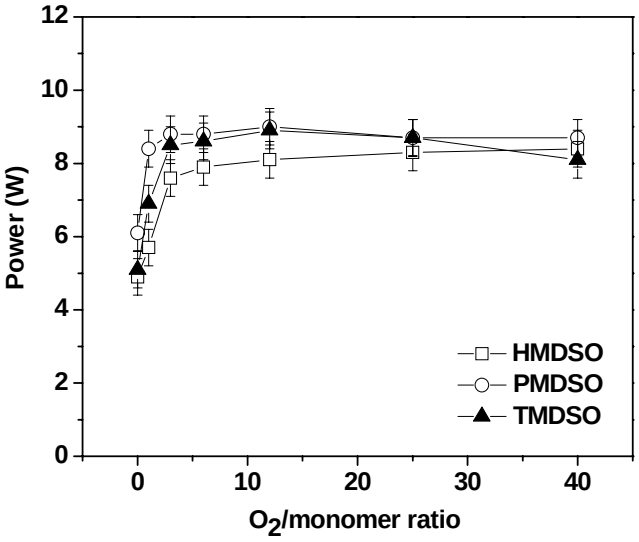

Figure 5.1.2: *Power delivered to the discharge as a function of the O_2 content in the feed.*

5.2 HMDSO/Ar/O_2 DBDs

5.2.1 Effect of gas residence time

Transparent and compact coatings without appreciable powder formation were deposited with Ar/HMDSO/O_2 feeds, while without oxygen an oily film was obtained. Powder deposition occurred in the downstream position out of the discharge zone especially at high O_2/HMDSO ratios.

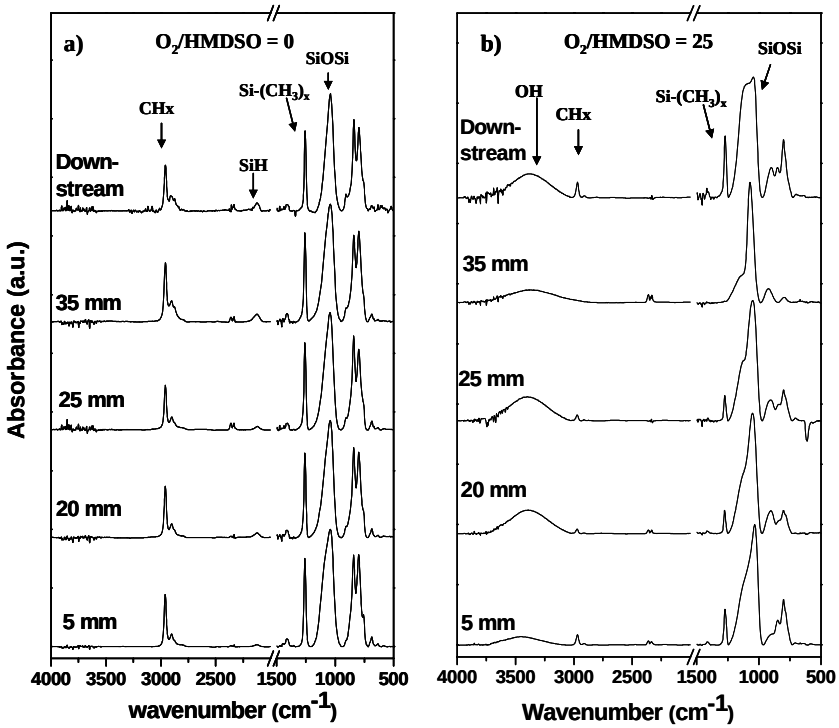

Figure 5.2.1: *FT-IR spectra of plasma-polymerized coatings obtained at different positions of the electrode region at a) O_2/HMDSO = 0 and b) O_2/HMDSO = 25.*

Due to the particular gas injection system both the chemical composition and the thickness of the deposit along the gas flow direction were evaluated. Figure 5.2.1 shows the FT-IR spectra at O_2/HMDSO = 0, 25 recorded at different position in the discharge length, i.e. at different gas residence time from the gas entrance to the downstream position. Without oxygen discharges the gas residence time does not

affect the coating chemistry, while at O_2/HMDSO = 25 a chemical evolution from an organic coating (the absorptions of Si-$(CH_3)_x$ symmetric bending around 1270 cm^{-1} and CH_x in the 2850 – 3000 cm^{-1} region are evident [3-5]) at the gas entrance, to an inorganic coating at the gas exit, is observed. In the downstream position (50-60 mm from the gas entrance) the powders collected exhibits an organic character. This trend is confirmed by XPS analyses at O_2/HMDSO = 25: the carbon content decrease from 39 to 5 % with gas residence time.

Both the position inside the discharge area and the gas feed composition affect the deposition rate (Figure 5.2.2)**.** At low oxygen content (O_2-to-HMDSO feed ratio = 1) a quasi-constant deposition rate is measured up to 40 mm from the gas injection point, while a trend with a maximum is recorded at O_2/HMDSO = 25.

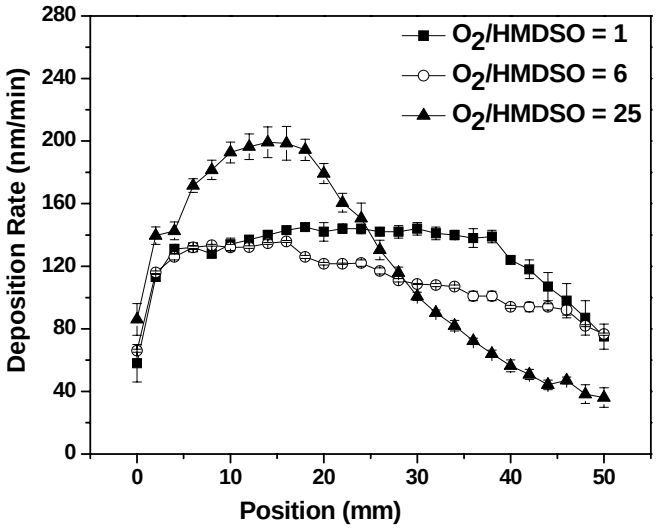

Figure 5.2.2: *Deposition rate profiles as a function of the position in the discharge area at different O_2/HMDSO ratio.*

5.2.2 Effect of the gas feed composition

Since the properties of the deposited coatings evolve with the gas residence time, the region from 20 to 30 mm from the gas entrance (the sample has been centred at 25 mm, i.e. at a gas residence time of 39 ms) was considered to study the effect of the gas feed composition on the deposition process.

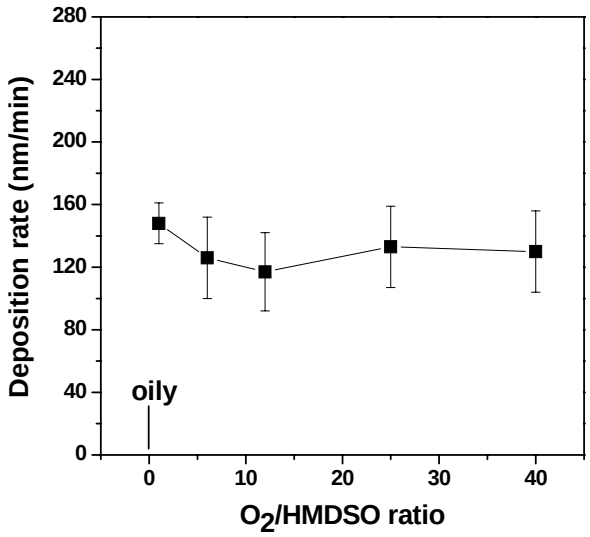

Figure 5.2.3: *Average deposition rate in the 20-30 mm region in the discharge area as a function of the O_2/HMDSO ratio.*

The deposition rate varies in the 120-150 nm·min^{-1} range and it is not significantly affected by the O_2 content (Figure 5.2.3). On the contrary the films chemistry is markedly affected by oxygen addition, as shown by the normalized FT-IR absorption spectra at various O_2-to-HMDSO ratios (Figure 5.2.4a). The FT-IR spectra of the deposits collected on a silicon substrate positioned in the downstream position are also reported for comparison in Figure 5.2.4b.

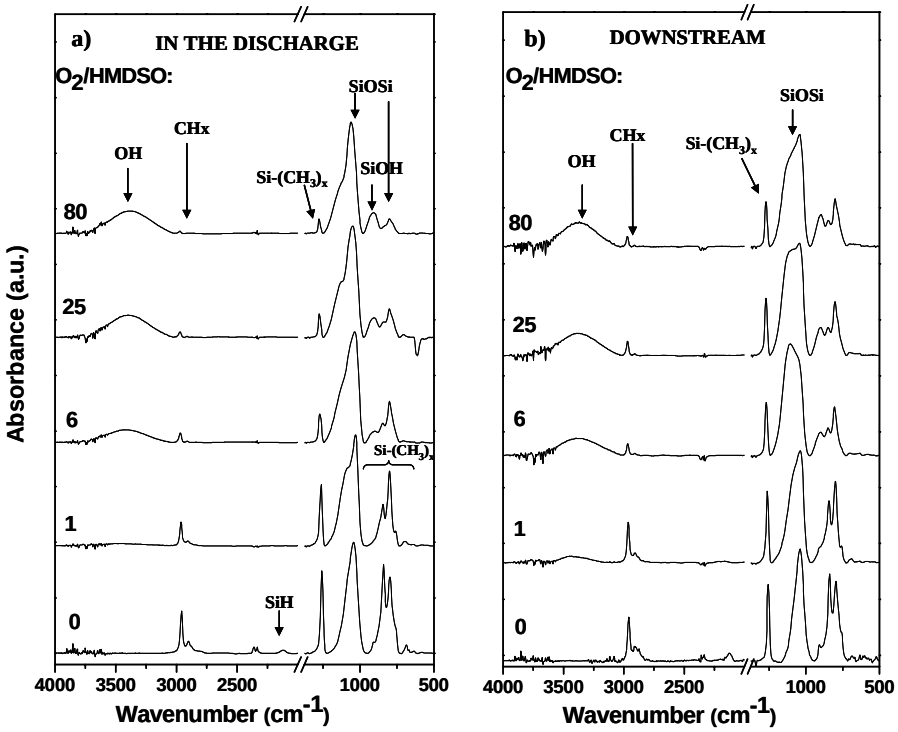

Figure 5.2.4: *a) FT-IR spectra of plasma-polymerized coatings obtained in the central region of the discharge zone at different O_2/HMDSO ratios; b) FT-IR spectra of the relative deposits obtained downstream of the electrode region.*

The coatings deposited, without oxygen, in the discharge zone show the typical features of silicone-like films: the intense Si-O-Si asymmetric stretching band at 1042 cm^{-1}, the Si-$(CH_3)_x$ symmetric bending at 1258 cm^{-1}, and the CH_x absorptions in the 2850 – 3000 cm^{-1} region (i.e. intense CH_3 asymmetric stretching at 2959 cm^{-1}, weak CH_3 symmetric stretching at 2874 cm^{-1}, and CH_2 asymmetric stretching at 2900 cm^{-1}) [3-9]. The absorptions in the 750 - 900 cm^{-1} region suggest the presence of di- and tri-substituted Si-$(CH_3)_x$ moieties [3-7, 10-12]: the intense peak at 841 cm^{-1}, along with the shoulder around 760 cm^{-1}, can be assigned to the Si-C rocking in Si-$(CH_3)_3$. The strong absorption at 796 cm^{-1} (which also contains a contribution due to Si-O-Si bending at 800 cm^{-1}), along with the small shoulder at 907 cm^{-1}, is due to Si-C rocking in Si-$(CH_3)_2$. Since without oxygen the typical OH absorption at 3200-3600 cm^{-1} is not evident, the contribution of Si-OH to the

shoulder at 907 cm^{-1} can be ruled out. The significant presence of Si-$(CH_3)_2$ (chain-propagating units), and Si-$(CH_3)_3$ (chain-terminating units), is further confirmed by the position of Si-$(CH_3)_x$ absorption at 1258 cm^{-1}. It has been reported, in fact, that the position of Si-$(CH_3)_x$ signal shifts to lower wavenumbers as the number of methyl groups bonded to silicon increases [4, 5, 13]. The absorptions of mono-substituted Si-CH_3, Si-$(CH_3)_2$ and Si-$(CH_3)_3$ are, in fact, generally observed at about 1275 cm^{-1}, 1260 cm^{-1} and 1255 cm^{-1} [4, 5, 13], respectively. The film also contains some Si-H units, as confirmed by the presence of the Si-H stretching at 2124 cm^{-1} [3, 5-9, 11, 14-17]; possible H-Si-O hybrid vibrations contribute to the shoulder at 760 cm^{-1} [14-17] ascribed to the Si-C rocking in Si-$(CH_3)_3$.

By adding O_2 to the gas feed, the absorptions of carbon containing groups (i.e. CH_x and $Si(CH_3)_x$) decrease but do not disappear also at high O_2-to-HMDSO ratios. The CH_3 asymmetric stretching shifts to higher wavenumbers for the more oxidized chemical environment (from 2959 cm^{-1} at O_2/HMDSO = 0, to 2970 cm^{-1} at O_2/HMDSO = 80); at O_2-to-HMDSO ratios higher than 6 the Si-$(CH_3)_x$ absorption moves up to 1274 cm^{-1}, suggesting the prevalence of mono-substituted Si-CH_3 units. This is also confirmed by the progressive reduction of the Si-C rocking in Si-$(CH_3)_3$ at 841 cm^{-1} and Si-$(CH_3)_2$ at 800 cm^{-1}. No Si-H signal can be detected as O_2 is added to the gas feed; on the contrary the broad OH absorption appears in the 3200 – 3600 cm^{-1} region, along with the intense signal at 905 cm^{-1} due to silanol (Si-OH) groups [6, 8-9]. The intense Si-O-Si asymmetric stretching slightly moves to higher wavenumbers, up to 1059 cm^{-1} at O_2/HMDSO = 80. An intense shoulder around 1084 cm^{-1}, ascribable to long siloxane chains, appears at O_2/HMDSO = 1. For higher O_2-to-HMDSO ratios the shoulder reduces and moves to 1123 cm^{-1}, indicating the presence of shorter Si-O-Si chains [3, 5-7, 13, 18]. The position of Si-O-Si asymmetric stretching is in agreement with the presence of carbon containing groups since in SiO_2-like coating this absorption falls at 1070 cm^{-1} and shifts to lower wavenumbers as the carbon content increases [4, 5].

The FT-IR spectra in the downstream position at O_2/HMDSO = 0-1 (Figure 5.2.4b) does not show significant differences with respect to the film deposited in the discharge region. At higher O_2 contents the deposit consists of powders and are more organic than in the discharge. Also the shape of Si-O-Si asymmetric stretching

is different in downstream position for the marked increase of the shoulder at 1100 cm^{-1}. This shoulder is a typical absorption of methyl polysiloxanes, and indicates a less dense, less ordered network of the collected powders with respect to the coating deposited inside the discharge [4, 5].

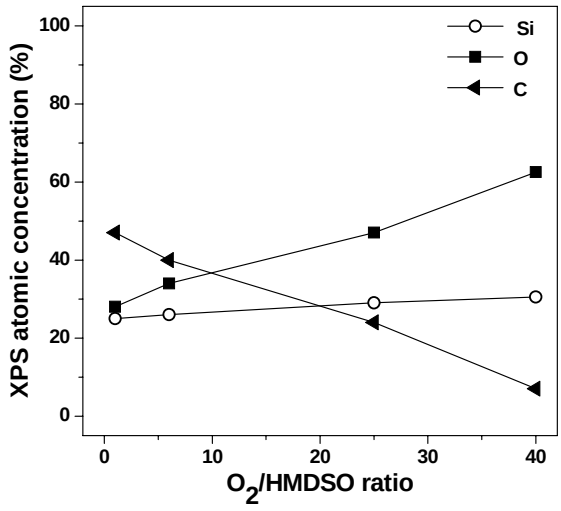

Figure 5.2.5: *XPS atomic concentrations as a function of the O_2 content in the feed.*

The XPS analyses of the coatings deposited in the discharge (Figure 5.2.5) confirm that by increasing the O_2-to-HMDSO ratio the carbon content decreases. The O/Si ratio at O_2/HMDSO = 25 is 2.05. The static, advancing and receding Water Contact Angles are shown in Figure 5.2.6. Static WCA decrease from 105° to 60° as a function of coating composition.

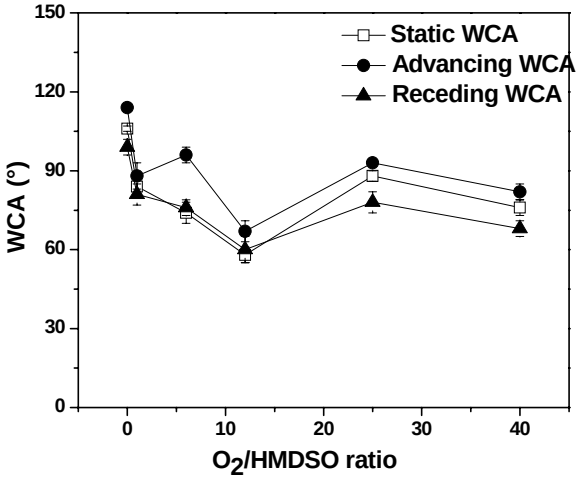

Figure 5.2.6: *Static, advancing and receding WCA as a function of the O_2 content in the feed.*

SEM images (Figure 5.2.7) show that quite smooth coatings are obtained up to an O_2-to-HMDSO ratio of 25, while at higher O_2 content powders are englobed in the coating. At the O_2-to-HMDSO ratio of 6, bubbles (Figure 5.2.7c), probably due to a thermically induced film detachment from the substrate, are detected. Neither the chemical nor the morphological analyses of the coatings explain the observed WCA trend: other surface effects could be involved.

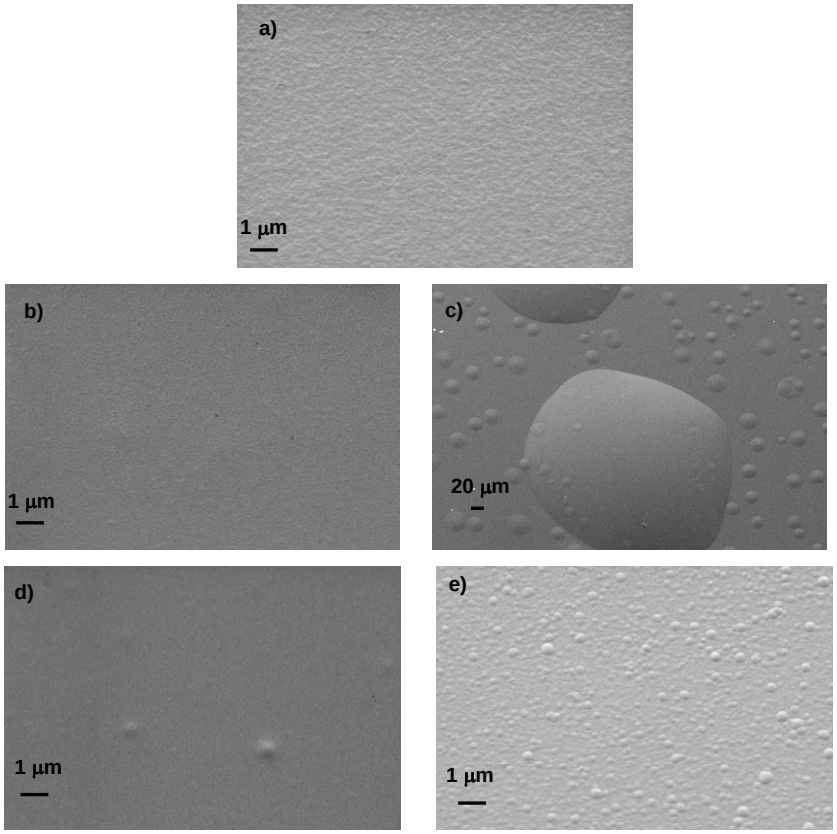

Figure 5.2.7: *SEM images of the coatings deposited at different O_2/HMDSO ratios: a) O_2/HMDSO = 1; b-c) O_2/HMDSO = 6: b) is the smooth surface among the bubbles in figure c); d) O_2/HMDSO = 25; e) O_2/HMDSO = 40.*

5.3 PMDSO/Ar/O_2 DBDs

5.3.1 Effect of gas residence time

Also with PMDSO containing feeds transparent and compact coatings were deposited, but in this case no oily films were obtained, and at high O_2 content in the feed an appreciable powder formation is detected in the discharge zone in the 2-6 mm region from the gas entrance. Abundant powder formation occurred also downstream the discharge zone as O_2 is added to the gas feed.

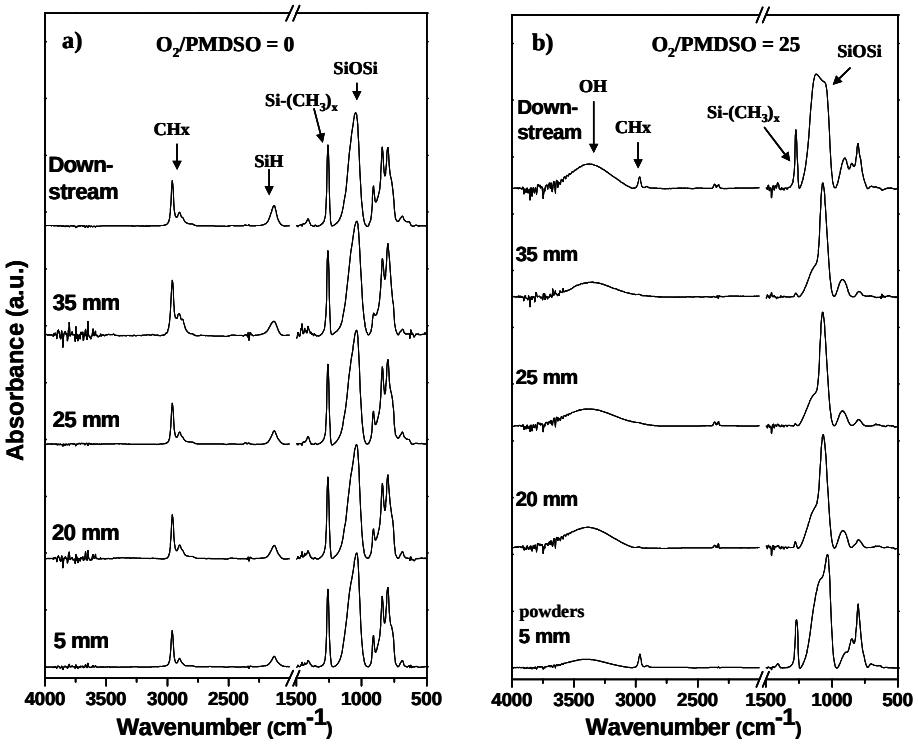

Figure 5.3.1: *FT-IR spectra of plasma-polymerized coatings obtained at different positions of the electrode region at a) O_2/PMDSO = 0 and b) O_2/PMDSO = 25.*

Also with Ar/PMDSO/O_2 the deposition process is affected by the gas injection system and a variation of film chemical composition and thickness are registered along

the gas flow direction. The FT-IR spectra, recorded at different gas residence time from the gas entrance and in downstream position, at O_2/PMDSO = 0, 25 (Figure 5.3.1a-b), show similar trend than for Ar/HMDSO/O_2. Without O_2 no variation can be observed in the discharge zone, while a chemical evolution from a silicone-like coating at the gas entrance, where powders are obtained, to a silica-like coating at the end of the discharge, is detected at O_2-to-PMDSO feed ratio of 25. XPS analyses confirm the carbon content decrease up to 2 % at increasing gas residence time. As for HMDSO, the powders collected in the downstream position are characterized by typical organic FT-IR spectra.

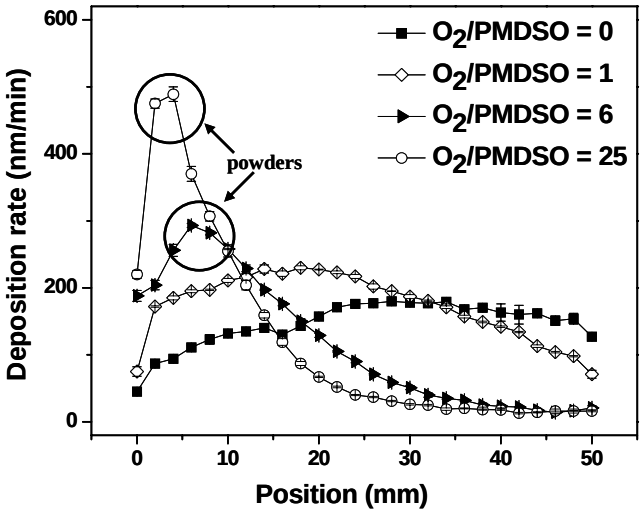

Figure 5.3.2: *Deposition rate profiles as a function of the position in the discharge area at different O_2/PMDSO ratio.*

The deposition rate profiles of Figure 5.3.2 show as the O_2 addiction to the feed affects the deposition rate along the flow direction.

5.3.2 Effect of the gas feed composition

The effect of the gas feed composition on the deposition rate was considered in the region centred at 25 mm from the gas entrance. In this case Figure 5.3.3 shows that the O_2 content significantly affects the deposition rate with a maximum of 200 nm·min^{-1} at O_2/PMDSO = 1.

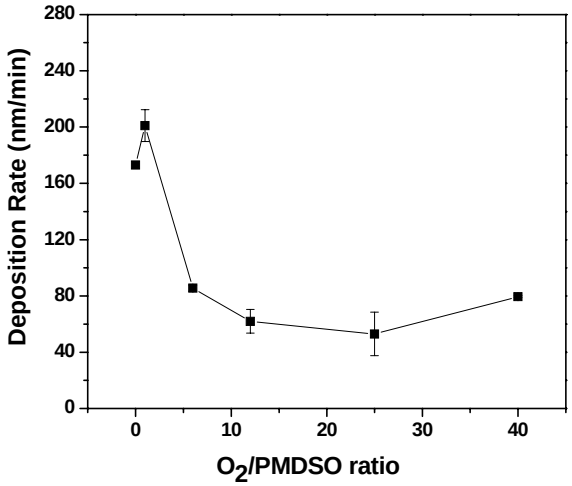

Figure 5.3.3: *Average deposition rate in the 20-30 mm region in the discharge area as a function of the O_2/PMDSO ratio.*

As expected, also the film composition significantly varies with oxygen addition, as shown by the FT-IR spectra of Figure 5.3.4, where also the deposit in downstream position are reported for comparison (Figure 5.3.4b).

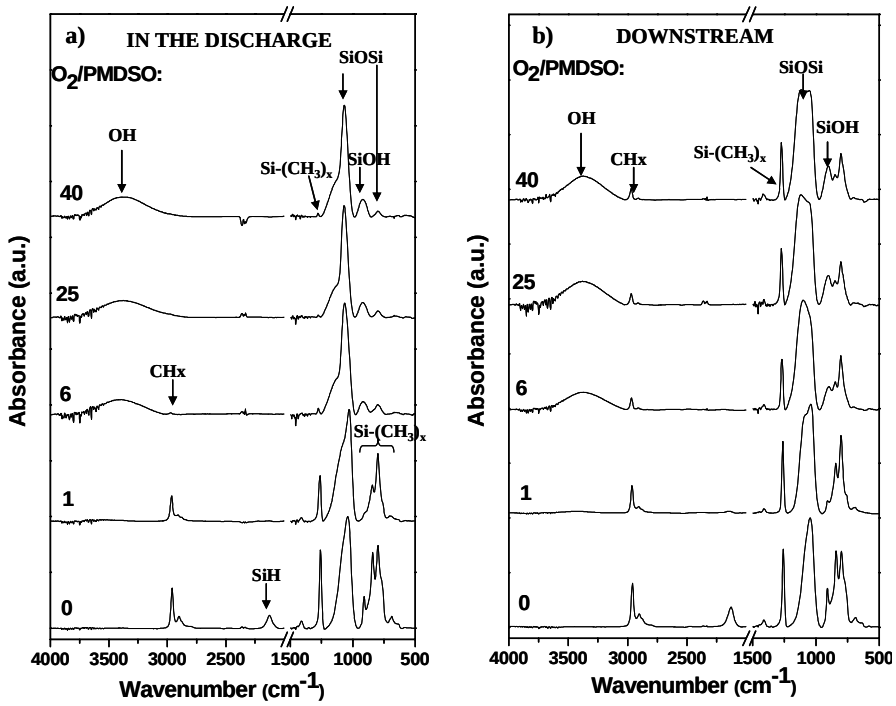

Figure 5.3.4: *a) FT-IR spectra of coatings at different O_2/PMDSO ratios; b) FT-IR spectra downstream of the electrode region.*

The coatings deposited in the discharge zone without oxygen show the same typical features of silicone-like films as found for Ar/HMDSO (see section 5.2.2); few differences can be evidenced respect to Figure 5.2.4a. The intensity of the absorptions at 841 cm^{-1}, assigned to the Si-C rocking in Si-$(CH_3)_3$, reduces, while the intensity of the signal at 798 cm^{-1}, due to Si-C rocking in Si-$(CH_3)_2$, enhances; a higher amount of Si-$(CH_3)_2$, chain-propagating units, is present due to the evident higher absorption at 909 cm^{-1}.

Increasing the O_2 content in the feed gas the absorptions of carbon containing groups decrease and almost disappear at O_2-to-PMDSO ratios higher than 6. The signal of Si-H disappears, while the broad OH absorption increases, along with the Si-OH signal at 920 cm^{-1}. The intense Si-O-Si asymmetric stretching moves to higher wavenumbers, up to 1068 cm^{-1} at O_2/PMDSO = 40, as in SiO_2-like films. The intense shoulder at

1087 cm^{-1} at O_2/PMDSO = 1 reduces and moves to 1140 cm^{-1} at higher O_2-to-PMDSO ratios, indicating the presence of short Si-O-Si chains or caged structure in the coating [3-5].

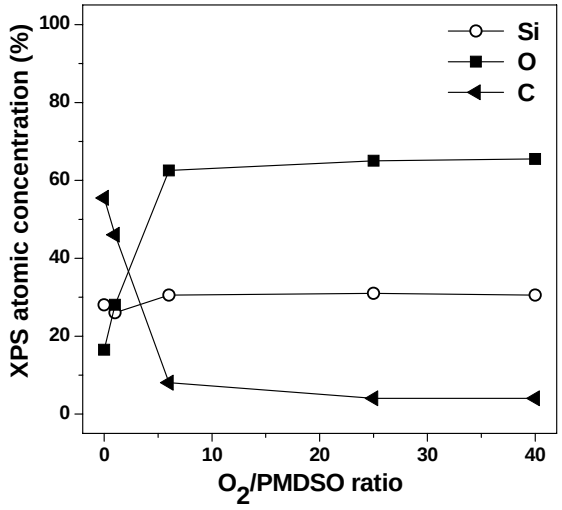

Figure 5.3.5: *XPS atomic concentrations as a function of the O_2 content in the feed.*

The trend in the downstream position (Figure 5.3.4b) is the same than with HMDSO. The XPS confirm the carbon content decrease from 55 % to 4 % with O_2 addition to the feed (Figure 5.3.5); at O_2/PMDSO = 6 the O/Si ratio is higher than 2 (2.15), probably for the presence of Si-OH groups.

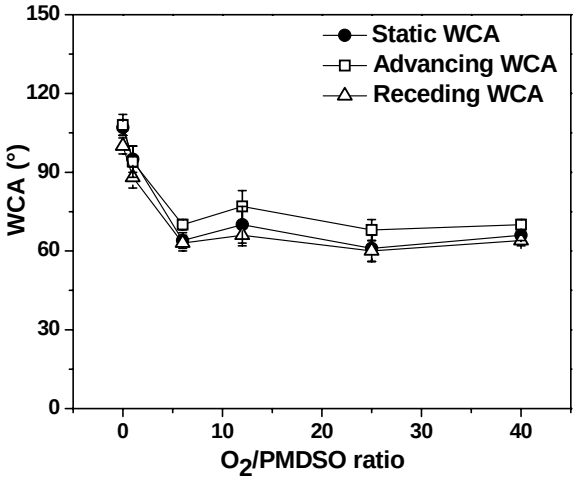

Figure 5.3.6: *Static, advancing and receding WCA as a function of the O_2 content in the feed.*

Static, advancing and receding WCA are reported in Figure 5.3.6. Static WCA decreases from 107° to 65° as a function of the carbon content in the film. Quite smooth coating are obtained at low O_2/PMDSO ratio, while for ratios higher than 25 powders are englobed in the coating (Figure 5.3.7). As found with HMDSO, at the O_2-to-PMDSO ratio of 6 bubbles (Figure 5.3.7c) are observed.

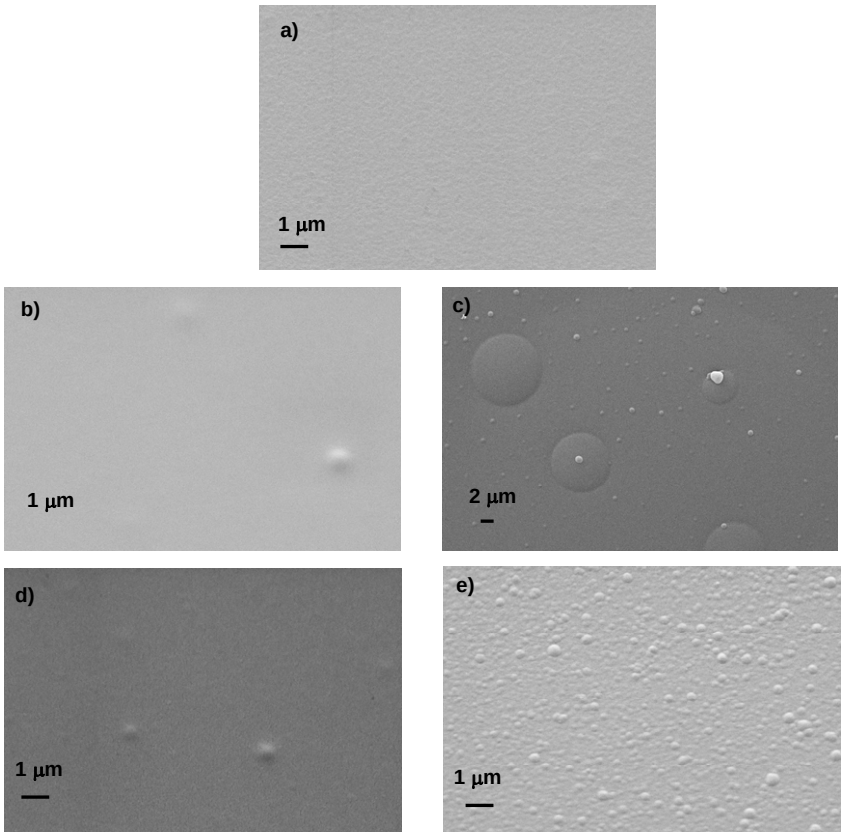

Figure 5.3.7: *SEM images of the deposited coatings at different O_2/PMDSO ratios: a) O_2/PMDSO = 1; b-c) O_2/PMDSO = 6: b) is the smooth surface among the bubbles in figure c); d) O_2/PMDSO = 25; e) O_2/PMDSO = 40.*

5.4 TMDSO/Ar/O_2 DBDs

5.4.1 Effect of gas residence time

Also with TMDSO containing feeds transparent and compact coatings were deposited; as O_2 is added to the feed an appreciable powder formation in the discharge zone, in the 2-6 mm region from the gas entrance, was detected. Also with TMDSO a great amount of powders was observed in the downstream position out of the discharge zone.

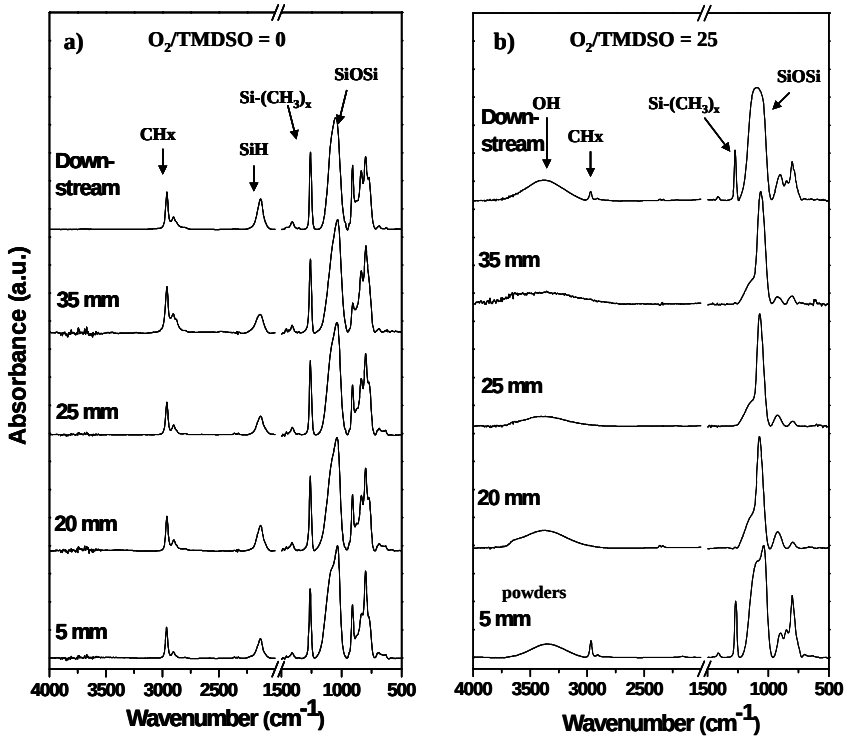

Figure 5.4.1: *FT-IR spectra of plasma-polymerized coatings obtained at different positions of the electrode region at a) O_2/TMDSO = 0 and b) O_2/TMDSO = 25.*

Also with TMDSO the gas injection system affects the chemical composition and the thickness of the coatings along the gas flow direction. The FT-IR spectra, recorded

at different gas residence time from the gas entrance and in downstream position, at O_2/TMDSO = 0, 25 (Figure 5.4.1a-b), show a similar behaviour than for HMDSO and PMDSO. As for PMDSO, the powders obtained at short gas residence time and the deposit collected in the downstream position at O_2/TMDSO = 25 have a silicone-like character.

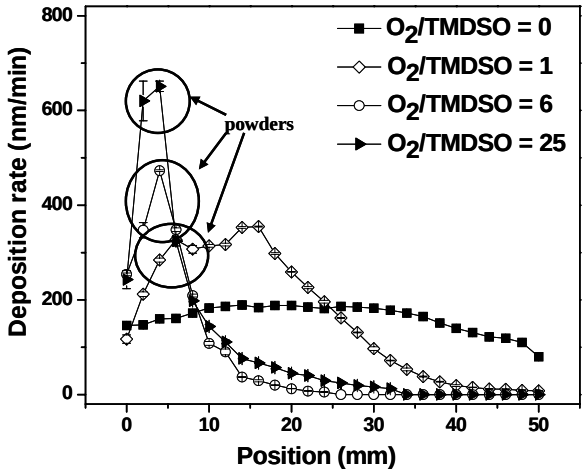

Figure 5.4.2: *Deposition rate profiles as a function of the position in the discharge area at different O_2/TMDSO ratio.*

The oxygen addition to the feed affects the deposition rate along the flow direction: the deposition rate profiles at different O_2-to-TMDSO feed ratio (Figure 5.4.2) show a similar trend than for PMDSO.

5.4.2 Effect of the feeding gas composition on deposited films

As for the other two precursors the effect of the O_2-to-TMDSO ratio was considered in the region centred at 25 mm from the gas entrance. As for PMDSO, the O_2 content significantly affects the deposition rate (Figure 5.4.3), with a maximum value of 170 nm·min^{-1} at O_2/PMDSO = 0. Also the film composition significantly varies with oxygen addition to the feed, as shown by the FT-IR spectra of Figure 5.4.4a; the deposit in downstream position are reported for comparison in Figure 5.4.4b.

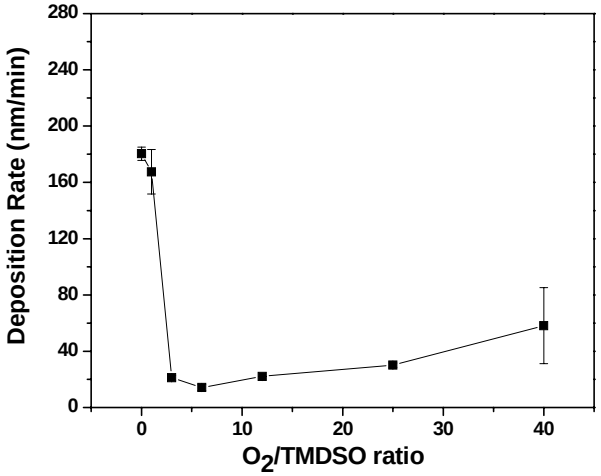

Figure 5.4.3: *Average deposition rate in the 20-30 mm region in the discharge area as a function of the O_2/TMDSO ratio.*

As found for HMDSO and PMDSO, without oxygen in the gas feed a silicone-like coating is deposited. Some differences can be noticed in the 700-900 cm^{-1} region: strong absorptions due to the Si-C rocking in Si-$(CH_3)_2$ are observed at 909 cm^{-1} and 798 cm^{-1}; more intense H-Si-O hybrid vibrations contribute to the signals at 835 and 770 cm^{-1} (the last one is also due to the Si-C rocking in Si-$(CH_3)_3$).

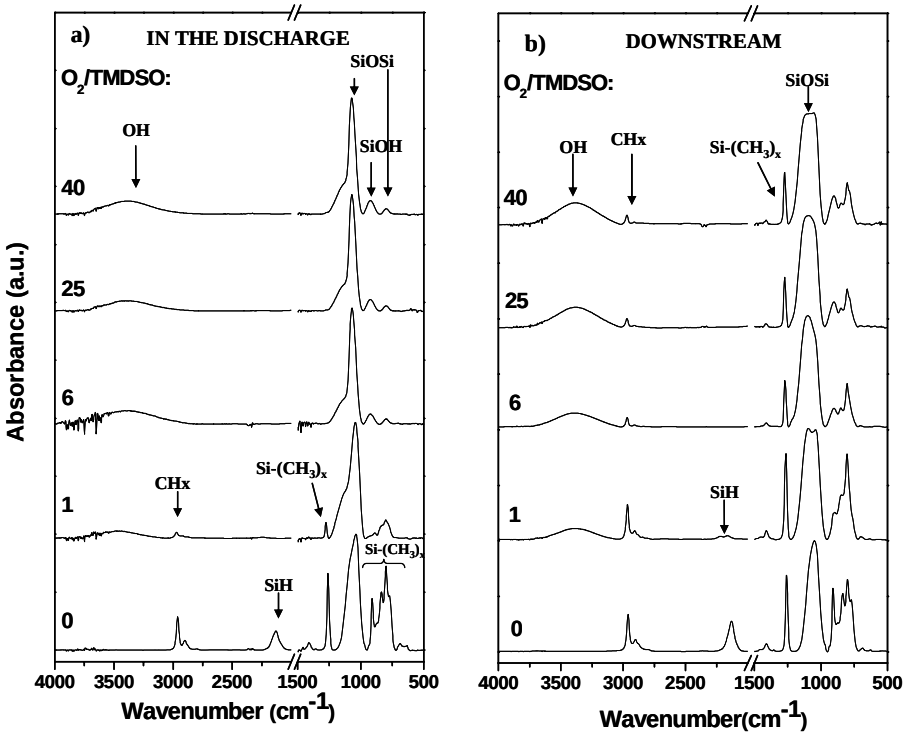

Figure 5.4.4: *a) FT-IR spectra of plasma-polymerized coatings obtained in the central region of the discharge zone at different O_2/TMDSO ratios; b) FT-IR spectra of the relative deposits obtained downstream of the electrode region.*

As O_2 is added to the gas feed the absorptions of carbon containing groups completely disappear at O_2-to-PMDSO ratios higher than 1; as confirmed also by the intense Si-O-Si asymmetric stretching at 1070 cm^{-1}, silica-like films are obtained. As for HMDSO and PMDSO, the Si-H signal disappears, while the OH absorptions increase; anyway, weaker OH signals and features at 3650 cm^{-1}, due to free Si-OH, not hydrogen-bonded to other Si-OH groups, are observed [4, 18].

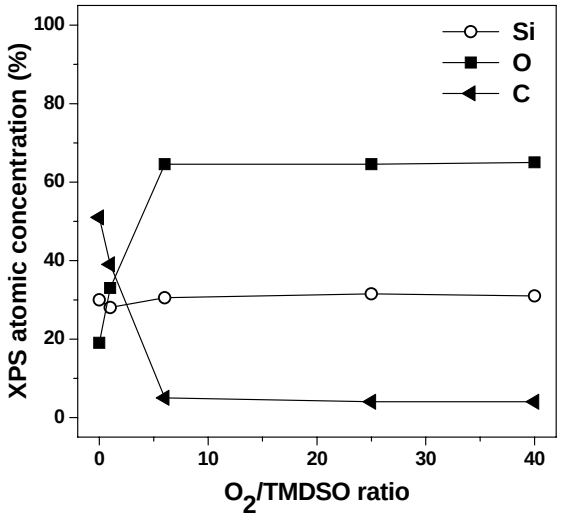

Figure 5.4.5: *XPS atomic concentrations as a function of the O_2 content in the feed.*

The same trend than with HMDSO and PMDSO is observed for the FT-IR spectra in downstream position (Figure 5.4.4b). XPS analyses (Figure 5.4.5) confirm the carbon content decrease from 50 % to 4 % with O_2 addition to the feed; an O/Si ratio higher than 2 (2.12), for the presence of Si-OH groups, was obtained for the silica-like coatings.

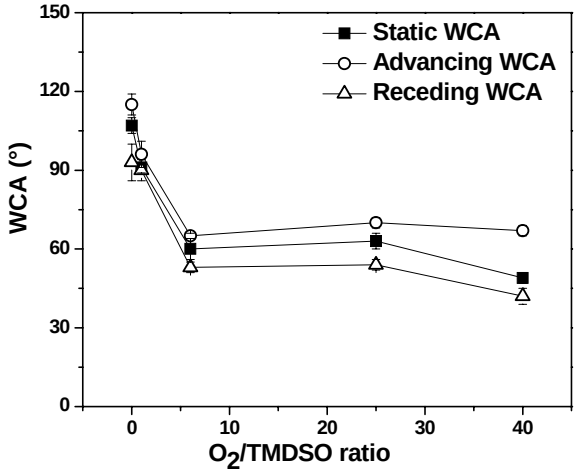

Figure 5.4.6: *Static, advancing and receding WCA as a function of the O_2 content in the feed.*

Static, advancing and receding WCA are shown in Figure 5.4.6. As for PMDSO, static WCA decreases from 107° to 50° at increasing O_2 content in the feed. Differently from the other two precursors grainy coatings, due to englobed powders, are obtained also at low O_2 content in the feed (Figure 5.4.7); the bubbles observed in the HMDSO and PMDSO coatings, are always present at O_2-to-TMDSO ratios higher than 6 (Figure 5.4.7 b-d).

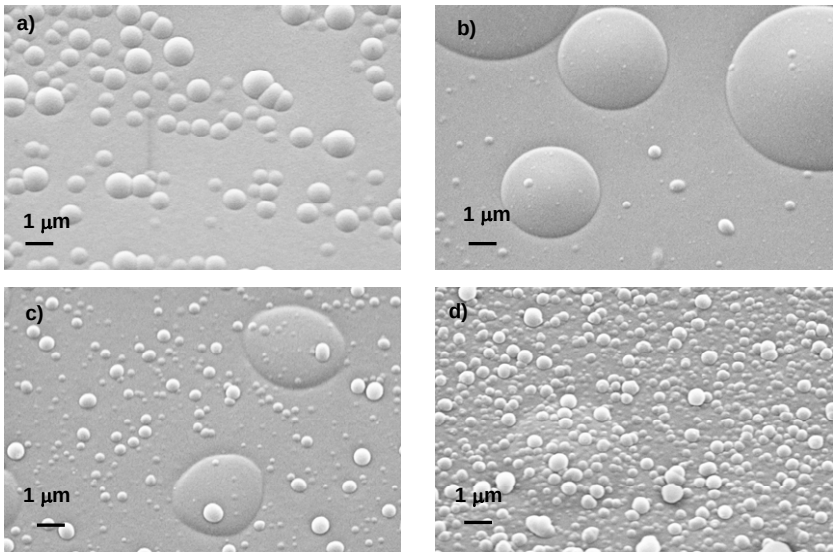

Figure 5.4.7: *SEM images of the deposited coatings at different O_2/TMDSO ratios: a) O_2/TMDSO = 1; b) O_2/TMDSO = 6; c) O_2/TMDSO = 25; d) O_2/TMDSO = 40.*

5.5 Discussion

The results presented in the previous sections show that, under the adopted experimental conditions, organosilicon thin films with tuneable properties can be deposited. The FT-IR spectra of the coatings obtained without O_2 suggest the deposition of poorly crosslinked coating with high structure retention of the starting monomer. The addition of O_2 to the feed affects the deposition process of the investigated disiloxanes in a different way. With HMDSO an appreciable amount of residual carbon is still present in the deposit, also at high O_2 content in the gas feed. With PMDSO the residual amount of residual carbon is lesser and it completely disappears with TMDSO. The FT-IR spectra of coatings deposited at a stoichiometric O_2-to-monomer ratio (Figure 5.5.1), i.e. O_2/HMDSO = 12, O_2/PMDSO = 10.5 and O_2/TMDSO = 9, clearly show that more oxidized coatings are obtained as the number of methyl units reduces in the precursor (TMDSO > PMDSO > HMDSO): only with TMDSO completely oxidized

coatings were obtained. The strong reduction of organic moieties could also explain the decrease of the deposition rate observed for PMDSO and TMDSO.

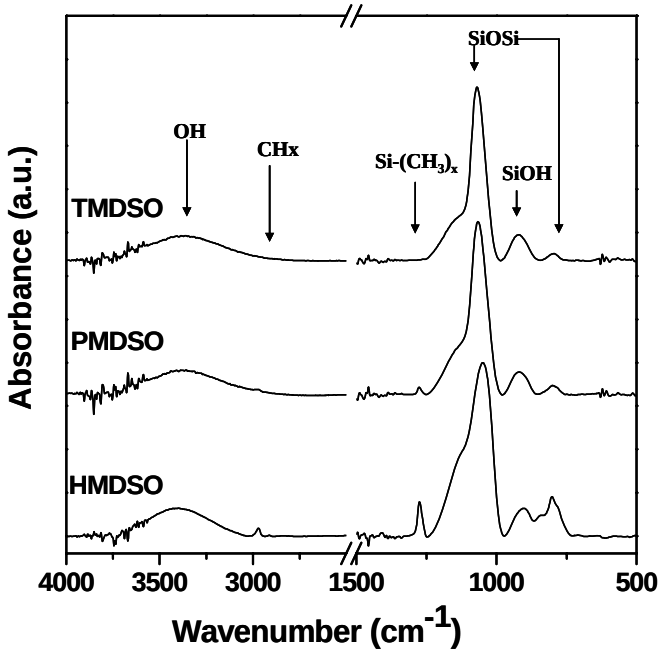

Figure 5.5.1: *FT-IR spectra of plasma-polymerized coatings obtained in the central region of the discharge zone at each O_2/Monomer stoichiometric ratio.*

The maxima observed in the trend of deposition rate as a function of the position in the discharge for the three precursors suggest that O_2 promotes the monomer fragmentation at the gas inlet, where organic coatings are obtained, and oxidation reactions at increasing gas residence time [19-20]; a contribution of the increasing power input to the enhanced fragmentation cannot be excluded. Thicker and dusty coatings were deposited at the entrance as more Si-H units are in the starting precursor: in comparable experimental conditions (i.e. same O_2/monomer ratio and similar power input) TMDSO seems more reactive than PMDSO and HMDSO. Morphological investigations support this statement as powders were always detected in the TMDSO

coatings, accounting for gas-phase nucleations occurring also in the discharge zone [21-22].

On the contrary in HMDSO and PMDSO fed discharges dusty coatings are obtained only at exceeding O_2 content (O_2-to-monomer = 40), while at lower O_2/monomer ratio powders were detected only downstream out of the discharge zone: since powders formation in the discharge zone has been reported for DBD fed with O_2 and HMDSO [23-24], it is reasonable to assume that under these experimental conditions, due to the high flow rate (i.e. low residence time) and the minor reactivity of HMDSO and PMDSO, if compared to TMDSO, the processes responsible for powder formation and deposition are scarcely efficient in the plasma zone.

REFERENCES

[1] U. Koghelschatz, *Plasma Chem. Plasma Process.* **2003**, *23*, 1.

[2] A. Fridman, A. Chirokov, A. Gustol, J. Phis. D: Appl. Phis. 38 (**2005**) R1-R24.

[3] A. Grill, D. A. Neumayer, J. Appl Phys, Vol. 94, No 10, 6697-6707, **2003.**

[4] A. Milella, J.L. Delattre, F. Palumbo, F. Fracassi, R. d'Agostino, J. Of Electrochemical Society, 153 (6) F106-F114 (**2006**).

[5] A. Milella, F. Palumbo, J.L. Delattre, F. Fracassi, R. d'Agostino, Plasma Process. Polym. **2007**, 4, 425-432.

[6] D. S. Wavhal, J. Zhang, M. L. Steen, E. R. Fisher, Plasma Process. Polym. **2006**, 3, 276-287.

[7] P. Supiot, C. Vivien, A. Granier, A. Bousquet, A. Mackova, D. Escaich, R. Clergereaux, P. Raynaud, Z. Stryhal, J. Pavlik, Plasma Process. Polym., **2006**, 3, 100-109.

[8] I. Vinogradov, D. Zimmer, A. Lunk, Plasma Process. Polym. **2007**, 4, S435-S439.

[9] I. Vinogradov, D. Zimmer, A. Lunk, *Plasma Process. Polym.* **2009**, *6*, DOI: 10.1002/ppap.200931102.

[10] C.Y. Wang, Z.H. Shen, Z.J. Zheng, Applied Spectroscopy, 54, 2, **2000**, 209-213.

[11] P. Raynaud, B. Despax, Y. Segui, H. Caquineau, Plasma Process. Polym. **2005**, 2, 45-52.

[12] Handbook of Plastic analyses, D. H. Lobo and J.V. Bonilla ed., **2003.**

[13] D.D. Burkey, K.K. Gleason, *Journal of The Electrochemical Society,* **2004**, 151 (5)**,** F105-F112.

[14] G. Lucovsky, J. Yang, S.S. Chao, J.E. Tyler, W. Czubatyi, Physical Review B, 28, 6, 3225-3233, **1983.**

[15] D.V. Tsu, G. Lucovsky, B.N.Davidson, Physical Review B, 40, 3, 1795-1805, **1989.**

[16] L. He, T. Inokuma, Y. Kurata, S. Hasegawa, Journal of Non-Crystalline Solids 185 (**1995**) 249-261.

[17] N.D. Gupta, P. Chaudhuri, Journal of Non-Crystalline Solids 289 (**2001**) 168-174.

[18] A. Milella, M. Creatore, M.A. Blauw, M.C.M. van de Sanden, Plasma Process. Polym. **2007**, 4, 621-628.

[19] I. Enanche, H Caquineau, N. Gherardi, T. Paulmier, L.Maechler, F. Massines, Plasma Process. Polym. **2007**, 4, 806-814.

[20] P.A. Premkumar, S.A. Starostine, H. de Vries, R.M.J. Paffen, M. Creatore, T.J. Eijkemans, P.M. Koenraad, M. van de Sanden, Plasma Process. Polym. **2009**, 6, 693-702.

[21] L.J. Ward, W.C.E. Schofield, J.P.S. Badyal, A.J. Goodwin, P.J. Merlin, Langmuir **2003**, 19, 2110-2114.

[22] L. O'Neill, L.-A O'Hare, S.R. Leadley, A.J. Goodwin, Chem. Vap. Deposition **2005**, 11, 477-479.

[23] K. Schmidt-Szalowski, Z. Rżanek-Boroch, J. Sentek, Z. Rymuza, Z. Kusznierewicz, M. Misiak, *Plasmas Polym.* **2000**, *5*, 173.

[24] S. Starostine, E. Aldea, H. de Vries, M. Creatore, M. C. M. van de Sanden, *Plasma Process. Polym.* **2007**, *4*, S440.

CHAPTER 6: RESULTS AND DISCUSSION: GAS PHASE ANALYSIS BY GC-MS INVESTIGATION

6.1 Optimization of the method

For a correct quantification of the amount of residual monomer the sampling yield of the liquid nitrogen trap was preliminarily evaluated. The effective flow rate of precursor injected into the reactor, was evaluated for each monomer by the reservoir weight variation per unit time (see section 4.3). The effective flow rate was than compared to the flow rate evaluated by sampling the precursors contained in the exhaust in plasma off condition and GC-MS analysis. As shown in Figure 6.1.1, it was found that the sampling yield increases at low flow rates and is the 100 % for precursor flow rates lower than 0.03 sccm. Under the working condition selected (1 sccm) the sampling yields is 29 % for HMDSO, 21 % for PMDSO and 28 % for TMDSO.

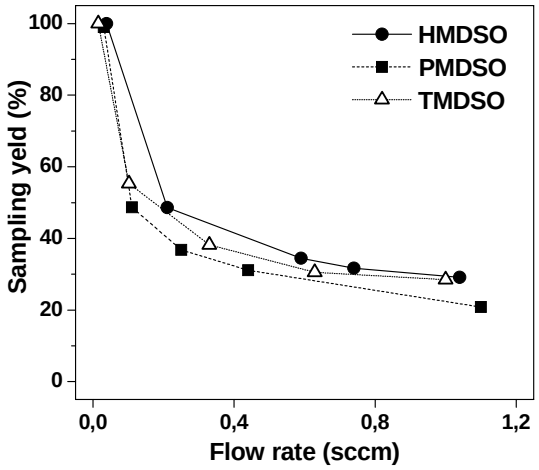

Figure 6.1.1: *Liquid nitrogen trap sampling yield as a function of the real precursors flow rate.*

The relation between real (Φ) and detected ($\Phi_{cold\ trap}$) flow rate can be expressed by equation 6.1.1. The constants A, B and C are reported for each precursor in Figure 6.1.2

$$\Phi_{\text{cold trap}} = A \cdot \exp(-\Phi/B) + C \qquad \text{eq. 6.1.1}$$

These calibration curves allows to calculate the real flow rates of HMDSO, PMDSO and TMDSO in the exhausts under plasma on conditions. Since the flow rates of all other compound present in the exhaust are lower than 0.01 sccm, a 100 % sampling yield was safely considered.

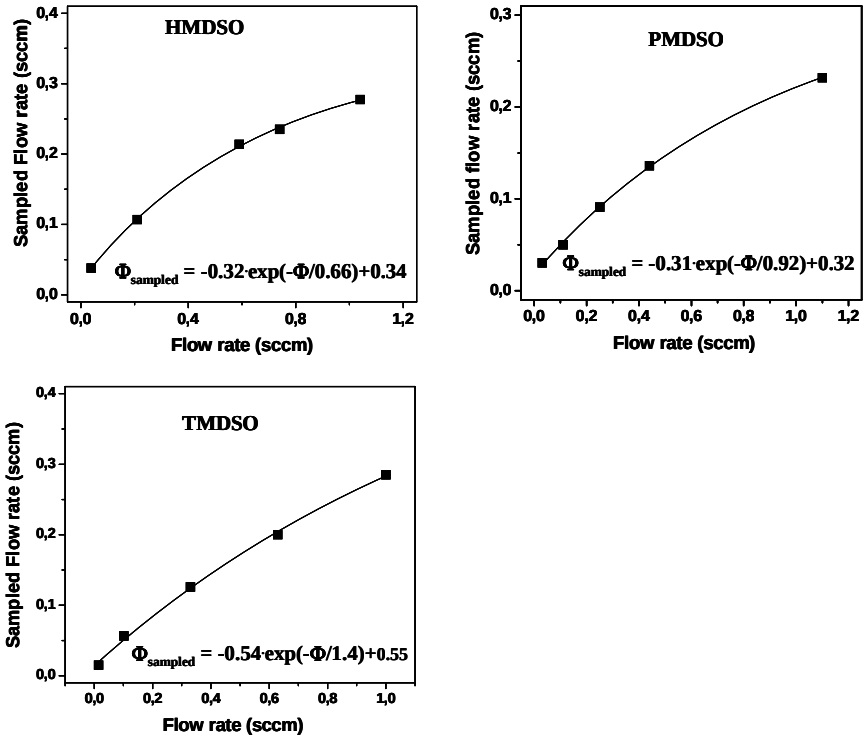

Figure 6.1.2: *Liquid nitrogen trap calibration curves evaluated for each precursor.*

6.2 Qualitative analysis of the exhaust

Typical chromatographic analyses of exhaust gas in Ar/HMDSO, Ar/PMDSO and Ar/TMDSO are shown in Figures 6.2.1, 6.2.2 and 6.2.3, respectively. Oxygen addition reduces the number of detectable species, even though a detectable amount of residual monomer is always present.

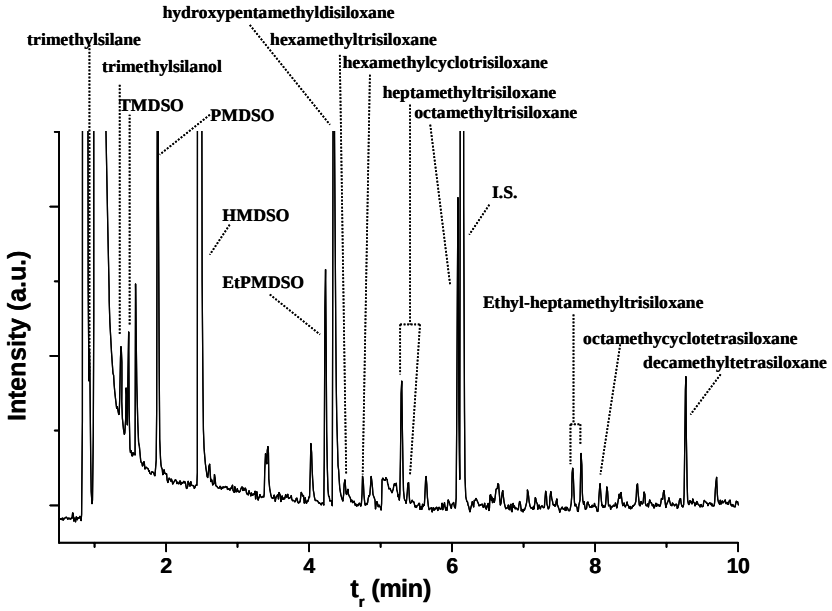

Figure 6.2.1: *Typical gaschromatogram of exhaust in Ar/HMDSO discharges.*

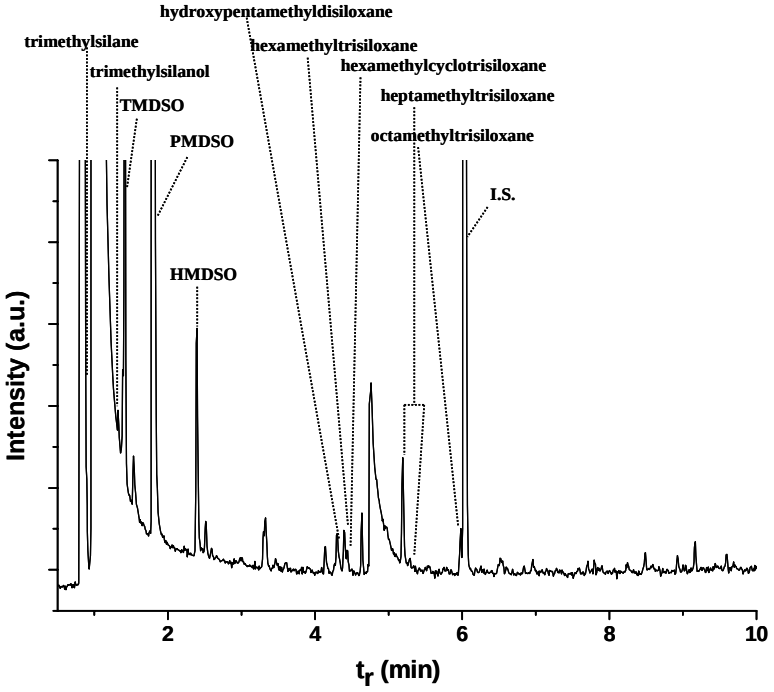

Figure 6.2.2: *Typical gaschromatogram of exhaust in Ar/PMDSO discharges.*

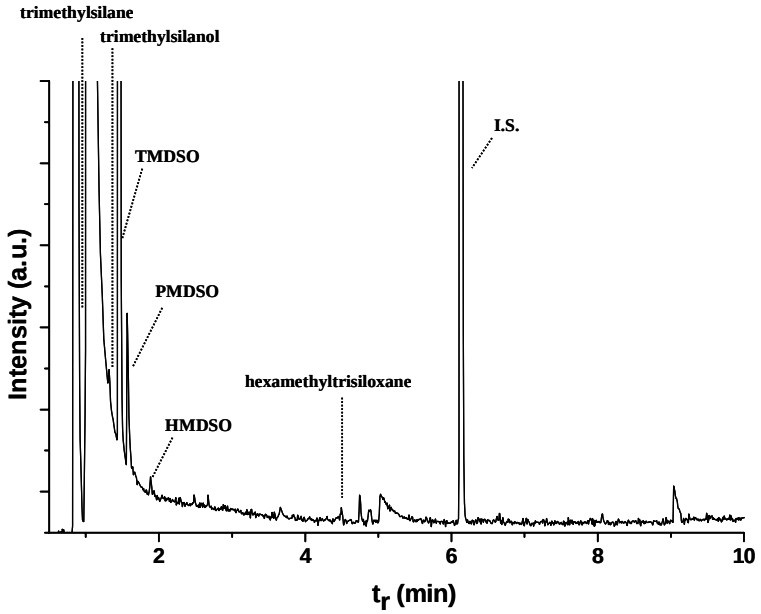

Figure 6.2.3: *Typical gaschromatogram of exhaust in Ar/TMDSO discharges.*

A list of the identified by-products detected in the exhaust gas is reported in Table 6.2.1: the number of detected species decreases with the number of $–CH_3$ units in the starting momomer (i.e. HMDSO>PMDSO>TMDSO). There are silanes with low molecular mass, (i.e. trimethysilane, tetramethylsilane ethyltrimethysilane), silanols (i.e. dimethylsilanol, trimethylsilanol and hydroxypentamethyldisiloxane) as well as linear and cyclic compounds with up to 5 silicon atoms and general formula $Me\text{-}(Me_2SiO)_n\text{-}SiMe_3$ (n = 1-4) and $(Me_2SiO)_n$ (n= 3-4), respectively, which derive from oligomerization processes: i.e. chain propagation and ring formation or expansion. As the Table 6.2.1 shows, heavier species were found only in the Ar/HMDSO exhaust, while in the Ar/PMDSO and Ar/TMDSO exhausts compounds with no more than 3 silicon atoms were detected. Considering the sampling procedure utilized, it seems reasonable to assume that heavier compounds (e.g. compounds containing more than five Si atoms) are not sampled for their low volatility, while light species (e.g., CO, CO_2, CH_4, SiH_4, etc.) are lost during manipulation of the condensate for their high volatility.

In agreement with FT-IR analyses of deposited films species containing one or two Si-H bonds and $-CH_2$ moieties (e.g. ethylpentamethyldisiloxanes) were also found in the Ar/HMDSO exhaust. These species could derive from the recombination of the active species formed by plasma activation; these recombination reactions could occur either in the plasma phase or outside the discharge zone and could involve both ionic and neutral species (such as radicals) leading to the stable products retained by the cold trap. On the contrary neither Ar/PMDSO nor Ar/TMDSO exhausts contain species with $-CH_2$ moieties, while, in spite of the reduced number of identified compounds, the presence of the Si-H unit was expected as it is contained in the starting precursors.

Table 6.2.1: *Identified species detected in the exhaust gas of Ar/HMDSO/O_2, Ar/PMDSO/O_2 and Ar/TMDSO/O_2 fed DBD.*

Compound	Formula	HMDSO	PMDSO	TMDSO
Trimethylsilane	$(CH_3)_3SiH$	✓	✓	✓
Tetramethylsilane	$(CH_3)_4Si$	✓	✓	✓
Dimethylsilanol	$(CH_3)_2HSiOH$		✓	✓
Trimethylsilanol	$(CH_3)_3SiOH$	✓	✓	
Ethyltrimethylsilane	$C_2H_5Si(CH_3)_3$	✓		
1,1,3,3-Tetramethydisiloxane	$(CH_3)_2HSi\text{-}O\text{-}SiH(CH_3)_2$	✓	✓	✓
Pentamethyldisiloxane	$(CH_3)_2HSi\text{-}O\text{-}Si(CH_3)_3$	✓	✓	✓
Hexamethyldisiloxane	$(CH_3)_3Si\text{-}O\text{-}Si(CH_3)_3$	✓	✓	✓
Ethylpentamethyldisiloxane	$(CH_3)_3SiOSi(CH_3)_2C_2H_5$	✓		
Hydroxypentamethyldisiloxane	$(CH_3)_3Si\text{-}O\text{-}Si(CH_3)_2OH$	✓	✓	
1,1,3,3,5,5,5-hexamethyltrisiloxane	$(CH_3)_2HSi\text{-}O\text{-}Si(CH_3)_2\text{-}O\text{-}SiH(CH_3)_2$	✓	✓	✓
Hexamethycycloltrisiloxane	$(SiO(CH_3)_2)_3$	✓	✓	
1,1,1,3,5,5,5-heptamethyltrisiloxane	$(CH_3)_3Si\text{-}O\text{-}Si(CH_3)H\text{-}O\text{-}Si(CH_3)_3$	✓	✓	
1,1,1,3,3,5,5-heptamethyltrisiloxane	$(CH_3)_3Si\text{-}O\text{-}Si(CH_3)_2\text{-}O\text{-}SiH(CH_3)_2$	✓	✓	
Octamethyltrisiloxane	$(CH_3)_3Si\text{-}O\text{-}Si(CH_3)_2\text{-}O\text{-}Si(CH_3)_3$	✓	✓	
1-Ethyl-1,1,3,3,5,5,5-heptamethyltrisiloxane	$C_2H_5\text{-}(Si(CH_3)_2O)_2\text{-}Si(CH_3)_3$	✓		
3-Ethyl-1,1,1,3,5,5,5-heptamethyltrisiloxane	$(CH_3)_3Si\text{-}O\text{-}Si(CH_3)(C_2H_5)\text{-}O\text{-}Si(CH_3)_3$	✓		
Octamethycycloltetrasiloxane	$(SiO(CH_3)_2)_4$	✓		
1,1,1,3,3,5,7,7,7-Nonamethyltetrasiloxanes	$CH_3\text{-}(Si(CH_3)_2O)_2 - Si(CH_3)H\text{-}O\text{-}Si(CH_3)_3$	✓		
1,1,1,3,3,5,5,7,7-Nonamethyltetrasiloxanes	$CH_3\text{-}[Si(CH_3)_2O]_3\text{-}Si(CH_3)_2H$	✓		
Decamethyltetrasiloxane	$(CH_3)_3Si\text{-}O\text{-}[Si(CH_3)_2]O]_2\text{-}Si(CH_3)_3$	✓		
2,2,4,4,5,5, 7-octamethyl-3,6-dioxa-2,4,5,7-tetrasilaoctane	$(CH_3)_3Si\text{-}O\text{-}Si(CH_3)_2\text{-}Si(CH_3)_2\text{-}O\text{-}SiH(CH_3)_2$		✓	
2,2,4,4,5,5, 7,7-octamethyl-3,6-dioxa-2,4,5,7-tetrasilaoctane	$(CH_3)_3Si\text{-}O\text{-}Si(CH_3)_2\text{-}Si(CH_3)_2\text{-}O\text{-}Si(CH_3)_3$	✓	✓	
Dodecamethypentasiloxane	$(CH_3)_3Si\text{-}O\text{-}[Si(CH_3)_2]O]_3\text{-}Si(CH_3)_3$	✓		

6.3 Quantitative analysis of the exhaust

6.3.1 Monomer depletion

Figure 6.3.1 shows that under all the explored experimental condition, apart slight differences among the three precursors, the amount of reacted monomer (see section 4.5.1) was always higher than 50 %.

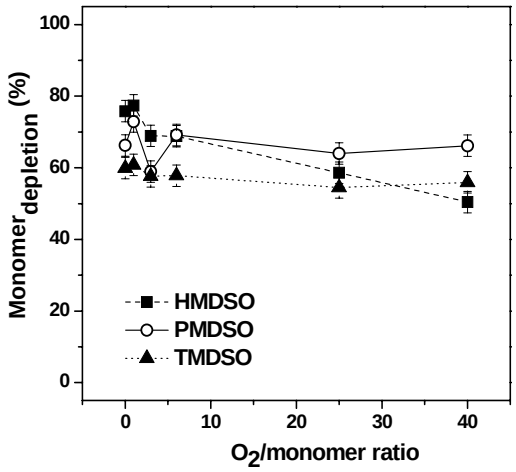

Figure 6.3.1: *Reacted HMDSO, PMDSO and TMDSO ($Monomer_{depletion}$) trend in the exhaust as a function of the O_2/HMDSO, O_2/PMDSO and O_2/TMDSO ratios in the feed, respectively.*

The oxygen addition to the gas feed does not improve the monomer activation/utilization since its depletion is always lower than without oxygen for HMDSO, or remains almost constant for PMDSO and TMDSO.

6.3.2 Quantification of silane and siloxane by-products

In the exhausts of all the three monomers the concentrations of the lowest molecular weight identified species (i.e. trimethylsilane and tetramethylsilane) decrease below the quantification limit increasing the O_2 content in the feed. As shown in Figure 6.3.2 very low amounts were detected in the PMDSO and TMDSO exhausts without O_2 in the feed if compared with the analogue from HMDSO discharges.

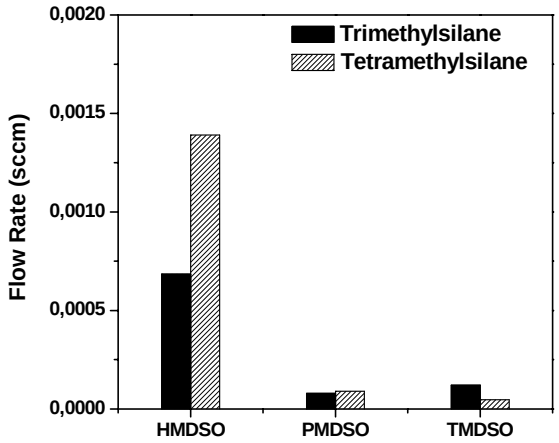

Figure 6.3.2: *Trimethylsilane and tetramethylsilane flow rate in the exhaust gas for Ar/HMDSO, Ar/PMDSO and Ar/TMDSO discharges.*

As shown in Table 6.2.1 the exhaust of each monomer contains the other two investigated precursors as by-product. Figure 6.3.3 shows that independently on the starting monomer, disiloxanes concentration steeply decreases with oxygen addition to the gas feed.

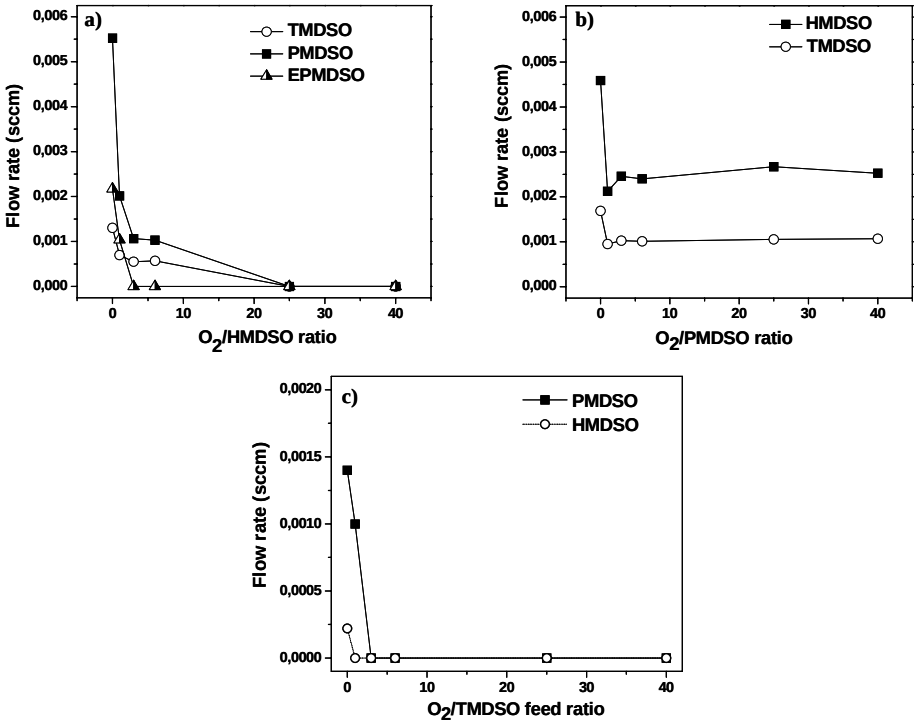

Figure 6.3.3: *Disiloxanes flow rate in the exhaust gas of each precursor as a function of the O_2/monomer ratio in the feed: a) TMDSO, PMDSO and ethylpentamethyldisiloxane (EPMDSO) flow rate in the exhaust gas as a function of the O_2/HMDSO ratio in the feed; b) HMDSO and TMDSO flow rate in the exhaust gas as a function of the O_2/PMDSO ratio in the feed; c) HMDSO and PMDSO flow rate in the exhaust gas as a function of the O_2/TMDSO ratio in the feed.*

Among the detected disiloxanes, pentamethyldisiloxane is the most abundant by-product both in HMDSO, where also the ethylpentamethyldisiloxane was taken into account, and in the TMDSO exhausts. On the other hand hexamethyldisiloxane and tetramethyldisiloxane do not decrease below the quantification limit at increasing O_2-to-PMDSO ratios.

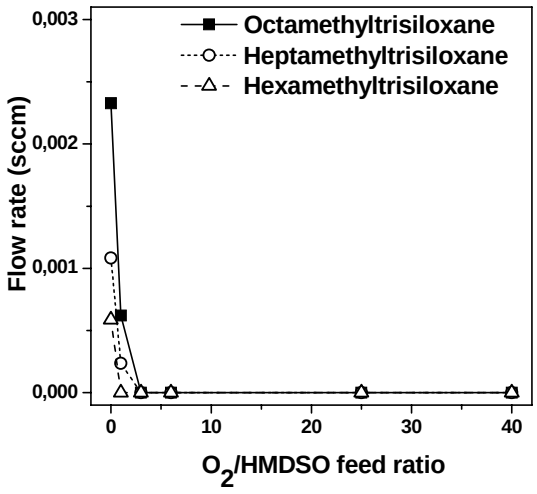

Figure 6.3.4: *Octamethyltrisiloxane, 1,1,1,3,5,5,5-heptamethyltrisiloxane and 1,1,3,3,5,5-hexamethyltrisiloxane flow rate in the exhaust gas as a function of the O_2/HMDSO ratio in the feed.*

Similarly methyltrisiloxanes concentrations decrease below the quantification limit increasing the O_2 content in the feed, as shown in Figure 6.3.4 for the HMDSO exhaust. Moreover it was observed that the relative abundance of trisiloxanes in the exhausts depends on the chemical composition of the starting monomer (Figure 6.3.5). With HMDSO the trisiloxane concentration is higher as the number of methyl groups in the molecule increases (i.e. octamethyltrisiloxane > 1,1,1,3,5,5,5-heptamethyltrisiloxane > 1,1,3,3,5,5-hexamethyltrisiloxane); with PMDSO, 1,1,1,3,5,5,5-heptamethyltrisiloxane, containing one Si-H bond, is the most abundant, while with TMDSO, although below the quantification limit, only 1,1,3,3,5,5-hexamethyltrisiloxane, containing two Si-H bonds, was detected.

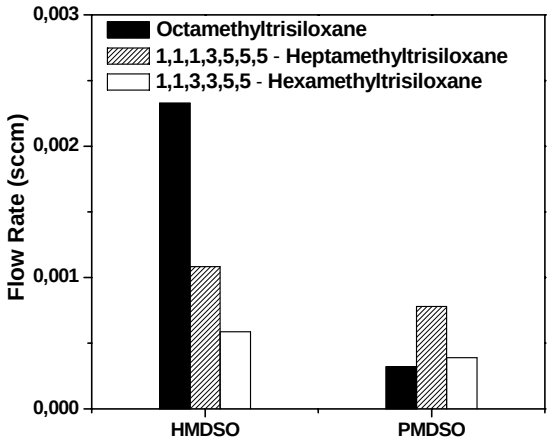

Figure 6.3.5: *Octamethyltrisiloxane, 1,1,1,3,5,5,5-heptamethyltrisiloxane and 1,1,3,3,5,5-hexamethyltrisiloxane flow rate in the exhaust gas of Ar/HMDSO and Ar/PMDSO discharges.*

6.3.3 Quantification of silanol by-products

In the exhaust of HMDSO containing plasma also the silanol (trimethylsilanol and hydroxypentamethyldisiloxane) concentration decreases with oxygen addition (Figure 6.3.6a) but, unlike the other species, they can be quantified also at high O_2 addition, since they are never below the quantification limit of the analytical procedure. On the contrary with PMDSO, the amount of trimethylsilanol remains almost constant, while the hydroxypentamethyldisiloxane flow rate significantly increase with oxygen addition to the feed (Figure 6.3.6b).

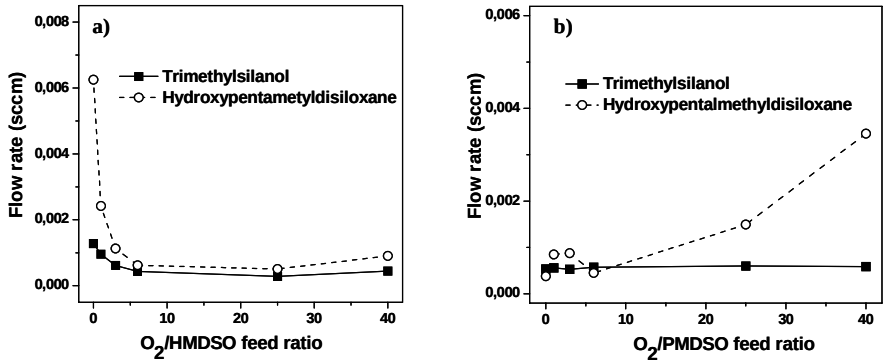

Figure 6.3.6: *Trimethylsilanol and hydroxypentamethyldisiloxane flow rate in the exhaust gas as a function of the a) O_2/HMDSO ratio, b) O_2/PMDSO ratio in the feed.*

6.4 Discussion

The results presented in the previous sections, in comparison with that shown in chapter 5, allow to make some hypothesis about the reactions occurring in the plasma phase and the deposition mechanism.

The list of by-products detected in the exhausts of the three monomers, compared with the FT-IR spectra of the deposited coatings discussed in the chapter 5, suggests that oligomerization could proceed mainly through condensation of precursors with a chemical structure close to that of the starting monomer, i.e. the pentamethyldisiloxanyl ($(CH_3)_3Si\text{-}O\text{-}Si(CH_3)_2$) units in HMDSO and PMDSO fed discharges, the tetramethyldisiloxanyl ($(CH_3)_2SiH\text{-}O\text{-}Si(CH_3)_2$) unit in TMDSO fed discharges. As reported in published works on low pressure plasmas, [1-3] the main HMDSO fragmentation route occurs via the loss of a methyl unit. This reaction path is further supported by the experimental evidence that, in HMDSO-containing DBDs without oxygen addition to the feed, apart from the unreacted monomer, pentamethyldisiloxane, $(CH_3)_3Si\text{-}O\text{-}Si(CH_3)_2H$, and hydroxypentamethyldisiloxane, $(CH_3)_3Si\text{-}O\text{-}Si(CH_3)_2OH$ are the most abundant species in the exhaust. Both compounds could be formed from one HMDSO molecule, with replacing a methyl group with -H and -OH, respectively.

This indicate that under the experimental conditions utilized, Si-CH_3 bond breaking plays an important role in HMDSO activation and film growth [4-6].

As the Si-H bond is weaker than Si-CH_3, the first most probable fragmentation step for PMDSO and TMDSO is Si-H bond cleavage [7-9], but since fully methylate polysiloxanes (e.g. HMDSO) are present, also methyl units are lost and recombine with available dandling bonds. Due to the presence of silanes in the exhausts of all monomers, the breaking of the Si-O bond cannot be neglected.

The progressive reduced number and amount of detected by-products in the exhaust of the three precursors (HMDSO>PMDSO>TMDSO) confirm the higher reactivity for compounds with lower number of methyl units (TMDSO>PMDSO>HMDSO). The dramatic reduction of oligomerization products with oxygen addition, observed for all the precursors, is realistically due to the oxidation of oligomerizing species.

The hypothesis about oxidation reactions occurring at higher gas residence time in O_2 containing feeds, discussed in the chapter 5, is supported by the fact that the shape of the deposition rate profiles obtained at higher O_2-to-monomer ratios (see sections 5.2.1, 5.3.1 and 5.4.1) cannot be ascribed to a complete monomer utilization since some residual monomer is always contained in the exhaust. Moreover, the increase of input power (see section 5.1), detected as a function of the oxygen content in the feed, does not result in an increase of the monomer utilization, as shown by the trends of the monomer depletion.

The observed decrease of the HMDSO depletion with oxygen addition could be due to the increases of the filamentary character of the discharge: the plasma is less homogeneous, more concentrated in the filaments and, therefore, the effective plasma volume is smaller, thus resulting in a overall less efficient monomer activation. The variation of the discharge regime with input power does not seem to affect the PMDSO and TMDSO utilization.

The decrease of HMDSO depletion with oxygen addition could be also ascribed to the fact that oxygen is not responsible of the HMDSO activation (i.e. the first step of the overall reaction): as it was already reported for HMDSO in RF low pressure plasmas [10] electron impact could be the main activation channel. This is a quite debated point since other authors observed different trends [11-12]. Another possibility is that the monomer activation is due to Ar metastables which are also responsible of oxygen

activation and therefore, when the O_2 content of the feed increases, the monomer activation is reduced because Ar metastables are mainly involved in oxygen activation [13].

On the contrary, in the case of PMDSO- and TMDSO-containing DBDs, besides electron impact or Ar metastables, oxygen molecules or atoms could be also responsible of monomer activation because they reasonably react with the Si-H units in hydrogen abstraction or insertion reactions [14]. The contribution of these reaction could balance the decrease of monomer depletion related to the reduction of the effective plasma volume due to the enhanced filamentary regime; as a consequence the PMDSO and TMDSO depletion remains almost constant as a function of the oxygen content in this feed. The occurrence of reaction of oxygen molecules/atoms with PMDSO could be further supported by the increasing hydroxypentamethyldisiloxane flow rate at higher O_2-to-PMDSO feed ratios. The different hydroxypentamethyldisiloxane trend in the HMDSO and PMDSO gas phase accounts for a different hydroxypentamethyldisiloxane formation mechanism that involve the starting monomer in the PMDSO discharges, while the pentamethyldisiloxanyl unit, due to the methyl abstraction, in HMDSO discharges.

Apart the hydroxypentamethyldisiloxane behaviour in the PMDSO gas phase, the general silanols decrease with O_2 addition to the feed could depend on the fact that oxygen promotes both the formation of Si-OH units and the oxidation of organic fragments to form CO_2 and H_2O. If the trends of silanols in the HMDSO exhaust are compared with the FT-IR spectra of the deposits collected inside the discharge and downstream at high O_2/HMDSO ratios (see section 5.2), it can be observed that higher amounts of Si-OH were detected in the coating when the silanols content in the exhaust is very low; this evidence suggests that the formation of the Si-OH groups in the coatings occurs mainly on the film surface through heterogeneous reactions during the growth process. Without oxygen addition to the feed, although the quantity of silanols in the exhaust is maximum (Figure 6.3.6), no absorption of Si-OH groups can be detected in the FT-IR spectra of deposits collected both in the discharge zone and downstream (Figure 5.2.1a). This evidence allows to enhance the hypothesis that silanols formed in the plasma phase, even at high concentrations, are not incorporated in the growing coating. The same conclusion cannot be expressed for PMDSO coatings

where, due to the particular hydroxypentamethyldisiloxane trend, the contribution of the silanols produced in the plasma phase cannot be completely ruled out at high O_2 content in the feed.

REFERENCES

[1] M. R. Alexander, F. R. Jones, R. D. Short, *Plasmas Polym.* **1997**, *2*, 277.

[2] M. R. Alexander, F. R. Jones, R. D. Short, *J. Phys. Chem. B* **1997**, *101*, 3164.

[3] D. Magni, Ch. Deschenaux, Ch. Hollenstein, A. Creatore, P. Fayet, *J. Phys. D: Appl. Phys.* **2001**, *34*, 87.

[4] A. Sonnenfeld, T. M. Tun, L. Zajíčková, K. V. Kozlov, H. E. Wagner, J. F. Behnke, R. Hippler, *Plasmas Polym.* **2001**, *6*, 237.

[5] I. Vinogradov, D. Zimmer, A. Lunk, *Plasma Process. Polym.* **2007**, *4*, S435.

[6] I. Vinogradov, D. Zimmer, A. Lunk, *Plasma Process. Polym.* **2009**, *6*, DOI: 10.1002/ppap.200931102.

[7] L.J. Ward, W.C.E. Schofield, J.P.S. Badyal, A.J. Goodwin, P.J. Merlin, Langmuir **2003**, 19, 2110-2114.

[8] L. O'Neill, L.-A O'Hare, S.R. Leadley, A.J. Goodwin, Chem. Vap. Deposition **2005**, 11, 477-479.

[9] B. Twomey, M. Rahman, G. Byrne, A. Hynes, L.-A O'Hare, L. O'Neill, D. Dowling, Plasma Process. Polym. **2008**, 5, 737-744.

[10] F. Fracassi, R. d'Agostino, F. Fanelli, A. Fornelli, F. Palumbo, *Plasmas Polym.* **2003**, *8*, 259.

[11] K. Li, O. Gabriel, J. Meichsner, *J. Phys. D: Appl. Phys.* **2004**, *37*, 588.

[12] D. S. Wavhal, J. Zhang, M. L. Steen, E. R. Fisher, *Plasma Process. Polym.* **2006**, *3*, 276.

[13] S. E. Alexandrov, N. McSporran, M. L. Hitchman, *Chem. Vap. Dep.* **2005**, *11*, 481-490.

[14] O. Horie, R. Taege, B. Reimann, N. L. Arthur, P. Potzinger, J. Phys Chem **1991**, 95, 4393-4400.

CONCLUSIONS

This thesis reported a fundamental study on the deposition of thin organosilicon films in Dielectric Barrier Discharges (DBDs) fed with Ar/HMDSO/O_2, Ar/PMDSO/O_2 and Ar/TMDSO/O_2 mixtures. The properties of the coatings produced with each disiloxane at different O_2 contents in the gas feed, were correlated to GC-MS analyses of the exhausts.

Without oxygen addition to the feed silicone-like coatings with high structure retention of the starting monomer were deposited. Several by-products, such as silanes, silanols and linear and cyclic siloxanes, were detected in the exhausts. The dissociation of the Si-CH_3 bond plays an important role in HMDSO activation, while the Si-H unit is also involved in PMDSO and TMDSO activation. The Si-H group is also supposed to be responsible of the enhanced reactivity of TMDSO and PMDSO with respect to HMDSO molecule. Both FT-IR spectra and GC-MS analyses show that the dimethylsiloxane (-Si$(CH_3)_2$O-) repeating unit can be considered to be the most important building blocks in the HMDSO oligomerization, while the hydromethylsiloxane (-SiH(CH_3)O-) repeating unit is also involved in TMDSO oligomerization processes; both these building blocks contribute to oligomerization in PMDSO DBDs.

The O_2 added to the feed enhances the filamentary character of the discharge and the delivered power and promotes the dramatic reduction of the concentration of by-products in the exhaust, realistically due to oxidation of oligomerizing species.

As also found in some cases in low pressure plasmas, oxygen addition to the gas feed does not improve the monomers activation, since the monomers depletion does not increase with O_2 content. Despite of the increased power, the smaller plasma volume available for the monomers activation, due to the enhanced filamentary regime with increasing O_2 content in the feed, was supposed to be responsible of the HMDSO depletion trend. Species responsible for the monomer activation (i.e. electrons, Ar metastables) are supposed to be involved also in oxygen activation, with the consequent decrease of the monomer depletion in the case of HMDSO.

In addition a different activation mechanism was supposed for the three precursors: for PMDSO and TMDSO reasonably hydrogen abstraction or insertion reactions of oxygen molecules or atoms with the Si-H units could balance the effect of the change of

the discharge regime and account for a stationary monomer depletion trend as a function of the O_2 content in the feed.

Oxygen addition strongly influences the chemical characteristics of the deposits and the composition of the exhausts. More crosslinked and inorganic coatings were deposited with increasing O_2 content in the feed, but, under the adopted experimental conditions, only with PMDSO and TMDSO completely oxidized coatings were obtained. As expected, the concentration of all organic by-products, except silanols, was reduced below the quantification limit as a function of the oxygen content in the feed.

Some evidences induce to claim that, in HMDSO fed discharges, the silanols contained in the deposits are formed through heterogeneous (plasma-surface) reactions during film growth and not from the contribution of silanol-containing species formed in the plasma; on the contrary for the Si-H containing precursors both heterogeneous and homogeneous reactions could contribute to the formation of Si-OH units in the deposits.

In the framework of this work, a reactor for the treatment, in continuum, of 30 cm long web of textile or paper, was built up, but not yet used. In the perspective of future research on the application of the deposition processes studied in this work to the textile treatment, the performances of the three precursors could be tested onto natural and synthetic fabrics. Anyway, as non oily, smooth coatings were generally obtained, PMDSO seems to be the more promising precursor.

CONCLUSION

Cette thèse présente une étude fondamentale sur le dépôt des couches minces d'organosiloxanes par des Décharges à Barrière Diélectrique (DBD), alimentées par des mélanges gazeux de Ar/HMDSO/O_2, Ar/PMDSO/O_2 et Ar/TMDSO/O_2. Les propriétés des couches minces obtenues à partir de chaque précurseur organosilicié, mélangé avec des quantités différentes de l'oxygène, ont été reliées aux analyses des gaz sortant du réacteur par GC-MS.

Sans ajout de l'oxygène au gaz alimentant la décharge, des couches minces contenant beaucoup de carbone et retenant la structure du précurseur de départ, ont été réalisées. Différents sous-produits, à savoir les silanes, silanols et siloxanes linéaires et cycliques, ont été trouvés dans le gaz sortant du réacteur. La dissociation de la liaison Si-CH_3 joue un rôle très important dans le procédé de l'activation du HMDSO, tandis que le groupe Si-H est impliqué dans l'activation du PMDSO et du TMDSO. Nous pensons que le groupe Si-H est aussi responsable de la majeure réactivité du PMDSO et du TMDSO par rapport au HMDSO. Les spectres FT-IR et les analyses par GC-MS montrent que l'unité de répétition diméthylsiloxane (-$Si(CH_3)_2O$-) peut être considérée comme étant le groupe de construction le plus important dans le procédé d'oligomérisation du HMDSO dans la décharge. Tandis que l'unité à répétition hydrométhylsiloxane (-$SiH(CH_3)O$-) joue aussi un rôle dans le procédé d'oligomérisation du TMDSO; tous les deux groupes de construction participent au procédé d'oligomérisation dans les décharges alimentées par PMDSO.

L'oxygène, ajouté au gaz d'alimentation, augmente la nature filamentaire de la décharge ainsi que la puissance injectée, et, en même temps, il favorise une forte réduction de la concentration des sous-produits dans le gaz sortant du réacteur, suite aux réactions d'oxydation des espèces chimiques oligomérisant.

Comme il à été déjà trouvé dans des procédés plasma à la basse pression, l'ajout d'oxygène au gaz d'alimentation de la décharge n'améliore pas l'activation du précurseur organosilicié, puisque le monomère n'ayant pas réagi ne diminue pas en augmentant l'oxygène. On pense que la raison pour cette tendance, pour le HMDSO en particulier, est due à l'augmentation du régime filamentaire de la décharge en introduisant une proportion plus importante d'oxygène dans le gaz d'alimentation. Même si en présence d'une concentration plus importante d'oxygène la puissance

injectée dans la décharge est plus importante, le volume du plasma disponible pour l'activation du précurseur est plus faible. De plus il se peut que les espèces responsables de l'activation du précurseur (électrons, métastables de l'Ar, etc.) soient consommées par l'oxygène et ses produits de décomposition, ce qui va conduire à un taux de décomposition du HMDSO plus faible.

En revanche dans les décharges alimentées par PMDSO et TMDSO, des réactions d'abstraction ou d'insertion des molécules ou des atomes d'oxygène avec les groupes chimiques Si-H pourraient raisonnablement compenser le changement du régime de la décharge et, au même temps, expliquer la tendance stationnaire de la conversion du PMDSO et du TMDSO en augmentant la proportion d'oxygène dans le gaz d'alimentation.

De plus, l'ajout d'oxygène influence fortement la composition chimique des dépôts et des gaz sortant du réacteur. Pour des proportions d'oxygène/monomère plus importante dans le gaz d'alimentation, des couches minces plus réticulées et plus inorganiques ont été obtenues. Un autre résultat important que nous avons obtenue est que dans les conditions expérimentales utilisées dans ce travail, les dépôts totalement oxydés exempte de carbone ont été obtenus seulement avec le PMDSO et le TMDSO. Comme attendu, en augmentant le rapport oxygène/monomère la concentration de tous les sous-produits organiques, sauf les silanols, diminue en dessous de la limite de la quantification de la technique d'analyse GC-MS.

Grâce aux résultats expérimentaux, il semblerait que dans le cas du précurseur HMDSO les groupements silanols détectés dans les dépôts se soient formés, pendant la croissance de la couche mince, par des réactions hétérogènes (phase plasma - surface), et non par les réactions homogène en phase gazeuse. En revanche, pour les précurseurs PMDSO et TMDSO, contenant le groupe Si-H, les réactions hétérogènes, ainsi que les réactions homogènes, pourraient contribuer à la formation des groupes Si-OH dans les dépôts. En ce qui concerne la qualité des films obtenus à partir des trois précurseur, le PMDSO semble le précurseur le plus prometteur, car des couches minces lisses et non-huileuses ont été obtenues uniquement dans le cas de ce monomère.

Dans le cadre de cette thèse, un réacteur, permettant de traiter des bobines de textile ou de papier de 30 cm de longueur en continu, a été conçu, mais faute de temps, nous n'avons pas pu de l'utiliser. Donc comme perspective de ce travail de recherche, il serait

intéressant d’évaluer les performances des couches minces obtenues à partir des trois précurseurs organosiliciés déposés sur les textiles naturels et synthétiques.

CONCLUSIONI

Questa tesi tratta uno studio fondamentale sulla deposizione di film sottili organosilanici in Scariche a Barriera di Dielettrico (DBDs) alimentate con miscele gassose di Ar/HMDSO/O_2, Ar/PMDSO/O_2 ed Ar/TMDSO/O_2. Le proprietà dei film prodotti a partire da ciascun organosilossano, e a diversi contenuti di O_2 nel gas di alimentazione, sono state correlate alle analisi GC-MS dei gas esausti.

In assenza di ossigeno nella miscela di alimentazione, sono stati depositati film di tipo siliconico, con elevata ritenzione della struttura del monomero di partenza. Nei gas esausti, invece, sono stati rinvenuti alcuni prodotti di ricombinazione, come silani, silanoli e silossani lineari e ciclici. La dissociazione del legame Si-CH_3 svolge un ruolo importante nell'attivazione dell'HMDSO, mentre anche l'unità Si-H risulta coinvolta nell'attivazione del PMDSO e del TMDSO. Si pensa altresì che il gruppo Si-H sia responsabile della più elevata reattività del TMDSO e del PMDSO rispetto all'HMDSO. Sia gli spettri FT-IR sia le analisi GC-MS mostrano che l'unità di ripetizione dimetilsilossano (-Si(CH_3)$_2$O-) può essere considerato il "building block" più importante nel processo di oligomerizzazione dell'HMDSO, mentre nel processo di oligomerizzazione del TMDSO è coinvolta anche l'unità di ripetizione idrometilsilossano (-SiH(CH_3)O-); entrambe queste unità contribuiscono all'oligomerizzazione del PMDSO nelle DBDs qui studiate.

L'aggiunta di O_2 al gas d'alimentazione aumenta sia il carattere filamentare della scarica, sia la potenza immessa, e, contemporaneamente, favorisce una forte riduzione della concentrazione dei prodotti di ricombinazione nei gas esausti, realisticamente a causa di reazioni di ossidazione che coinvolgono le specie oligomerizzanti.

Com'è stato riscontrato anche in alcuni casi in plasmi a bassa pressione, l'aggiunta di ossigeno al gas d'alimentazione non migliora l'attivazione del monomero, dal momento che l'abbattimento del precursore non aumenta all'aumentare dell'O_2. Si pensa che, nonostante la potenza immessa aumenti con l'O_2, l'andamento dell'abbattimento dell'HMDSO sia dovuto alla riduzione del volume di plasma disponibile per l'attivazione del monomero, causato dal maggior carattere filamentare della scarica. Le specie responsabili dell'attivazione del monomero (elettroni, metastabili dell'Ar, etc.) sono probabilmente coinvolti anche nell'attivazione dell'ossigeno, provocando, pertanto, la diminuzione dell'abbattimento dell'HMDSO.

Un diverso meccanismo d'attivazione è stato ipotizzato per i tre precursori organosilanici: per il PMDSO ed il TMDSO, reazioni di astrazione di idrogeno o di inserzione di atomi o molecole di ossigeno con il gruppo Si-H potrebbero, plausibilmente, bilanciare l'effetto del cambiamento del regime di scarica e giustificare, pertanto, l'andamento costante dell'abbattimento di tali precursori in funzione della quantità di O_2 contenuta nel gas di alimentazione.

L'aggiunta di O_2, inoltre, influenza fortemente la composizione chimica sia dei film depositati, sia dei gas esausti. All'aumentare del contenuto di O_2 nel gas di alimentazione, si ottengono film via via più inorganici e reticolati, ma, nelle condizioni sperimentali adottate in questo lavoro, film completamente ossidati, cioè senza carbonio, sono stati ottenuti solo con il PMDSO ed il TMDSO. Come atteso, la concentrazione di tutti i prodotti di ricombinazione, fatta eccezione per i silanoli, si riduce al di sotto del limite di quantificazione della tecnica analitica GC-MS in funzione del contenuto di O_2 nella miscela di alimentazione della scarica.

Alcune evidenze sperimentali inducono ad affermare che, nelle scariche alimentate con HMDSO, le funzionalità Si-OH individuate nei film depositati si formino durante la crescita del film per reazioni di ossidazione eterogenee (fase plasma - superficie), e non ci sia alcun contributo da parte dei silanoli che si formano nella fase plasma; al contrario, per i precursori contenenti l'unità Si-H (PMDSO e TMDSO), reazioni di ossidazione sia eterogenee sia omogenee potrebbero contribuire alla formazione dei gruppi Si-OH contenuti nei film.

Nell'ambito di questo progetto di ricerca è stato progettato e costruito, ma non ancora utilizzato, un reattore in grado di trattare substrati di tessuto o di carta lunghi fino a 30 cm. Pertanto, nell'ottica del prosieguo di tale attività di ricerca, volta ad applicare al trattamento dei tessuti i processi di deposizione studiati in questa tesi, si dovrebbero testare su tessuti sia naturali sia sintetici i film ottenuti con tutti e tre i disilossani indagati. Ad ogni modo il PMDSO sembra il precursore più promettente, dal momento che sono stati ottenuti film non oleosi e generalmente lisci.